DEVELOPMENT OF AN EXPERIMENTAL METHODOLOGY FOR MEASUREMENT OF OIL RETENTION AND ITS EFFECT ON THE MICROCHANNEL HEAT EXCHANGER

By

PRATIK S. DEOKAR

Bachelor of Engineering (Mechanical)

University of Pune

INDIA

2010

Submitted to the Faculty of the
Graduate College of the
Oklahoma State University
in partial fulfillment of
the requirements for
the Degree of
MASTER OF SCIENCE
December, 2013

DEVELOPMENT OF AN EXPERIMENTAL METHODOLOGY FOR MEASUREMENT OF OIL RETENTION AND ITS EFFECT ON THE MICROCHANNEL HEAT EXCHANGER

Thesis Approved:

Dr. Daniel E. Fisher

Thesis Adviser

Dr. Lorenzo Cremaschi

Dr. Jeffrey Spitler

ACKNOWLEDGEMENTS

I am thankful to Dr. Lorenzo Cremaschi and Dr. Daniel Fisher for their guidance, encouragement, and support throughout my research at Oklahoma State University. I would like to express my deep gratitude to my friends and research companions: Ardiyansyah Yatim, Roshan Revankar, Andrea Bigi, Ehsan Moallem, Ramprasad Chandrasekharan, and Kedar Pai who helped and encouraged me to complete my thesis work. I am so happy to have worked with Tommy Hong, Kody Jones, Xiaoxiao Wu, Shanshan Cai, Auvi Biswas, Jeremy Smith, Gabriele Corti, Stefano Marelli and all of the undergraduate students in and around the Psychrometric Chamber and Air Flow Lab. My appreciation also goes to the members of the BETSRG lab.

I wish to express my deep gratitude to my parents who have always helped me in making decisions throughout my life, without whom the graduate studies would have been impossible.

Acknowledgements reflect the views of the author and are not endorsed by committee members or Oklahoma State University.

Name: PRATIK S. DEOKAR

Date of Degree: DECEMBER, 2013

Title of Study: DEVELOPMENT OF AN EXPERIMENTAL METHODOLOGY FOR MEASUREMENT OF OIL RETENTION AND ITS EFFECT ON THE MICROCHANNEL HEAT EXCHANGER.

Major Field: MECHANICAL ENGINEERING

Abstract:

In HVAC and refrigeration systems, the lubricant is used only because the compressor requires it for lubrication and sealing. A small portion of the oil circulates with the refrigerant flow through the cycle components, while most of the oil stays in the compressor. The circulating oil, which is missing from the compressor, can form a fairly homogeneous mixture with the liquid refrigerant or it can exist as a separate oil film inside the small tubes and headers of a microchannel heat exchanger. Each heat exchanger in the refrigeration cycle has different oil retention characteristics, and large amounts of oil retention cause a change in heat transfer and an increase in pressure drop. As a result, proper oil management is necessary in order to improve the compressor reliability, to increase overall efficiency of the system, and to minimize system cost by avoiding redundancy and wasted energy.

The thesis focuses on developing methodologies for oil retention experiments on the microchannel heat exchanger working as a condenser and adopted in systems for commercial refrigeration and air conditioning applications. An experimental test facility is designed, built, and calibrated for injecting the oil into a microchannel heat exchanger in a controlled fashion. The methodologies allow accurate measurements of the oil circulation ratio (OCR), heat transfer penalty factor ($HTPF$), and pressure drop penalty factor ($PDPF$) under different operating conditions. The oil retained in the microchannel heat exchanger can also be measured. The refrigerant in this work is R-410A and the oil used is ISO VG 32 grade Mixed Acid POE. The microchannel heat exchanger can also be tested as an evaporator in the same test facility by making minor modifications to the fluid circuitry.

A total of five levels of oil circulation ratios (OCRs) are investigated: OCR = 0, 0.5, 1, 3, and 5 percent by weight. The tests are done at the refrigerant flow rates of 400 lb/h (0.05 kg/s) and 600 lb/h (0.076 kg/s), and at the refrigerant (R-410A) saturation temperatures of 85°F (29.4°C), 105°F (40.6°C), and 130°F (54.4°C). The data for the $HTPF$s, $PDPF$s and oil retentions are provided as a function of OCRs, refrigerant flow rates, and refrigerant saturation temperatures to prove the effectiveness of the methodology.

TABLE OF CONTENTS

Chapter Page

LIST OF TABLES

Table Page

LIST OF FIGURES

Figure Page

CHAPTER I

I. INTRODUCTION

1.1 Introduction

The compressor is the heart of the vapor compression cycle systems; it can be reciprocating, rotary, screw, scroll type, or centrifugal depending on the type of application. In a vapor compression cycle system, the lubricant exists only because the compressors require it. A small portion of the oil circulates with the refrigerant through the cycle components, while most of the oil stays in the compressor. It is essential to have lubrication of the compressor to prevent wear and friction between the mating components. Oil provides a seal between the high and low pressure sides inside the compressor, it does a good job of removing wear debris, it removes the heat generated by the friction and power loss of the electric motor, and it dampens the noise by foaming. Thus, the lubricant serves to extend the life of the compressor. For example, polyol ester (POE) is used as a lubricant with HFC refrigerants like R-410A and R-134a in all types of compressors (ASHRAE 2010).

When the refrigerant leaves the compressor at high velocity, it carries away some fraction of the oil which is entrained in it. The oil separator used on the discharge line is not always 100% efficient or may have lost its efficiency over time, thus a fractional amount of the oil is carried along with the vapor refrigerant to the next component after the separator. The interval required and the ability for the oil to be carried back to the compressor from the system is a complex

function of interdependent parameters like the geometry of the system and its components, fluid viscosities, refrigerant vapor velocity, fluid densities, surface tension of fluids with each other and with the metal they contact, surface of the fluid carrying tubes or channels, load on the heat exchangers, and the temperature and pressure at which the particular component is operating. The design of the layout of the pipelines, condenser, evaporator, suction line, and other system components should be such that the lubricant is effectively removed from them without clogging or being trapped in the tubes, channels or corner pockets, which increases the pressure drop and causes heat transfer degradation in the heat exchangers.

The oil-refrigerant mixture composition is different in different sections of the refrigeration cycle, as the solubility of the refrigerant in oil depends on the pressure and temperature at that particular section. The refrigerant and oil can form a fairly homogeneous mixture in the liquid state, or the oil can exist as a separate film inside the refrigeration system components such as liquid lines, suction lines, heat exchangers, or the small tubes and headers of a microchannel heat exchanger. The amount of oil retained in these components is affected by the system condition at that moment. Cremaschi et al. (2005) point out that the oil retention is high if the concentration of oil in the oil-refrigerant mixtures is high, but retention is low if the refrigerant mass flux is high. Every component in the system has its own oil retention characteristics depending on its geometry and operating conditions. Oil retention in the heat exchanger results in a change in the heat transfer rate and an increase in the pressure drop. It is essential to have proper oil management through the refrigeration cycle to ensure that a sufficient amount of oil always returns to the compressor, avoiding its failure, improving the operational reliability, and preventing excessive pressure rise and heat transfer drop, which adversely affects the overall efficiency of the system.

The presence of the oil has a significant impact on the heat transfer rate and pressure drop in the microchannel heat exchanger-condenser or evaporator, because the thermodynamic and

transport properties of the resulting oil-refrigerant mixture are different from those of pure refrigerant. Predicting the thermodynamic performance of the microchannel heat exchanger is possible only when the contributions of the individual refrigerant and oil components in the oil-refrigerant mixture are known. Many of the experiments performed on heat exchangers to date are based on pure refrigerants or neglect the presence of the lubricant (even if it is present because of the use of pre-charged compressors). The use of such experimental results may bias the design or modeling of the heat exchangers.

Analytical and experimental studies of oil retention in the microchannel tubes, heat exchangers, suction line, liquid line, and discharge line with various refrigerant and oil pairs can be found extensively in the literature. However, oil retention studies in the microchannel heat exchangers using R-410A / POE (ISO VG 32 grade) and R-134a / POE (ISO VG 32 grade) mixtures do not exist and are important for future design considerations. This research project tries to fill in these gaps in the oil retention studies by providing experimental results of oil retention and its effects on the microchannel heat exchanger. This study will facilitate improvements in the design of microchannel heat exchanger, help in proper oil management in order to improve the compressor's reliability, increase the overall system efficiency, and minimize system cost by avoiding redundancy and waste of energy.

1.2 Thesis Objectives

The objectives of this thesis are as follows:

1.2.1 Construct an experimental facility capable of measuring the oil retention and its effect on the heat transfer and pressure drop in a microchannel heat exchanger when used as a condenser in R-410A air conditioning systems and R-134a commercial refrigeration systems.

1.2.2 Develop the procedures for experimentation and data analysis.

1.2.3 Conduct preliminary experiments of all possible combinations of the following parameters:

a. Refrigerant mass flow rates [400 lb/h (0.05 kg/s) and 600 lb/h (0.076 kg/s)]

b. Oil circulation ratios [0%, 0.5%, 1%, 3%, and 5%]

c. Saturated temperatures of R-410A [85°F (29.4°C), 105°F (40.6°C), and 130°F (54.4°C)]

1.2.4 Provide preliminary data for the Heat Transfer Penalty Factor ($HTPF$) and the Pressure Drop Penalty Factor ($PDPF$) due to oil retention in microchannel heat exchangers. The $HTPF$ and $PDPF$ data should be a function of oil circulation ratios (OCRs), refrigerant flow rates, and refrigerant saturation temperatures.

1.3 Significant Contributions to Improve Experimental Methods

1.3.1 Initially a Vapor Compression Cycle System was constructed for experimentation. The system was then converted to a Pump-Boiler System because of problems with the former system. This research project directly compares these two experimental set-ups for the first time and provides a quantitative comparison of the oil retention measurements' experimental methodology.

1.3.2 In the oil measurement experiments, the use of the Pump-Boiler System, with gear pump, displayed various advantages over the use of the Vapor Compression Cycle System, with a single speed scroll compressor. In the Pump-Boiler System the mass flow rate could be controlled instantaneously by varying the speed of the gear pump, the bladder accumulator dampened the fluctuations in the mass flow rate, control of the superheat at the microchannel heat exchanger inlet was possible with the help of a superheater, and the system required less supervision.

1.3.3 The use of the Coriolis mass flow meter contributed to extremely small uncertainty in the measured mass flow rate of the injected oil-refrigerant mixture, which means that the uncertainty in the solubility dominates the error in the OCR. Accurate measurement of the solubility value of the injected oil-refrigerant mixture by the gravimetric method instead of relying on the solubility data from the literature considerably reduces the uncertainty in the calculated OCR and is a unique feature of this project. A methodology was also devised to predict the injection mass flow rate of the oil-refrigerant mixture to get the desired OCR at the microchannel heat exchanger.

1.3.4 An unconventional duct between the heat exchanger and the nozzle bank was used. The in-house calibration of the nozzle bank when applied to the equations presented in ANSI/ASHRAE Standard 41.2 (ASHRAE 1987) gave correct air volume flow rates ($CFMs$). The CFM values were further used in the heat transfer calculations.

1.3.5 Mapping tests performed at the "no oil injection tests" (or OCR=0% tests) provided mapping points to determine the surface fits for the heat transfer and pressure drop as a function of pure refrigerant flow rates and saturation pressures at the microchannel heat exchanger. The surface fits were used to interpolate the "no oil" condition heat transfer ($Q_{air@OCR=0}$) and pressure drop ($\Delta P_{@OCR=0}$) for any system conditions observed during the oil injection test.

CHAPTER II

II. LITERATURE REVIEW

2.1 History

Since humans started understanding the importance of storing food, they started using cool caves or ice for that purpose. They also started to invent technologies to improve the environment inside their houses. In 1300 BC Windcatchers, a passive ventilation and cooling system, were used by the Egyptians. An ancient refrigerator from 300 BC, the "Tong Bing Jian - Bronze Ice box", was excavated in 1978 from the Zenghouyi Tomb in China. In the 200s, the Romans built aqueducts to bring fresh water to the cities, and this water was passed through ducts in the walls of their homes to provide cooling. The roots of the modern vapor compression cycle are first noticed in the 19th century. A few of the key events as described by EPA (2013), Green (2012), Moe (2011), and Roger's Refrigeration (2012) are presented below; these events have a major impact on the development of modern refrigeration and air-conditioning industries.

1748 Artificial refrigeration was demonstrated by William Cullen at the University of Glasgow by boiling ethyl ether in a partial vacuum.

1758 Benjamin Franklin and John Hadley used quick evaporation of alcohol and other volatile liquids to cool down objects below the freezing temperature of water.

1820 Michael Faraday made the same discovery in England, but with ammonia when he compressed and liquefied it.

1834 The first practical machine was built by Jacob Perkins. It was based on the same technology and used ether as a refrigerant.

1842 An American physician, John Gorrie, designed and built an air cooling apparatus which made ice by evaporation and compression of the liquid ammonia, which he used to cool the air of his patients in a hospital in Apalachicola, Florida.

1851 John Gorrie was granted the U.S. patent for mechanical refrigeration.

1856 An American businessperson, Alexander C. Twinning, introduced the first commercial refrigerator.

1866 Carbon dioxide (CO_2) was first used as a refrigerant.

1905 On October 3, Léon Creux, an engineer from the Republic of France, patented the scroll compressor technology (Creux 1905). It only became feasible to mass manufacture and use scroll compressors in air conditioning units after the mid-1970s, when high precision machining was able to create scrolls with very small tolerances in their design.

1920s Initially the research only focused on finding refrigerants for the air conditioning and refrigeration systems that would provide effective cooling. The objectives were fulfilled by using refrigerants like ammonia (NH_3), chloromethane (CH_3Cl), propane, and sulfur dioxide (SO_2). However they were highly toxic, flammable, or explosive.

1928 The team of Thomas Midgley, Albert Henne, and Robert McNary at the Frigidaire division of General Motors synthesized dichlorofluoromethane, R-12, the first CFC. They announced it publicly in **1930** and trademarked it as Freon. They were safe alternatives to the chemicals used before them, odorless and toxic only in extremely large doses. CFCs came to dominate first refrigeration and later HVAC industries.

1931 The commercial production of R-12 to be used in residential refrigeration. Willis Carrier developed the first centrifugal chiller for commercial use.

1950s Hydrochlorofluorocarbons (HCFCs) were added to the portfolio of refrigerant alternatives.

1970s Concerns began to surface about the thinning of the ozone layer and whether CFCs may be in part responsible.

1973 Prof. James Lovelock reported finding trace amounts of refrigerant gases in the atmosphere.

1974 Sherwood Rowland and Mario Molina predicted that chlorofluorocarbon refrigerant gases would reach the high stratosphere and there damage the ozone.

1985 The "ozone hole" over the Antarctic was discovered.

1987 The Montreal protocol went into effect. It is an international treaty that established phase-out dates for the use and production of ozone-depleting substances. According to this protocol, CFCs were to be replaced with HCFCs and HFCs, and then HCFCs were to be phased out. Developed countries were to phase out CFCs in 1993 and achieve a 50% reduction in HCFCs by 1998.

1990s The HFCs were developed as a substitute for CFCs and HCFCs (HFCs are ozone-friendly and energy efficient, have low toxicity and flammability, but have high global warming potential (GWP)). Global warming arose as the new threat from refrigerants, which acted as greenhouse gases.

1990 Rowland and Molina's prediction was proved correct. The Montreal protocol -The London Amendment changed the ozone-depleting substances (ODS) emission schedule. The requirement of completely phased out CFCs, halons, and carbon tetrachloride was by 2000 in developed countries and 2010 in developing countries. Methyl chloroform was added to the list, with phase out year of 2005 in developed countries and 2015 in developing countries.

1992 The Montreal protocol -The Copenhagen Amendment changed the ozone-depleting substances (ODS) emission schedule and called for complete phase out of CFCs, halons, carbon tetrachloride, and methyl chloroform by 1996 in developed countries. It planned for the HCFC phase out for developed countries, beginning in 2004.

1996 All CFC (R-11, R-12) production stopped in developed countries, but the use of recycled CFCs continued.

1997 The Montreal protocol -The Montreal Amendment called for phase out HCFCs in developing countries and methyl bromide in developed and developing countries by 2005 and 2015, respectively. The Kyoto Protocol of the United Nations Framework Convention on Climate Change (UNFCCC) went into effect. This protocol targeted phasing out the refrigerants responsible for global warming, like HFCs, in developed countries. The CFCs and HCFCs were not included, as they were already covered by the Montreal Protocol.

1999 The Montreal Protocol -The Beijing Amendment tightened the control on the production and trade of HCFCs. Bromochloromethane was added to the list, with phase out by 2004.

2004 The Montreal Protocol schedule called for 35% reduction in HCFCs consumption and production in developed countries. No production and no import of HCFC-141b in the U.S.

2006 The EU adopted regulation of fluorinated greenhouse gases, which makes stipulations regarding the use of FCs and HFCs with the intention of reducing their emissions.

2010 The Montreal Protocol schedule called for 75% reduction in HCFCs consumption and production in developed countries. The sales of new Freon-based air conditioners were stopped. No CFCs for developing countries. No new equipment with HCFC-22 in the US, but the use of recycled R22 in equipment manufactured before 1/1/2010 could continue. No production and no import of HCFC-142b and HCFC-22 in the U.S.

2011 The HFOs were scheduled to replace HFC-134a in the new automobile models in Europe. The U.S. Environmental Protection Agency's minimal allowable leakage rates for equipment with more than 50 lbs. of refrigerant charge over a 12-month period are 35% for commercial refrigeration, 35% for industrial process refrigeration, and 15% for comfort cooling. Venting the refrigerant is prohibited for any equipment during service or retirement.

2015 The Montreal Protocol schedule is for HCFC consumption and production, which is to be reduced by 90% in developed and 10% in developing countries. In the U.S., addition to the

HCFC-141b, HCFC-142b and HCFC-22 restrictions, no production or importing of any other HCFCs, except for use as refrigerants in equipment manufactured before 1/1/2020.

2020 The Montreal Protocol schedule is for HCFC consumption and production, which is to be reduced by 99.5% in developed and 35% in developing countries. No new equipment with HCFC-123 in developed countries.

2025 The Montreal Protocol schedule is for HCFC consumption and production, which is to be reduced by 67.5% in developing countries.

2030 The Montreal Protocol schedule is for HCFC consumption and production, which is to be reduced by 100% in developed and 97.5% in developing countries. No new R123 for service in developed countries. No HCFCs in new equipment in developing countries, but the use of recycled R123 can be continued. The US, Mexico and the Federated States of Micronesia will phase-down HFCs.

The question arises about the use of existing equipment when the refrigerant in them is phased out. This problem can be solved by using the same refrigerant after recycling, replacing the equipment, or recovering and destroying the phased out refrigerant and switching to a new compatible refrigerant which will not affect the operating conditions and efficiency of the system. Consumers should purchase energy-efficient and reliable systems which already use environment friendly refrigerants. Products with (Environmental Protection Agency's and the Department of Energy's) Energy Star® label can save 10% to 40% on the heating and cooling bills every year (EPA 2012). As of today, equipment that displays the Energy Star® label has a SEER value of at least 13. The Seasonal Energy Efficiency Ratio, or SEER, is defined as the ratio of the total heat removed from the conditioned space during the annual cooling season and the total electrical energy consumed by the air conditioner or heat pump during the same season, expressed in Btu/W-h (AHRI 2008).

2.2 Refrigerants R-410A and R-134a

Hydroflurocarbons (HFCs) were introduced as substitutes for the ozone-depleting chloroflurocarbons (CFCs) and hydrochloroflurocarbons (HCFCs), which have been gradually phased out. The properties of the new HFCs are similar to those of as the phased-out refrigerants and do not require major modifications to the system components. However, the HFC mixtures are ozone-friendly, they have high GWP and so are not completely friendly to the environment. Mineral oil was used along with the CFCs and HCFCs because of its high miscibility. Reduced miscibility affects the return of the oil to the compressor in Vapor Compression Cycle Systems. Hence for retrofits or new systems utilizing HFC refrigerants, highly miscible synthetic lubricants (like POE) were developed. These expensive synthetic lubricants, being hygroscopic in nature, introduces moisture in the system if exposed to the atmosphere before charging, and also caused irritation if they came in contact with skin (Mohanraj et al. 2011).

R-410A is one such alternative. R-410A is a near-azeotropic mixture of 50 wt. % HFC-32 and 50 wt. % of HFC-125. A composition tolerance of $^{+0.5\%}_{-1.5\%}$ for R-32 and $^{+1.5\%}_{-0.5\%}$ for R-125 is allowed by ASHRAE (Bivens and Yokozeki 1998). R-410A belongs to the safety group of A1: much less toxic and less flammable (ASHRAE 2007, 2009) with zero ozone depletion potential (ODP), but with a very high global warming potential (GWP, 100 years) of 2100 (ASHRAE 2009), and its retrofits have higher working pressures (EPA 2012). R-410A is manufactured and sold under various trade names, including GENETRON® AZ-20, SUVA® 410A, Forane® 410A, and Puron®. The letter "A" in the R-410A identifies the percentage of R-32 and R-125 in it. Bivens and Yokozeki (1998) present data for change in the composition of the HFC mixture inside an R-410A storage tank when the liquid level drops from 85% to 2% while the refrigerant is extracted isothermally: at 77°F (25°C) the composition changed by a maximum of 0.4%, and at 104°F (40°C) it changed by a maximum of 0.5% in both R-32 and R-125 proportions. They also

showed that refilling the tank with fresh R-410A changed the composition further, but within an acceptable limit.

R-134a is another alternative; it also belongs to the group of A1 (ASHRAE 2007, 2009), with zero ozone depletion potential (ODP) but a high global warming potential (GWP, 100 years) of 1430 (ASHRAE 2009). R-134a is manufactured and sold under various trade names, including Forane® 134a, Genetron® 134a, Suva® 134a, and Dymel® 134a. The letter "a" in the R-134a ies the type of isomer, that is, even though all tetrafluoroethanes have the same molecular formula, the unique structural formula of R-134a is 1,1,1,2-tetrafluoroethane.

Industrial process refrigeration, industrial process air conditioning, household and light commercial air conditioners, cold storage warehouses, ice skating rinks, very low temperature refrigeration, non-mechanical heat transfer systems, refrigerated transport, commercial ice machines, vending machines, motor vehicle air conditioners, water coolers, household refrigerators and freezers, residential dehumidifiers, reciprocating and screw chillers, centrifugal chillers and other such systems utilizing ozone-depleting CFC-12, HCFC-22, R-500 (73.8 wt.% CFC-12 and 26.2 wt.% of HFC-152a) and blends containing HCFC-22 and/or HCFC-142b were retrofitted with R-134a, and the ones using HCFC-22 and blends containing HCFCs were retrofitted with R-410A or R-134a. (EPA 2012)

This section concentrates only on R-410A and R-134a because these two refrigerants are the primary heat transfer fluids used in the thermal system described in this study.

2.3 Studies of Microchannels

A microchannel heat exchanger consists of tubes with multiple parallel channels; in the case of a condenser, the tubes are cooled by air flowing over its fins. The use of multichannel tubes reduces the internal volume of the heat exchanger and thus the charge of the system. Each channel provides a high surface-to-volume ratio and an increased condensation heat transfer coefficient compared to the conventional large round tubes. The construction of multi-louvered fins over the microchannel tubes helps in reducing the air side pressure drop and increasing the heat transfer to the air.

Microchannel heat exchangers have improved the performance of air conditioning, refrigeration, and heat pump systems, and their benefits are mentioned in numerous studies (Garimella 2003, Jacobi et al. 2005). Kandlikar et al. (2006) have compiled studies done on microchannels. Two-phase flow regime studies have been done in microchannels using air–water, air-oil, and nitrogen-water pairs. The flows were adiabatic flows, that is, they flow without rejecting heat, and the experimental tests were performed at atmospheric pressures in order to simplify the experiment facilities. In these experimental facilities, the gas and liquid flow rates were controlled to get desired qualities, while a heater and cooler maintained the temperature of the mixture. The low-pressure tests helped in gaining optical access in the tubes to visualize the flow patterns. Once the experiments were done, the fluids (air, water, and nitrogen) could be expelled to the atmosphere, unlike harmful refrigerants. Such studies have the disadvantage of extrapolating their results to other fluids like refrigerants, as the properties of air-water, air-oil, and nitrogen-water mixtures are considerably different from the two-phased refrigerant. The adiabatic flows with the same vapor-liquid ratio and flow pattern in the entire tube/channel gave no information about the change that is observed in the actual non-adiabatic phase changing flow.

Extrapolation from large round-tube correlations to smaller multi-channel tube geometries in microchannel heat exchangers could introduce errors in pressure drop and heat

transfer predictions because the flow regimes and their transitions, which depends on the gravity, shear, viscous, and surface tension forces, are different in microchannel tubes from those in larger diameter tubes.

A probabilistic two-phase flow map model (Jassim and Newell 2006) for the refrigerant flow through the microchannel (in the absence of oil) can predict the pressure drop and void fraction over a wide range of qualities (0 to 1) and mass fluxes (50 kg/m2-s ≥ mass flux ≥ 300 kg/m2-s). In the same setup as Jassim and Newell (2006), Nino (2002) observed the flow regime in the microchannel tube at different sections along its length, they observed that at the same section of the tube, simultaneous liquid, intermittent, vapor, and annular flow regimes are present in different channels. The weightages (also called time fractions) were given to each flow regime based on its likelihood to occur at every section of the tube: the liquid time fraction, the vapor or high quality time fraction, the intermittent time fraction, or the annular time fraction. The summation of the time fraction values of all flow regimes at a particular section is one. This time fraction of a particular flow regime when multiplied with the flow regimes' pressure drop model gives the pressure drop at that section of the tube due to that flow regime. The modeling approach with oil and refrigerant in the heat exchanger can be simplified by using the equation by Baustian et al. (1986), which calculates the density of the oil-refrigerant mixture based on local oil concentrations. The specific heat, surface tension, and thermal conductivity can be calculated using the local oil mass fraction, according to Jensen and Jackman (1984). A simplified modeling of the heat exchanger was done by Iu (2007), who used the modeling approaches recommended by Shen and Groll (2005) to calculate the oil-refrigerant mixture properties. The probabilistic two-phase flow map modeling technique by Jassim and Newell (2006) can be extended to include the oil in the channels along with the refrigerant if it is possible to extrapolate the time fraction values.

2.4 Theory of Lubricants with the Refrigerants

The lubricant, synthetic or natural, is selected such that it does not react with the refrigerant used in the system and is still efficient in lubricating the compressor. To enhance the lubricant, additives are added which improve its lubricity, anti-wear, anti-corrosion, antifoaming, thermal stability, oiliness, and oxidation inhibition properties.

The lubricant (oil) used in the system mentioned in thesis report is Emkarate RL 32-3MAF, which is an ISO VG 32 synthetic polyol ester (POE) lubricant with additives less than 1%. POE - ISO VG 32 has a midpoint viscosity of 32 cSt at 40°C or approximatly 150 SSU at 104°F (ASTM 2007). This report uses the terms “lubricant” and “oil” interchangeably.

The amount of refrigerant dissolved in the lubricant depends on the pressure, temperature, and chemical structure. The percentage of the refrigerant dissolved increases with an increase in the pressure and/or decrease in the temperature. The HFC refrigerants are highly polar compounds and have less miscibility with the non-polar mineral oil lubricants (Yokozeki et al. 2000). For example, halogenated refrigerants like R-134a and R-410A are highly miscible in synthetic lubricants like POE, while mineral oils are not soluble in HFC refrigerants like R-134a and refrigerant blends using R-32 (ASHRAE 2010). The coefficient of performance (COP) of the R-134a refrigeration system has been observed to be higher by 5% when the miscible POE oil was used instead of the immiscible mineral oil (MO) (Schnur et al. 2000).

The viscosity of the lubricant decreases if its temperature rises or if the less viscous refrigerant is dissolved in it. An appreciable drop in viscosity can hamper the sealing action of the lubricant inside the compressor. The viscosity drop can be avoided by using a high-viscosity grade lubricant with higher viscosity index, which prevent a drop in the viscosity below the critical limit and will maintain less change in its viscosity over a given temperature range. However, lubricant oil with low viscosity and viscosity index at a lower evaporator temperature

can be helpful for returning the oil to the compressor with high velocity refrigerant gases. The lubricant thus needs to have balanced properties so the system performance is not compromised in any stage of the refrigeration cycle. The coefficient of performance (COP) of the R-410a system with low viscous POE 32 (ISO VG 32 grade) increased by 3.5% because of the increase in the evaporative capacity compared to a system with the higher viscous POE 68 (Schnur et al. 2000).

When the refrigerant is dissolved in the lubricant (high lubricant concentration, or oil-rich solution) or the lubricant is dissolved in the refrigerant (high refrigerant concentration, or refrigerant-rich solution), the parent/solvent fluid cannot be treated as a pure fluid, as its composition has been changed because of the solute. Different pressures and temperatures are observed at different stages of the refrigeration cycle; hence the refrigerant or lubricant solution, whichever fluid is of interest, will differ in its composition.

Refrigerant and lubricant pairs can be classified into three types: completely miscible, partially miscible, and totally immiscible. Miscibility is the ability of one fluid to mix in all proportions with the second fluid; it can be considered as lubricant in refrigerant or refrigerant in lubricant. The proportion in which the refrigerant mixes in the lubricant is termed as solubility; its unit of % w/w is the ratio of the mass of refrigerant (solute) to the mass of lubricant (solvent) at the same temperature and pressure expressed in a percentage.

In the case of a **completely miscible** pair, at a particular temperature the refrigerant and the lubricant are mutually soluble in all proportions. There will be only a liquid phase, or one liquid phase (made of the refrigerant and the lubricant) and one gaseous phase (consisting of only pure refrigerant) under the equilibrium condition. In the gaseous phase, only pure refrigerant vapor exists because the vapor pressure of the lubricant is much lower than that of the pure refrigerant. In the liquid phase, the lubricant will be dissolved in the refrigerant (in the evaporators and the condensers) or the refrigerant will be dissolved in the lubricant (inside the compressor). In Figure 1, P_1^{o} and P_2^{o} are the pure refrigerant's saturated pressures at temperatures t_1 and t_2, respectively. At pressure P_1 and temperature t_1 only one composition W_1 of the liquid is possible at an equilibrium condition, and this is represented by point E_1. If the temperature is increased to t_2, some of the refrigerant will evaporate from the refrigerant and lubricant liquid mixture or solution, reducing its composition to W_2 which is represented by point E_2.

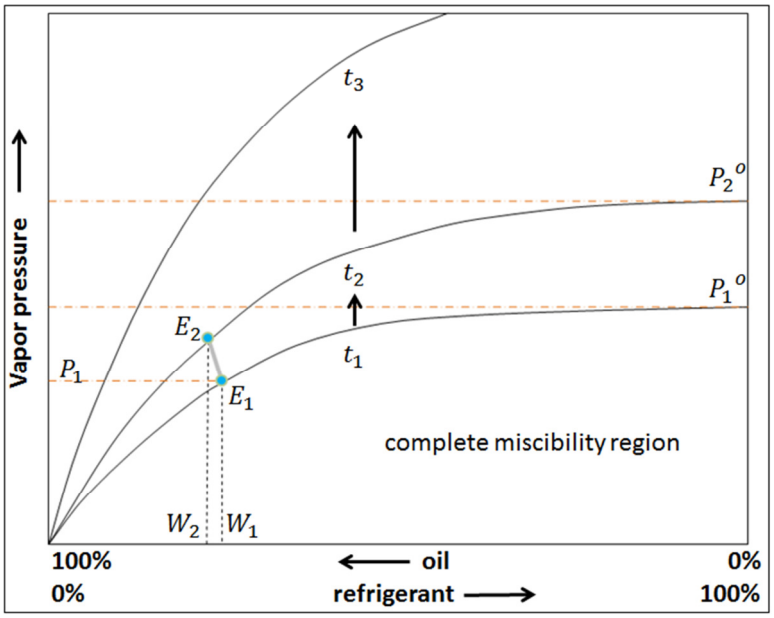

Figure 1: Pressure-Temperature-Solubility diagram for completely miscible refrigerant/oil solutions, ASHRAE (2010).

In Figure 2, point C at the apex of the dotted dome represents the critical solution temperature (CST) t_3. The CST is the temperature above which the refrigerant and the lubricant mixture are completely miscible. The region below this point C and to the left of the dotted dome represents a region with a lubricant-rich solution, which is completely miscible. The region under the dotted dome is the **partially miscible** region. In this region, the liquid separates into two liquid phases: one is a refrigerant-rich solution and the other is a lubricant-rich solution. These two solutions are then immiscible with each other. The region below this point C and to the right of the dotted dome represents a region with a refrigerant-rich solution, which is also completely miscible. Under this dotted dome, or in the partially miscible region, the points E_1 (lubricant-rich solution – composition W_1) and E_2 (refrigerant-rich solution – composition W_2) on the temperature line t_1 represent the two phases that coexist in equilibrium at pressure P_1. One such case of equilibrium between the R-410A and POE oil pair as seen through the sight glass of the oil reservoir is shown in Figure 3, in the figure the refrigerant-rich solution being less dense tries to settle below the refrigerant-rich solution.

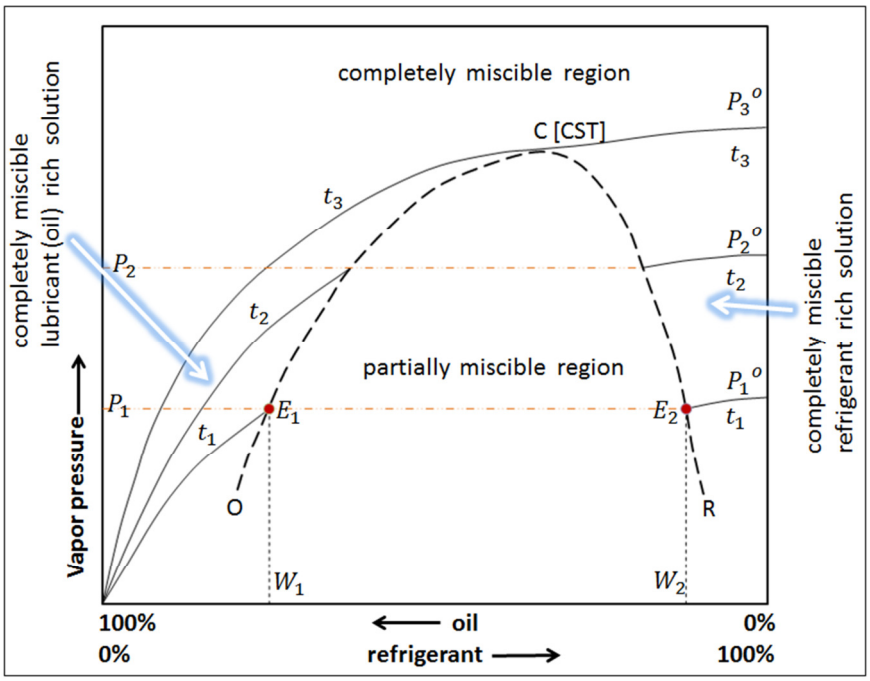

Figure 2: Pressure-Temperature-Solubility diagram for partially miscible refrigerant/oil solutions, ASHRAE (2010).

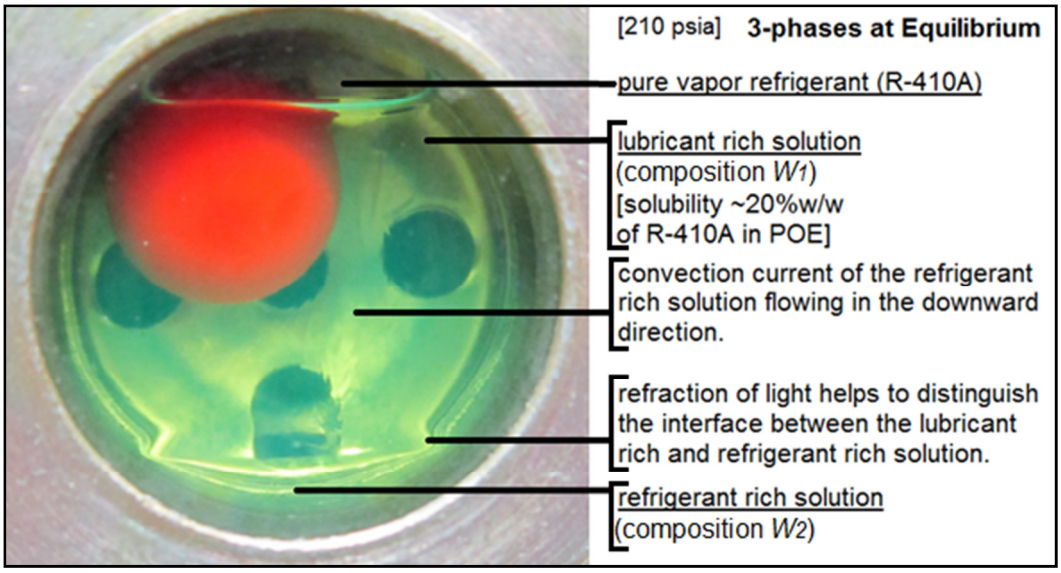

Figure 3: Three phases at equilibrium (R-410A vapor, POE rich solution, and R-410A rich solution)

For some of the lubricant and refrigerant **totally immiscible** pairs, the partial miscibility dome is so wide and the CST is so high that their mutual solubility can be neglected. In this case, the two liquid phases that coexist in equilibrium at a certain temperature and pressure will have an extremely lubricant-rich solution and an extremely refrigerant-rich solution. These two individual phases will have the same properties as their pure composition.

When the refrigeration system is operating, the compressor's oil sump or crank case has a lubricant-rich solution. However, when the system stops and pressure needs to equalize between the low inlet pressure side of the compressor and the evaporator, equalization drives more refrigerant from the refrigerant-rich solution in the evaporator towards the compressor, diluting the lubricant-rich solution, which is not good for the next system startup. Once the compressor stops, its temperature drops and may reach the ambient temperature. If the lubricant and the refrigerant solution inside the compressor are partially miscible and if their temperatures drop below the CST, the lubricant-rich phase and the refrigerant-rich phase separate. These two phases form layers on top of each other because of the differences in their densities. The lubricity, anti-wear, anti-corrosive properties of the refrigerant-rich solution are much less than that of the

lubricant; the compressor components in contact with the refrigerant-rich solution, when stopped and during the startup, are likely to get damaged, because of its inferior properties. The viscosity of the refrigerant-rich layer is also much lower than that of the lubricant and, because of this, the liquid refrigerant may enter the compression chamber, which is very undesirable for the compressor's operation at startup.

When the refrigerant-rich solution is discharged from the compressor, it carries diluted lubricant with it. The compressor also loses some of its lubricant in the form of entrained particles which gain momentum from the high velocity refrigerant exiting at the discharge. The problem is worse if the refrigerant and the lubricant pair are totally immiscible.

The condenser operates at a relatively higher temperature than the rest of the refrigeration system components. At this high temperature when the vapor refrigerant condenses, the lubricant dissolves in it and a refrigerant-rich solution is formed. If the lubricant is not dissolved in the refrigerant, in case of a totally immiscible pair, then this nearly pure lubricant with less density floats on the liquid refrigerant in the form of droplets or forms a continuous stream, which in turn will be rolled or pushed along the wall of the tubes. In the case of a partially miscible pair, the lubricant-rich solution will be flushed by the liquid refrigerant-rich solution. The lubricant-rich solution may become trapped in stagnant pockets unreached by the liquid refrigerant solution. In these cases, the ability of the refrigerant solution to flush the lubricant solution strongly depends on the viscosity of the lubricant solution, their miscibility, and surface tension interactions with each other and with the walls of the heat exchanger tubes.

The evaporator, on the other hand, works at lower temperatures than the rest of the refrigeration system components. In the case of a partially miscible refrigeration/lubrication pair, if the temperature is below the CST, then the phases separate into refrigerant-rich solutions and lubricant-rich solutions. One more phase is added inside the evaporator when the refrigerant

evaporates from the refrigerant-rich solution. Thus, there are three phases inside the evaporator, similar to the equilibrium phases seen in Figure 3. If the solution pair is completely miscible, then two phases are present under equilibrium, a completely miscible refrigerant/lubricant solution and pure vapor refrigerant. If the solution pair is totally immiscible, the three phases that can exist in equilibrium are the nearly pure refrigerant, the nearly pure lubricant and the vapor refrigerant. The fluid that exits the evaporator is mostly the liquid lubricant or the lubricant-rich solution and the vapor refrigerant, as almost all the refrigerant evaporates.

The lubricant-rich solution is encountered in the initial stage inside the condenser. In the later stage, or outlet, of the condenser, the lubricant-rich solution is negligible as the fluid then turns into the refrigerant-rich solution because of refrigerant condensation and dissolution with the lubricant. While in the evaporator, the lubricant-rich solution is negligible in the initial stage and as the refrigerant evaporates, it becomes a lubricant-rich solution. This lubricant-rich solution travels at a very low speed in the heat exchanger because of high viscosity. The viscosity depends on the solubility of the refrigerant in the lubricant: the higher the solubility, the lower is the viscosity. This lubricant-rich solution is pushed by the sheer force exerted on it by the less viscous refrigerant-rich solution and the vapor refrigerant. As the lubricant does not evaporate or condense like the refrigerant, the heat transfer to or from the heat exchanger also depends on the sensible heat of the lubricant. The lubricant-rich solution exiting from the evaporator, or the suction line, is carried by high velocity refrigerant vapor, which transfers momentum to the lubricant-rich solution.

Further discussion will be related to the R-410A - POE pair and the R-134a - POE pair, as they are the primary fluids used for this experiment.

The ASHRAE Handbook – Refrigeration (ASHRAE 2010) contains charts for various oil-refrigerant pairs showing their solubility, density, and viscosity changes with temperature and pressure. The data of solubility for R-410A and ISO VG 32 grade Mixed Acid POE are found only in the paper by Cavestri and Schafer (2000), while that for R-134a and ISO VG 32 grade Mixed Acid POE (EMKARATE RL32S) are in Cavestri (1993, 1995). The data from these references are used in the current thesis work. These references also provide solubility, density, and viscosity data for several other refrigerant-lubricant pairs. The authors used an Oscillating Body Viscometer in experiments having a count of at least 0.06 cP (0.06 mPa·s). Their viscometer also included a densitometer, which could measure density up to 0.0003 oz/in^3 (0.0005 g/mL). The viscometer consisted of a cylindrical bob oscillating in the test fluid, the viscosity was determined by measuring the rate of sinusoidal decay of the bob's oscillations using a linear variable differential transformer. In all their experiments they used a temperature-compensated 360° rotation Bourdon tube gauge for pressure measurement having an error of ±0.2 psia (±0.0013 MPa), while the RTDs and J type thermocouples were calibrated to show an error of ±0.2°F (±0.1°C). The calibration of the setup using particular standards gave an accuracy of ±0.1% for low viscosity solutions and ±1.5% for high viscosity solutions, and the densitometer had an error of ±0.3%. The solubility of the refrigerant in the oil was measured by measuring the weight of the samples in an evacuated light weight glass. The authors do not give the error for the measured solubility, but the method they used gave reproducible results within ±0.5%.

2.5 Previous Work in Investigation of Oil Retention

The literature review shows the types of experimental setups used for oil retained measurements in the system components such as heat exchangers, suction or discharge lines of the compressor, or a custom made test section to analyze the heat transfer and pressure drop characteristics along with the oil retained.

Scheideman and Macken (1975) and Scheideman et al. (1977) oil retention measurement system was designed to simulate the compressor suction line and the discharge line. This system had a closed vapor refrigerant loop where the pressures and the flow rates were maintained by a compressor. Oil separators placed on the discharge line, after the compressor, filtered the oil from the vapor refrigerant in concentrations as low as 50 ppm before the refrigerant entered the test section. The test sections were either vertical or horizontal large tubes, greater than 0.5 in. (12.7 mm) in diameter depending on the geometry of testing. The temperature and pressure were controlled by heating the vapor refrigerant using strip heaters or by cooling it using an external refrigeration unit. The cooling of the vapors could also be achieved by condensing a portion of refrigerant vapor, throttling and mixing it back with the main stream. Before being injected into the test section from the inlet reservoir, the oil was preheated using the energy from the vapor refrigerant in a heat exchanger. Another set of separators was placed after the test section for recovering and returning the oil into the return reservoir. The oil was then transferred manually from the return reservoir to the inlet reservoir. The first three types of injection methods shown in Figure 4 were tested: injection into the copper tube with a porous bronze annular section which is in series with the main refrigerant copper tube, injection inside the main copper tube using a spray nozzle, and injection using hypodermic tubing at the center and perpendicular to the main refrigerant line. Scheideman and Macken (1975) and Scheideman et al. (1977) pointed out that the pressure measurements were independent for these three methods of oil injection 3 ft. (0.9 m) before the first pressure tap; also the flow patterns developed quickly to achieve the mixture's

equilibrium pattern and were same for all cases. The oil thickness in the glass viewing port was measured using an attached micrometer whose shaft/probe traversed inside the tube in a perpendicular direction till the probe's tip touched the level of the oil.

For the experiment discussed in this report, the injection position of the oil upstream/before the microchannel heat exchanger is approximately 2.5 ft. (0.76 m) before the first pressure tap, to ensure that the mixture equilibrium is achieved and that the pressure measured remains independent of the method of oil injection. The oil injection method consists of small diameter copper tubing connected in a perpendicular direction and nearly flush with the inside surface of the main refrigerant line. Figure 4-(d) shows a graphical image while Figure 17 (see page 47) shows an actual image of this injection method. When the injected oil reaches the intersection, it gets carried by the high velocity refrigerant.

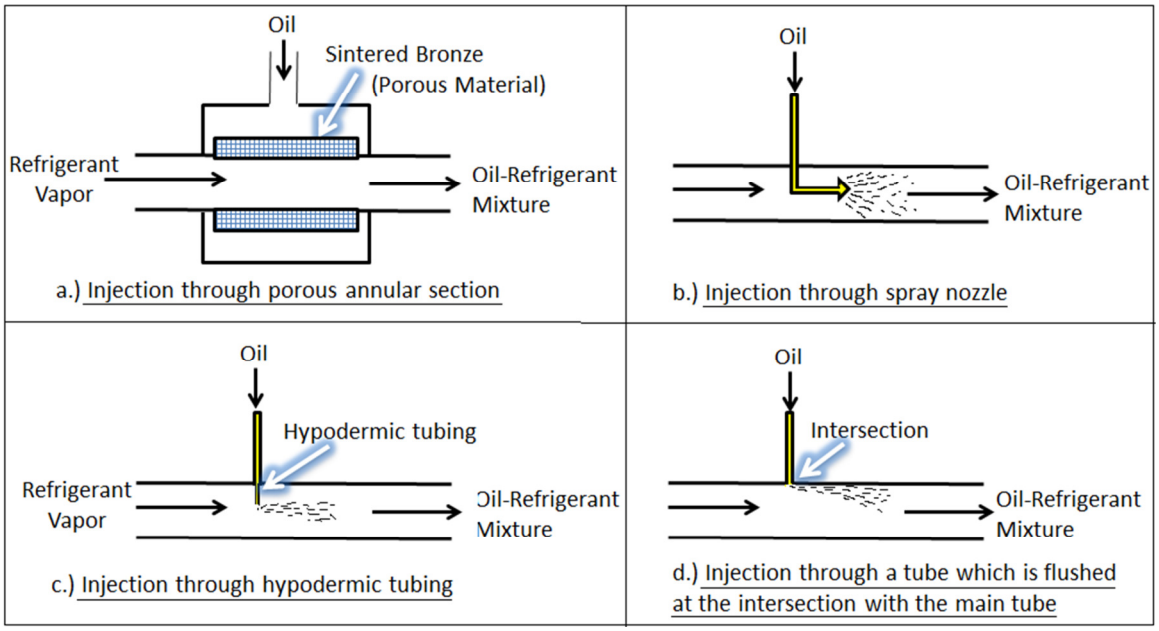

Figure 4: Oil injection methods; (a), (b), and (c) are described and used by Scheideman and Macken (1975), while (d) is used in the current work.

Sheth and Newell (2005) modified an R-22 standard window air conditioning unit, modifications were made to the unit so that the compressor discharge line, the condenser, the liquid line, the evaporator, and the suction line could be isolated using shut off valves to get the

oil holdup data in them. Once the stable operation was achieved, the compressor was shut off, and simultaneously all of the shut off valves were closed to trap the oil and refrigerant in their respective components. Each of the components was then removed from the loop and weighed to measure the oil and the refrigerant trapped. Sheth and Newell does not introduce oil from an external source while the system was operated and tested, instead relying on the oil that was already charged in the compressor. They also compared the experimental data with the void fraction model by Graham et al. (1999), which predicted mass quantities for refrigerant and oil in the tubes. The difference between experimental and predicted refrigerant mass quantities was within 20%; however, the experimental oil mass holdup data differed from the predicted data for the evaporator and the condenser. The large difference was attributed to the changes made in the tube circuitry and the geometry of the tubing, which consisted of 90 degree rises and bends after the condenser causing the holdup amount in the condenser to increase with the number of experiments performed. They suggested avoiding the use of sharp bends in the lines, which cause sudden changes in refrigerant velocities and can affect the holdup mass.

The oil retention in a smooth and 18° helical microfinned round copper tube having 3/8 in. (9.53 mm) O.D. was investigated by Crompton et al. (2004) at various mass flux, but at the same saturation temperature of 95°F (35°C). The refrigerant/oil pairs in the study were R-134a/POE, R-134a/PAG (where PAG is polyalkylene glycol), R-134a/AB (where AB is alkylbenzene), R-22/AB and R-410A/POE. The test rig consisted of a receiver tank sitting in a hot water bath; it received condensed oil-refrigerant mixture from the condenser placed after the test section. The energy from the hot water evaporated the refrigerant inside the tank and increased the system pressure. The liquid oil-refrigerant mixture from the bottom of the receiver tank was cooled in a heat exchanger and then pumped through the system loop at a controlled mass flow rate. To achieve the desired quality at the test section inlet, the pumped fluid was further heated in a special heat exchanger consisting of a long, flattened copper tube of serpentine

geometry, which was layered between aluminum plates and had electric strip heaters on the outside. This innovative configuration enhanced efficient heat transfer and prevented the heaters from burnout. The test section had an actual oil holdup section and a visualization section parallel to it. Once the steady state was achieved, the oil holdup test section was bypassed, then isolated with special ball valves at both ends, and the section was then detached from the main loop to measure the oil retained.

The method of maintaining the system pressure is the major difference between Crompton et al.'s (2004) system and the focused experimental system described in this report. The former used a heated receiver tank before the pump and an electric preheater before the test section to maintain desired pressure. The experimental facility described in this report uses an evaporator after the pump, the condition of the air at the microchannel heat exchanger, the temperatures at the oil reservoirs, and the valve positions of the pressure equalization lines to maintain the pressure inside the system. The information is discussed in detail in section 3.1.4 Pump-Boiler System and the Test Section.

Sundaresan and Radermacher (1996) use a residential 3-ton split heat pump to investigate the effect of miscibility on oil return by comparing R-407C/MO with R-407C/ POE and R-22/MO. R-22 shows partial miscibility with MO. The refrigerant HFC-407C was developed to replace R-22 in new or existing residential and commercial air-conditioners and heat pumps that had positive displacement compressors. The recommendation is to have a lubricant change to POE since the solubility and miscibility of R-407C in MO is much lower than in POE. The authors wanted to check the possibility of replacing costly POEs with less costly MO. Their system was operated without a crank case heater and an accumulator. The scroll compressor was installed with a graduated sight tube, which measured the level of liquid oil and refrigerant in the crank case while the tests were performed. The top of the sight tube was at the level of the suction inlet, and the bottom of the sight tube was at the lower level of the crank case. They performed a

"simulated oil pump out test" in which the oil was drained from the crank case and injected into the compressor discharge line. In a period of 30 minutes of operation, the oil was returned to the compressor for the tests with R-22/MO pair and the R-407C/POE pair, but the lost oil did not return in the test with R-407C/MO pair.

Whenever the refrigeration vapor travels vertically upward at a lower mass flow rate than the critical velocity, the lubricant-rich film flows downward along the surface of the pipe instead of being transported upward by the vapor refrigerant at the core. The flow visualization experiments were carried out on a vertical pipe with an 8 mm inside diameter by Mehendale and Radermacher (2000) to find the critical vapor flow rate of R-22, R-407C, and R-410A for preventing flow reversal in miscible POE lubricant and immiscible MO lubricant film, and also for two-phase refrigerant with immiscible lubricant. The experimental results for superheated refrigeration vapor flows when compared with the correlation by Jacobs et al. (1976) predicted lower critical mass flow rates then needed. Their parametric studies showed that the pipe's inside diameter has more dominating effect on the critical refrigerant mass flow rate, than the density of the vapor, the density of the film, or the viscosity of the film. The miscible oil did not separate from the liquid refrigerant in R-22/MO, R-410A/POE, and R-407C/POE while flowing upward in a pipe; thus, no oil film flow reversal was observed.

An oil injection-extraction method was developed by Lee (2003) to investigate the oil retention in each component of an air-conditioner vapor compression cycle system with carbon dioxide as a refrigerant. The test facility consisted of an oil loop and refrigeration loop, where the latter was a modified carbon dioxide automotive air-conditioning system. In this system, the compressor's rotational speed was altered to get the desired refrigerant mass flow rate. Centrifugal oil separators were installed on the compressor discharge line, which collected the oil from the compressor discharge and then sent it back to the compressor's suction. The test facility also made use of flow visualization sections to observe flow patterns of the oil-carbon dioxide

mixture, and check whether the oil extractor and the oil separators were working efficiently. The oil loop consisted of a helical oil separator to extract oil from the test section to the oil accumulator, a capacitance level sensor inside the oil accumulator to measure the extraction oil volume rate, a gear pump to inject the oil at the desired OCR from the oil reservoir, a Coriolis mass flow meter to measure the injected oil, and oil lines from the mass flow meter to the injection ports at desired locations on the test section (refer to Figure 5).

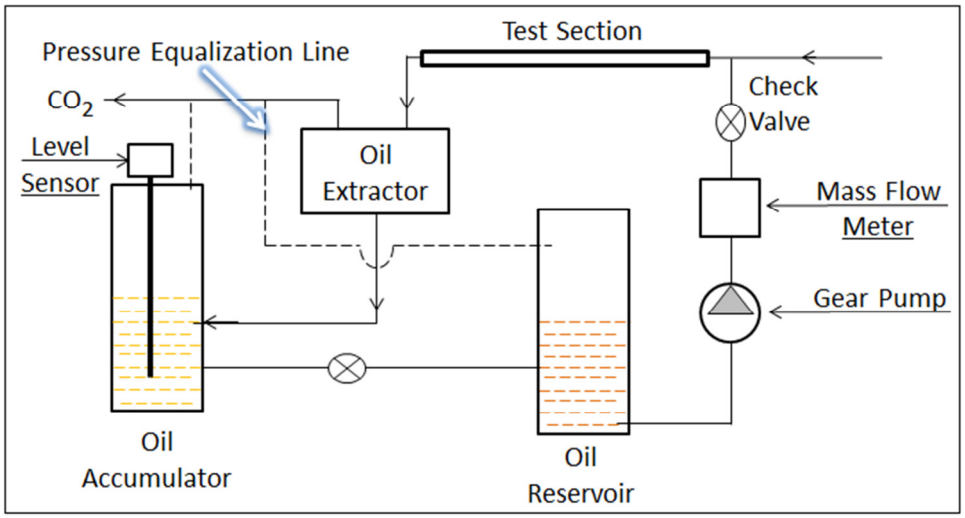

Figure 5: Schematic of the closed oil loop use by Lee (2003).

Lee's experiments showed that with increases in OCR, the oil volume retained in the heat exchanger and suction line increased, while a drop in the volume of oil retained with an increase in the refrigerant mass flux and a simultaneously drop in $PDPF$ (pressure drop penalty factor) were observed.

Cremaschi et al. (2005), using a setup similar to Lee's (2003), measured the oil retention in fin and tube evaporators and condensers in air conditioning and refrigeration systems. The refrigerants used were R22, R410A, and R134a in combination with mineral oil (MO), polyol ester (POE), and polyalkylene glycole (PAG), where the POE and PAG are synthetic lubricants. The effects of different refrigerant mass fluxes, solubility, and miscibility were experimentally investigated.

Zoellick and Hrnjak (2010) used a pump system instead of a vapor compression cycle system to investigate the oil retention and pressure drop in the horizontal and vertical suction lines. R-410A and R-22 were tested along with their respective miscible lubricants. In the pump system, the subcooled refrigerant and the cold oil were pumped by their respective gear pumps to a plate heat exchanger-evaporator. The refrigerant was vaporized and mixed with the oil in the evaporator to attain the necessary equilibrium, after which the mixture was supplied to transparent horizontal and vertical test sections for visual observations and pressure drop measurements. A helical liquid separator placed after the test section separated the vapor refrigerant and the liquid oil. The liquid oil was sent to the oil tank, while the vapor refrigerant was condensed and circulated in the system. The test sections were isolated during the steady state condition, then removed and weighed to measure the amount of oil retained.

The research and project work done by Cremaschi (2004), Cremaschi et al. (2004), and Cremaschi et al. (2005) formed the basis of the current research project. The system design and analysis procedure mentioned in these reference papers are used in this work. Initially the system was designed and constructed as a Vapor Compression Cycle System, but it was later changed to a Pump-Boiler System because of the difficulties faced with the former system in oil retention measurements.

CHAPTER III

III. EXPERIMENTAL METHODOLOGY

Section 3.1 Experimental Apparatus explains the construction of the experimental test setup and the position in the system of the various important components such as the microchannel heat exchanger, gear pumps, sub cooler, and evaporator. It gives a short description of the psychrometric chamber in which the microchannel heat exchanger is kept. The start and end positions of the test section are defined. The oil injection and extraction systems are also described in detail.

Section 3.2 Comparison between Vapor Compression Cycle System and Pump-Boiler System first explains the construction of the Vapor Compression Cycle System, then the difference between the two systems is clarified on a P-h diagram. It also describes the operational and oil management issues with the Vapor Compression Cycle System and the advantages of using the Pump-Boiler System in the oil retention experiments.

Section 3.3 Instrumentation and Errors gives the technical specifications and uncertainties of all the sensors used in the system. This section is followed by 3.4 Specification of the Components, which provides information about the suppliers or the manufacturers, model numbers, specifications, and descriptions of the components used either on the Pump-Boiler System or the Vapor Compression Cycle System.

Section 3.5 Dimensions of the Microchannel Heat Exchanger provides the dimensions which were actually measured and not provided by the manufacturer.

Section 3.6 Test Procedure explains all the steps involved to get the system into operating condition, inject the oil, extract the oil, and measure the parameters required for successful determination of the oil retained and its effect on heat transfer and pressure drop.

3.1 Experimental Apparatus

3.1.1 Air Conditioning Loop

A schematic cross-section of the Psychrometric Chamber and the positions of the various components and instrumentation used for the calculation of heat transferred and the pressure drop measurements are shown in Figure 6.

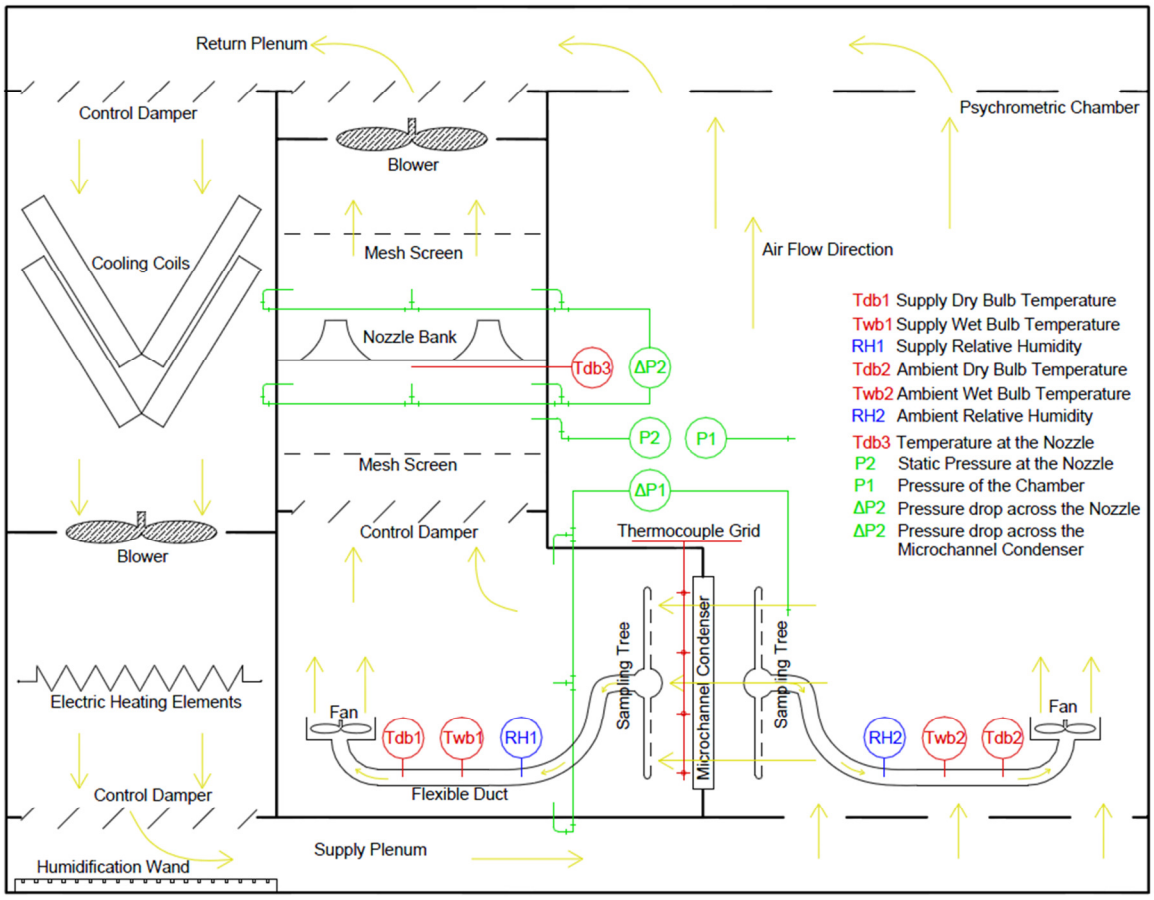

Figure 6: Air conditioning loop inside the psychrometric chamber.

The microchannel heat exchanger, which acts as the condenser in the Pump-Boiler System, has been installed inside the psychrometric chamber. The psychrometric chamber helps to control the condition of the air flowing across the microchannel heat exchanger by using its cooling coils, electric heaters, and humidification units. The design and specification of the Psychrometric Chamber can be found in the paper by Cremaschi and Lee (2008). The chamber has temperature, differential pressure, and relative humidity sensors for the air property measurements, while the nozzle bank on the air supply duct on the downstream side of the microchannel heat exchanger helps in the calculation of the air flow rates.

3.1.2 Microchannel Heat Exchanger – Position

The microchannel heat exchanger is placed inside the psychrometric chamber, while the remaining components in the test setup are installed outside the chamber. This section describes the position of the microchannel heat exchanger inside the chamber, the instrumentation, and the fluid lines to the microchannel heat exchanger using images for clarity and emphasis. Figure 7 shows the side of the microchannel heat exchanger exposed to the ambient air.

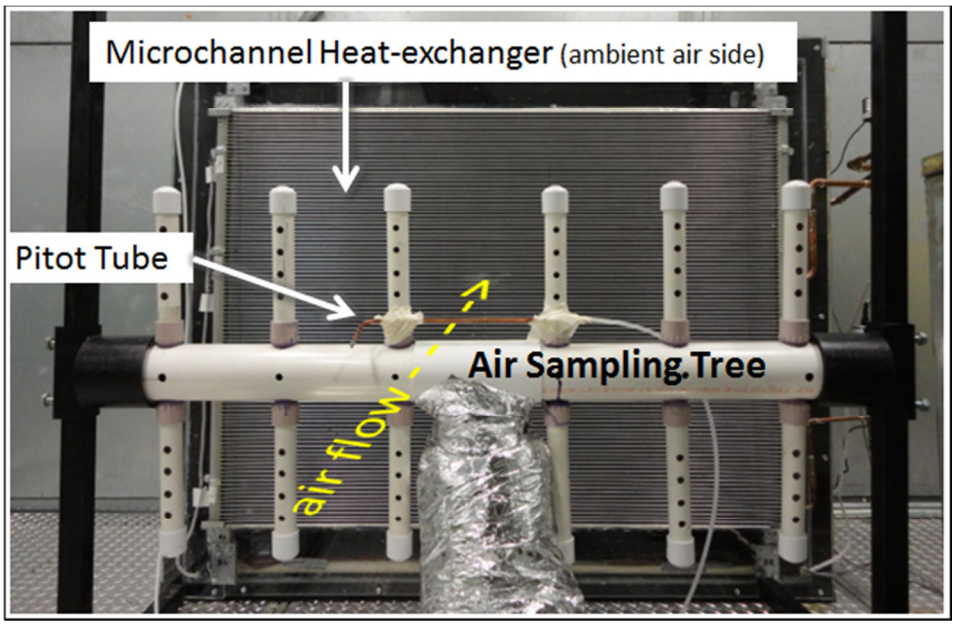

Figure 7: Side of the microchannel heat exchanger exposed to the ambient air.

The position of the microchannel heat exchanger in the duct (having a chamber approach) is such that it has the same face velocity of air over its entire slab. Figure 8 is the image, as seen from inside the duct, of the air supply side of the microchannel heat exchanger. Because of space limitation the oil, liquid, and vapor lines entered the chamber through its wall, travelled inside the air supply duct, and emerge from the inner left wall of the duct as seen in Figure 8, upon which they were connected to the microchannel heat exchanger's header. Figure 9 shows the fluid lines coming out of the duct on the air (ambient) side and connecting to the microchannel heat

exchanger. The connecting lines inside the air supply duct are insulated to prevent their thermal interference with the air supply.

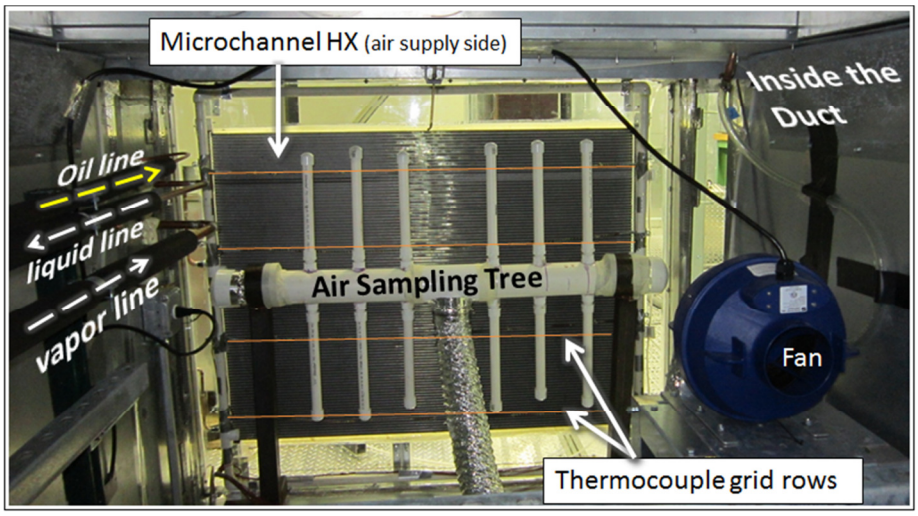

Figure 8: Side of the microchannel heat exchanger facing the air supply duct.

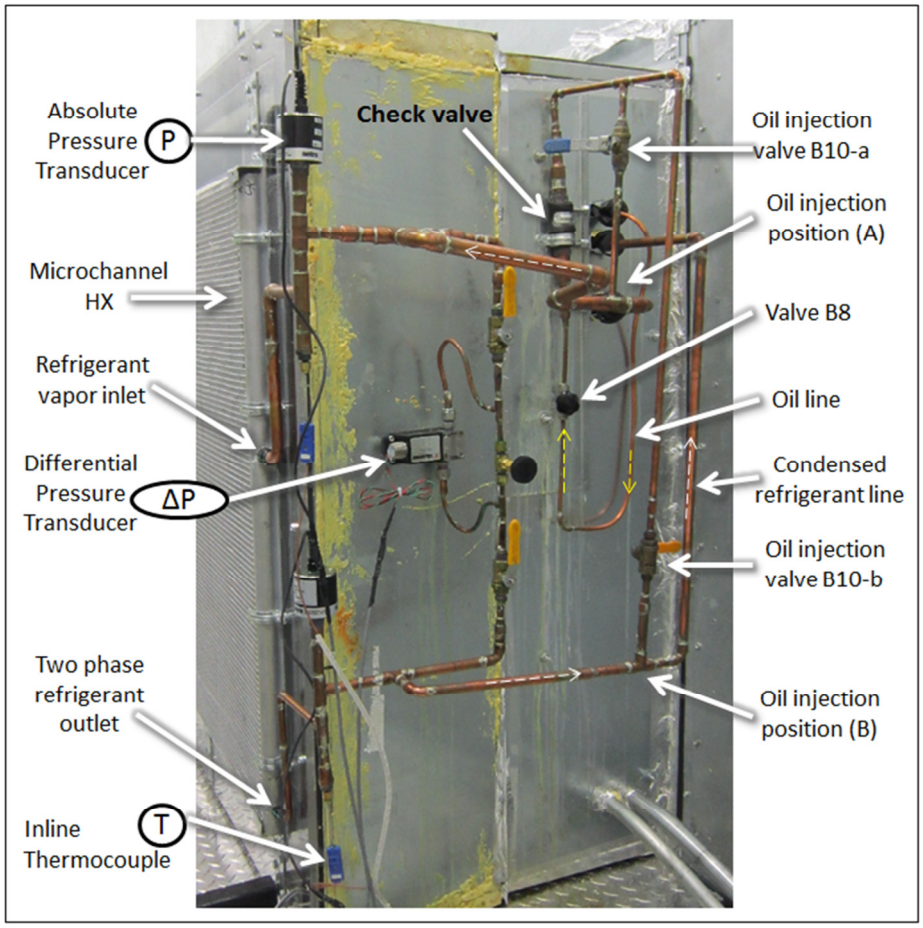

Figure 9: Instrumentation and configuration of refrigerant and oil lines connecting the microchannel heat exchanger.

A grid of 18 welded thermocouples was used on the air supply side and was placed 1 in. away from the microchannel heat exchanger slab. The grid has 4 horizontal rows; starting from the top each row has 4, 5, 5, and 4 thermocouples. Figure 9 also shows the position of the inline thermocouple and the pressure transducer on the refrigerant vapor supply line and the refrigerant liquid (or two-phase) return line. The differential pressure transducer connected between the supply and return lines measures the pressure drop inside the microchannel heat exchanger. In the event of excess pressure drop across the supply and return lines, the ball valves in series with the differential pressure transducer are closed to isolate the transducer. The differential pressure transducer can also be protected by opening the needle valve, which is parallel to it, causing the pressure on both the sides of the transducer's diaphragm to balance and prevent its failure.

3.1.3 Air Sampling Device

The sampling devices on the two sides of the microchannel heat exchanger, one exposed to the ambient air and the other on the side exposed to the supply air, were constructed according to ANSI/ASHRAE Standard 41.1 (ASHRAE 1986). The following section gives the description of the components of the sampling device and how they work.

The sampling trees shown in Figure 7 and Figure 8 were similar in construction. Each sampling tree was constructed of a horizontal 4 in. (10.16 cm) diameter PVC pipe, the ends were capped, and the center was connected to a flexible duct. The horizontal PVC pipe has 12 vertical branches made of 1.5 in. (3.81 cm) diameter PVC pipes. Holes drilled into the branches face the air flow. The construction of the tree helps to mechanically collect small samples of air (collected through these holes) over a large region, mix them in the central horizontal PVC pipe, and then transport the mixture further through the flexible duct.

Figure 10, an extension of Figure 8, shows that the flexible duct carries the sampled air from the sampling tree to the relative humidity measurement probe. Further, the sampled air gets carried through a long PVC pipe to the dry bulb and wet bulb temperature-measuring RTDs. The long PVC pipe assists in having a fully developed flow before the air reaches the temperature sensors. The wet bulb probe has its own water reservoir in which its wick is dipped. A separate tank (seen in the top left corner of Figure 10) supplies distilled water to this reservoir whenever the water level drops below a certain level.

In-line centrifugal fan/blower helps to overcome the pressure drop in the 4 in. diameter flexible duct and the long PVC pipe from the sampling tree to the dry and wet bulb RTDs, inducing a sufficient air flow velocity of around 1000 ft/min (around 5 m/s) over the temperature sensors. The in-line centrifugal fan/blower from Suncourt Inc. Centrax (Model #TF104-CRD 4") has a capacity to have a flow rate of 200 cfm at least resistance. The flow rate at the temperature

sensors is measured using a differential pressure transducer and a Pitot tube during the calibration phase. The blower then returns the sampled air back to the main airstream (on the downstream side of the sampling tree).

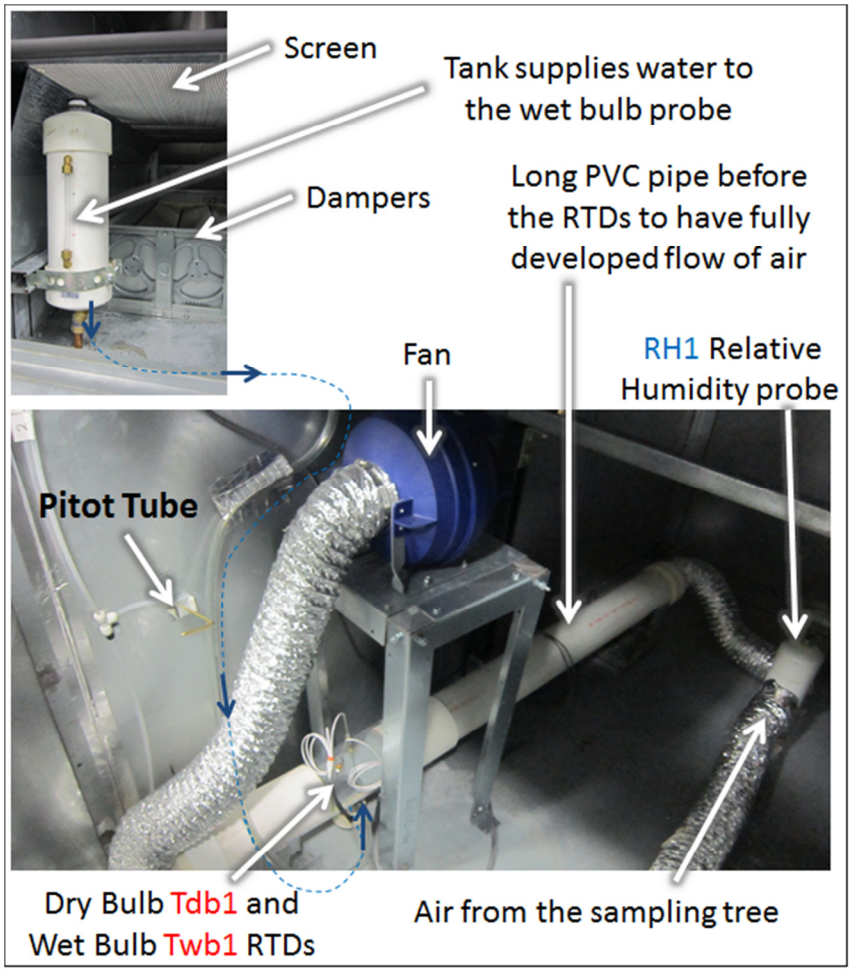

Figure 10: Instrumentation on the sampling device placed inside the air supply duct.

3.1.4 Pump-Boiler System and the Test Section

The schematic in Figure 11 and the actual image in Figure 12 show the positioning of the Pump-Boiler System components. Figure 13 presents the different states of the refrigerant on a *P-h* diagram, as the refrigerant flows through different components in the Pump-Boiler system. The microchannel heat exchanger-condenser is placed inside the psychrometric chamber, while the remaining components are placed outside the chamber. The following paragraph describes the working of the refrigerant circuit components in the direction of the fluid flow downstream from the microchannel heat exchanger.

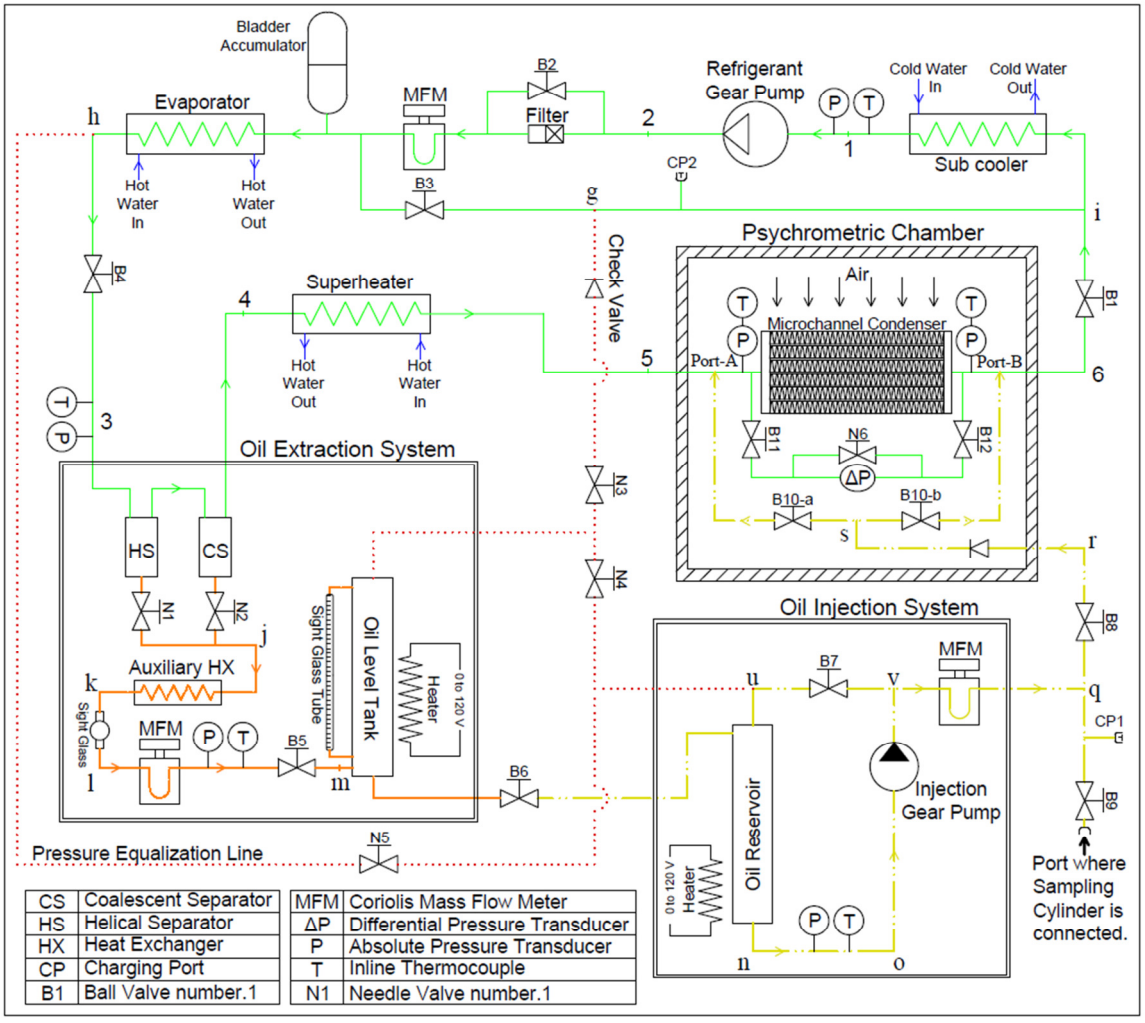

Figure 11: Schematic of the test facility with the Pump-Boiler System.

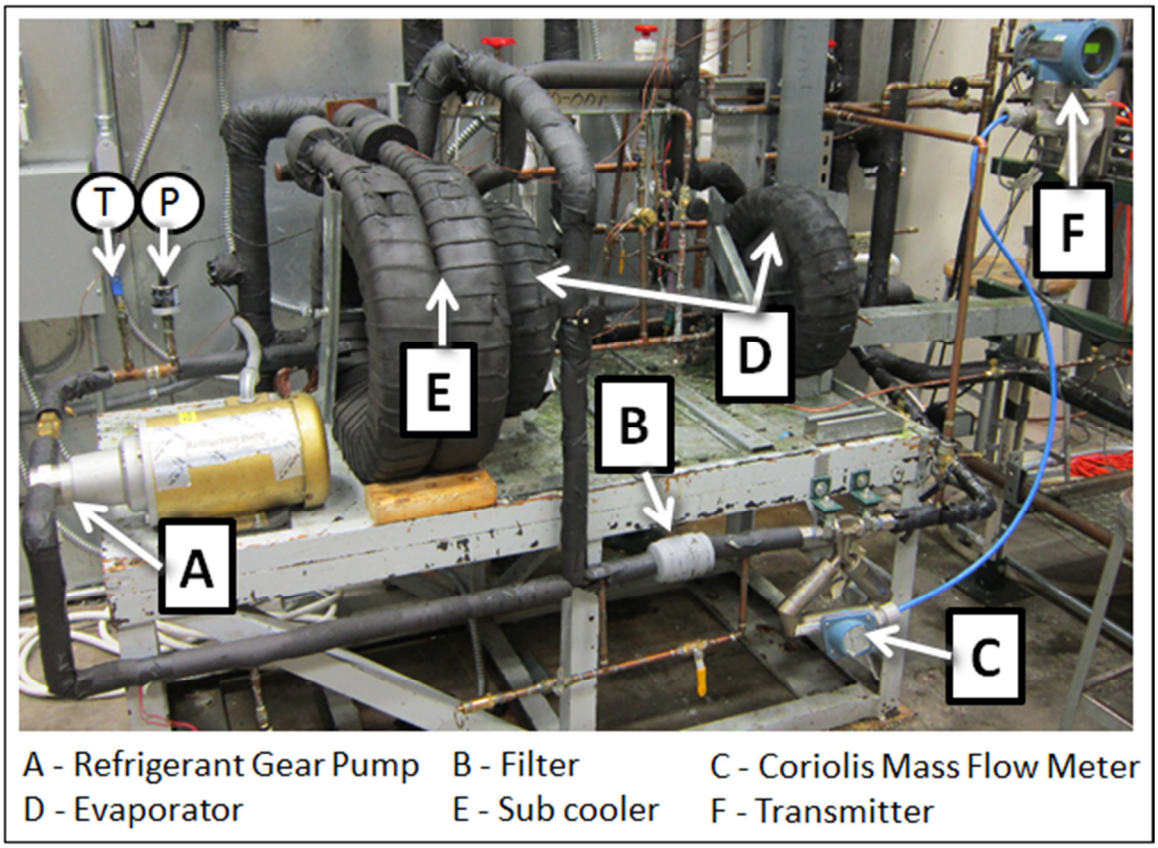

Figure 12: Setup of the Pump-Boiler System's components.

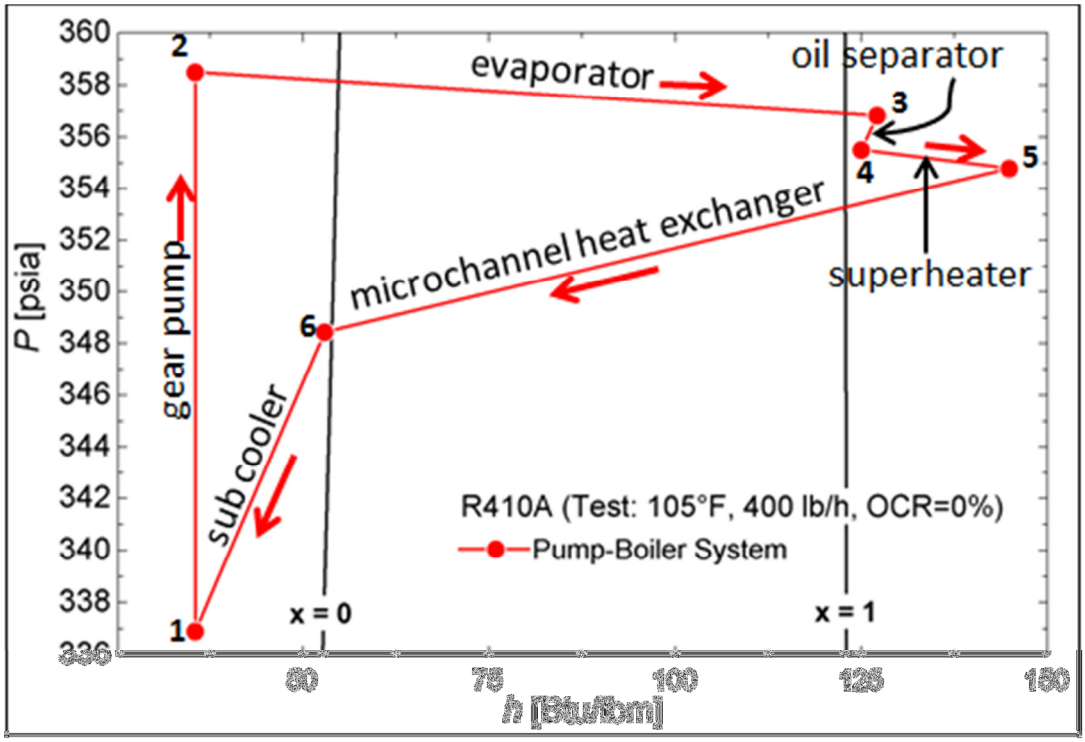

Figure 13: *P-h* diagram of the Pump-Boiler System.

In this section the start and end points of the test sections are defined. The hot water loop for the refrigerant superheater, the oil injection and extraction systems are discussed in detail in later sections.

The condensed refrigerant (or oil-refrigerant mixture) from the microchannel heat exchanger (state 6 in Figure 13) is transported to the secondary condenser or sub cooler (component E in Figure 12). This sub cooler is a coaxial water-to-refrigerant heat exchanger, and it ensures that all fluid entering the refrigerant gear pump is in a liquid phase (state 1 in Figure 13). The mass flow rates through the microchannel heat exchanger can be easily controlled by changing the rotational speed of the refrigerant gear pump (component A in Figure 12) and thus its volumetric discharge.

The refrigeration gear pump by Micropump [Model #GC-M25.JVS] can supply fluid at a rate of 0.48 gallon per 1000 revolutions (1.82 ml/rev) at a maximum differential pressure of 125 psi (862 kPa). The pump's rotational speed depends upon the frequency of the alternating voltage supplied to it by the Variable Frequency Drive (VFD). The VFD is manufactured by Baldor Electric Company [Model #VS1SP21-1B]. The VFD requires a 3 phase input of 230 V at 60 Hz, and is configured for the motor of the gear pump. The electric motor of the gear pump is of 1 hp and can rotate at 3450 rpm; the motor is manufactured by Baldor.Reliance Super-E motors [Model #CEM3545].

Refrigerant filter-dryer (component B in Figure 12) is placed after the refrigerant gear pump to removes any moisture, dirt, acid, and sludge from the liquid refrigerant. The filter-dryer is manufacturer by Parker Hannifin Corp. Sporlan Division [C-083-S-HH 3/8]. The mass flow rate of the liquid refrigerant (or oil-refrigerant mixture) transferred by the refrigerant gear pump is measured accurately using the Coriolis mass flow meter (component C in Figure 12). The Coriolis mass flow meter is manufactured by Micro Motion Inc. [CMF025], its specifications and

uncertainty are discussed in details in later section on Instrumentation. The liquid refrigerant or oil-refrigerant mixture (at state 2 in Figure 13) is then vaporized/boiled inside two parallel evaporators (component D in Figure 12). These evaporators are also coaxial water-to-refrigerant heat exchangers. The vaporization of the refrigerant with the help of hot water increases the system pressure.

The helical separator and coalescent separator are placed in series after the evaporator to prevent the entrained oil droplets in the refrigerant vapor (at state 3 in Figure 13) from flowing to the test section. The helical separator is manufactured by Henry Technologies Inc. [Model #S-5188] and is designed for a flow rate requirement of 10 cfm for 10 tons of refrigeration capacity. The coalescent separator is manufactured by Temprite [Model #925R] and can separates up to 0.05 microns particles. Both the separators were selected with no internal float valves, the presence of the float valves in the early separators caused problems like sticking of the internal valves and pulsating oil flow at its drain. These separators are also the main components of the oil extraction system, which extracts the oil during the actual tests.

The vapor refrigerant from the separators (at state 4 in Figure 13) is further heated in the superheater before being supplied to the test section (at state 5 in Figure 13). The test section includes the microchannel heat exchanger, sub cooler, refrigerant gear pump, filter, mass flow meter, evaporator and all the fluid lines before the separator, the test section circuit in Figure 11 is (Port-A)-(Port-B)-6-i-1-2-h-3.

Figure 11 also shows the positions of the pressure transducers and the inline thermocouples on the lines that help monitor the system while operating it. The charging ports are used to charge and recover the refrigerant from the system.

Figure 14 shows the hot water loop for the refrigerant superheater. The superheater loop consists of a centrifugal water pump (component A in Figure 14), an inline water heater

(component B in Figure 14), a superheater (plate heat exchanger) (component D in Figure 14), in a closed loop. This loop also has an expansion tank (component C in Figure 14), and safety devices: safety valve (component E in Figure 14) and flow switch (component F in Figure 14).

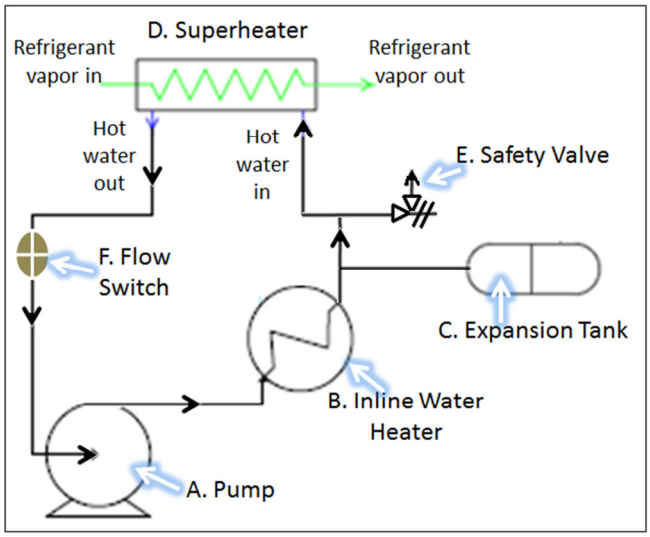

Figure 14: Hot water loop for the refrigerant superheater.

The superheater (plate heat exchanger) transfers the energy from the hot water to the vapor refrigerant to achieve necessary superheat before it enters the microchannel heat exchanger. The plate heat exchanger used, model GB400L-14, is manufactured by GEA, it has a total of 14 plates with heat transfer area of 16 ft^2. The centrifugal water pump, model: 1400 – 50 –A, is manufactured by Taco and operates at 3450 rpm. It pumps the water at a minimum of 1.5 gpm through the inline water heater to prevent the burnout of the heating element. The inline heater used, model: NWHSRG 06-024P-E1, is manufactured by Chromalox and has a heating capacity of 2 KW. This being a closed loop requires an expansion tank, model: HFT- 15, and is manufactured by Bell and Gosset.

A 1 gallon capacity bladder accumulator from McMaster-Carr [59595K12] is installed after the refrigerant gear pump, which helped stabilize the mass flow rate of the refrigerant in the system. Plot (a) of Figure 15 shows that the refrigerant mass flow rate kept on rising during the

injection test in the absence of the accumulator; the use of the accumulator helped to attain a constant mass flow rate, as shown in Plot (b) of Figure 15.

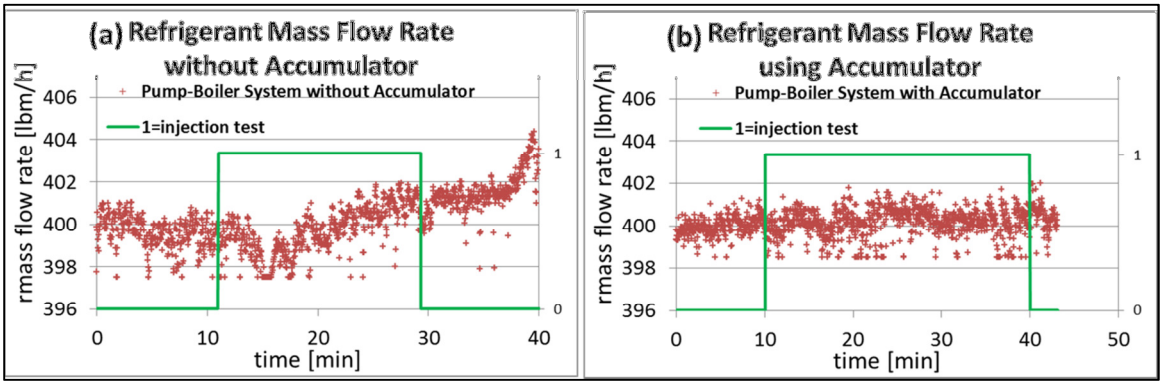

Figure 15: Stabalization of the refrigerant mass flow rate by the use of an accumulator during the injection test.

3.1.5 Oil Injection System

The oil used for the experimentation is Emkarate™ RL 32-3MAF, which is an ISO VG 32 grade Mixed-Acid Polyol Ester (POE) lubricant/oil. The following section describes the components used for controlled oil injection into the test section. Refer to the schematic from Figure 11 and the image in Figure 16 for this section. The oil reservoir, injection Coriolis mass flow meter, injection gear pump, electric heaters, pressure equalization line, and fluid lines with valves are the components of the entire oil injection system.

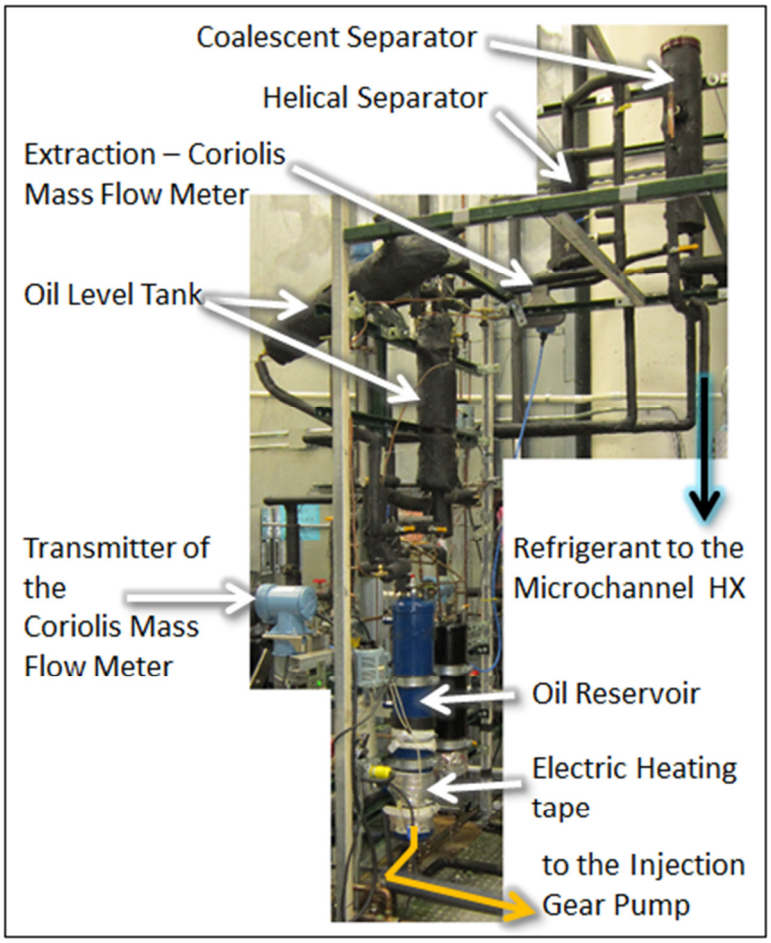

Figure 16: Components of the oil extraction and injection systems.

The oil reservoir from Emerson Climate Technologies [Model #AOR-4], which holds the injected oil-refrigerant mixture (the oil and the refrigerant soluble in it) has a capacity of 4 gallons

(15.1 L). Before the injection test, the temperature and pressure of this tank were maintained at a constant by using an electric heater tape and pressure from the pressure equalization line.

The electric heater tape, from OMEGA Engineering Inc. [Model #FWH171-060], has maximum input of 120 V, for usage of 624 W, with heating capacity of 5.2 W/in^2. The voltage supply to the heater tapes is from a variable transformer, manufactured by Superior Electric [Model #3PN116C], which helps in controlling the heat generated by the heater tape. The opening of valve N5 over the pressure equalization line determines the rate at which the refrigerant vapor enters the oil reservoir from the system, and the opening of this needle valve is kept so small that the rate of flow of the vapor refrigerant to the oil reservoir is negligible. (Refer to Figure 11 for the pressure equalization circuit between nodes u and h.)

The injection gear pump continuously circulated the oil in the 2.5 ft (0.88 m) tall oil reservoir to help mix it and prevent any stratification. In Figure 11 the circulation circuit is v-u-n-o, during the injection test the circulation is stopped by closing ball valve B7, and the injection to the test section is started by opening ball valve B8. The injection mixture follows either the circuit n-o-v-q-r-s-(port-A) or the circuit n-o-v-q-r-s-(port-B), depending upon the opening and closing of valves B10-a and B10-b.

The circulation during the injection test is stopped because the same injection gear pump is used to inject the oil-refrigerant mixture from the bottom of the oil reservoir to the test section. The Coriolis mass flow meter placed after the injection gear pump measured the flow rate of the injected oil-refrigerant mixture to the test section. The Coriolis mass flow meter, injection gear pump, gear pump motor, and the VFD used on the oil injection system are similar to the ones described in the previous section.

A metered amount of this oil is then injected either upstream at position/port-A or downstream at position/port-B of the microchannel heat exchanger/condenser using appropriate

valves (B10-a) and (B10-b), respectively (Figure 11). The check valve (from McMaster-Carr, [Model #7768K14]) installed on the oil injection line prevents any back flow of the oil/refrigerant from the system to the oil reservoir. (Refer to Figure 11 for check valve between nodes r and s.)

The oil injection port consists of a small diameter copper tube connected perpendicular to the refrigerant lines of the test section at port-A and port-B. The intersecting copper tube is nearly flush with the inside surface of the main refrigerant line (Figure 17) at the injection ports. The injected oil is carried with the high velocity refrigerant at the intersection. Injection port-A is around 2.5 ft. (0.76 m) before the first pressure tap to ensure that a fully developed flow is achieved and the pressure measurement remains independent of the method of oil injection. The section between injection port-A and the microchannel heat exchanger's inlet has a total of eight sharp elbows, shown in Figure 9. This configuration helps to mix the refrigerant vapor and the oil before the mixture enters the heat exchanger.

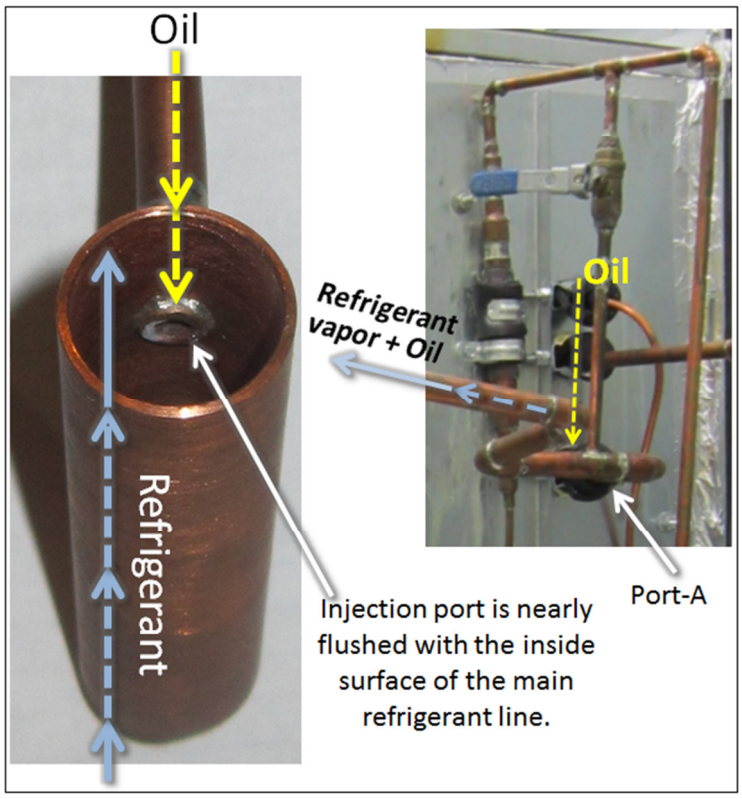

Figure 17: Oil injection method at the inlet of the microchannel heat exchanger.

3.1.6 Oil Extraction System

The helical and coalescent separators, extraction Coriolis mass flow meter, auxiliary heat exchanger, oil level tank, electric heaters, pressure equalization line, and check valve form the main components of the oil extraction system. The schematic in Figure 11 and the image in Figure 16 should be referred to for this section. This section explains why the components are necessary and how they work.

The refrigerant vapor escapes from the helical and coalescent separators' oil outlet (oil drain) to the oil level tank during the pre-injection test, during the injection test the refrigerant vapor escapes along with the extracted oil-rich fluid at the oil outlet. The separators cannot prevent the escape of the vapor refrigerant because of the absence of an internal float valve. The helical and coalescent separators are not 100% efficient in separating the entrained oil in the vapor refrigerant, but the vapor refrigerant going to the test section from the separators has a negligible amount of entrained oil. A sample extracted after the separators for testing the amount of oil in the refrigerant showed that these separators in series have very high efficiency, about 99.9% based on the ASHRAE sampling method.

The Coriolis mass flow meter placed on the oil outlet/extraction line of the separators does not work well if it has a slug flow flowing through it; the slug flow will be present because of the mixture of the escaped vapor refrigerant and the extracted oil-rich liquid. The auxiliary heat exchanger condenses the escaped vapor refrigerant during the pre-injection and injection test (refer the Oil Extraction System schematic in Figure 11), so the Coriolis mass flow meter always has the liquid phase flowing through it. The auxiliary heat exchanger is not used if a single (liquid) phase is flowing through the Coriolis mass flow meter. The auxiliary heat exchanger is a tube in tube, double pass, water to refrigerant (with oil and refrigerant flowing through the inner

tube) heat exchanger, has an overall length of 1 ft., and it is constructed in the lab using copper tubes.

A small sight glass [from McMaster-Carr, Model #1138K64], with 1.5 in. length of viewing glass, is installed after the auxiliary heat exchanger and before the Coriolis mass flow meter. (Refer to Figure 11 for the sight glass placed between nodes k and l, and refer to Figure 32 for the actual image of the extracted oil in the sight glass.) The sight glass is used to monitor the flow (either slug due to two-phase flow or single-phase flow) to the Coriolis mass flow meter, it also helps to note the time of oil extraction from the oil separators. Similar sight glass is also installed before the refrigerant gear pump to confirm that liquid refrigerant enters the refrigerant gear pump (not shown in Figure 11).

The oil and the escaped refrigerant further travels to the oil level tank from the Coriolis mass flow meter. The oil level tank actually is not a single tank but is made up of two steel cylinders and a copper tube in parallel. Both the steel cylinders have a volume of 1 gallon, and are manufactured by Swagelok, Model [#304L-HDF8-1GAL]. Two sight glass tubes from McMaster-Carr [Model # 1106K76] , with 18 in. length of viewing glass, are installed in parallel at different elevations over the copper tube of the oil level tank set up, which is graduated and calibrated to measure the volume of fluid extracted in the oil level tank set up. Figure 65 (refer to Appendix A, page no.156) shows the detailed schematic of the oil level tank system. One steel cylinder is vertical and the other is tilted; this orientation helps the mixture level to rise at a faster rate in the lower section of the oil level tank system, and as the mixture starts filling the tilted tank, the rate of rise decreases.

A large amount of charge is removed from the system when the escaped refrigerant (from the separators) is transferred to the oil level tank. To have a steady state operation, it is necessary to send the now liquid refrigerant in the oil level tank back to the system; if not done, the system

pressure and the mass flow rate in the test section will keep on dropping as the system's refrigerant charge is reduced. The problem is solved by vaporizing the refrigerant inside the oil level tank using an electric heater and sending it back to the system through the pressure equalization line. This pressure equalization line is connected back to the system at node g (Refer to Figure 11 for node g); the pressure at node g is lower than it is at the oil level tank, which is near the inlet of the sub cooler. The check valve [from McMaster-Carr, Model #7775K12] was over the pressure equalization line prevents any back flow of the vapors from the system to the oil level tank. Figure 18 shows the mass balance over the oil level tank, the amount of oil-refrigerant mixture going in, storage of the mixture, and the refrigerant vapors coming out during a steady state injection test.

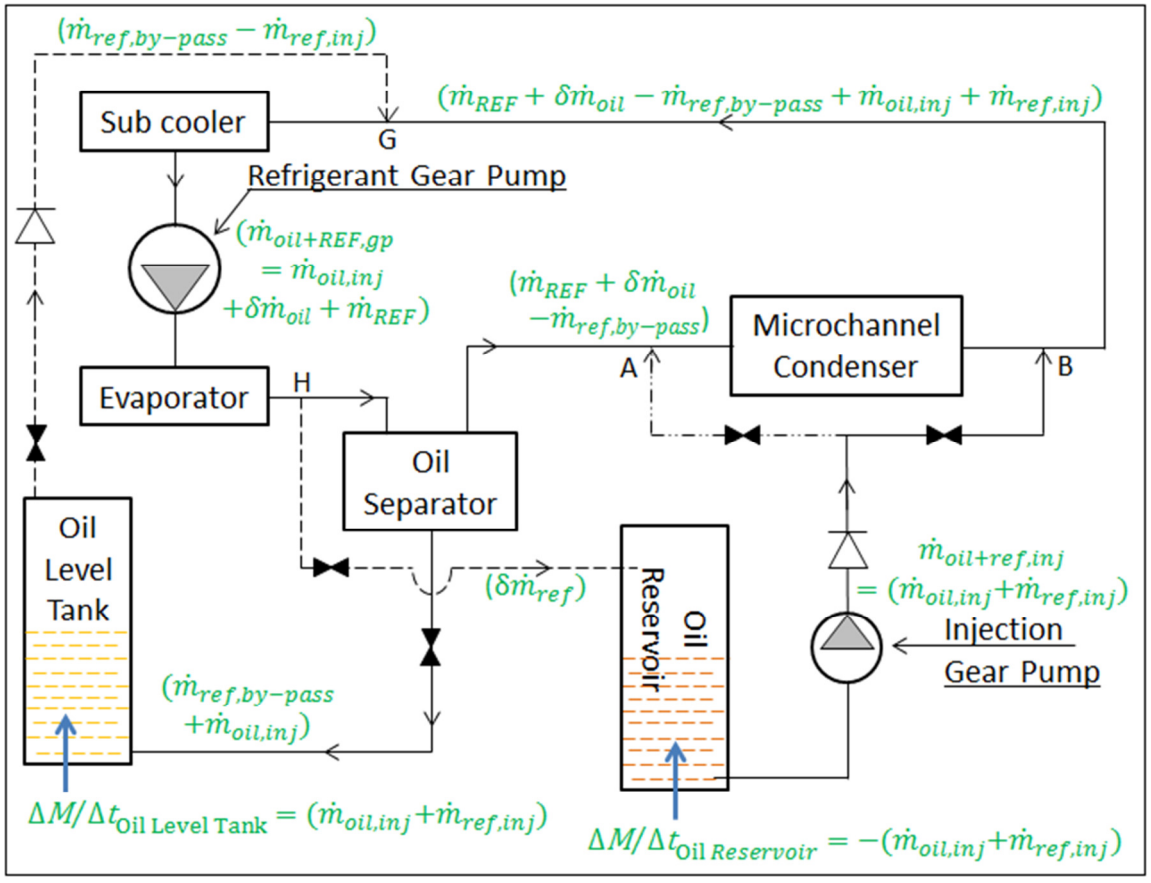

Figure 18: Mass balance on the Pump-Boiler System components.

3.1.7 Fluid Transportation Lines

Copper and copper alloy tubes were used to construct the fluid transportation lines in the test setup. These hard drawn or annealed (soft) tempered tubes were connected to the refrigeration system components by either threaded, flared, compression or soldered joints. The soldered/sweated joints were preferred over brazed joints, as they could be easily disconnected when needed for system modification. According to ASME Standard B31.9 (ASME 1996), the tin 95% - antimony 5% soldered joints are rated for internal working pressure of 500 psi (34.4 bar) at 100°F (37.7°C) and 200 psi (13.8 bar) at 250°F (121.1°C) when used for copper tubes of less than 1 in. nominal size. The copper tubes used in actual refrigeration services such as air-conditioning and refrigeration units should be according to ASTM Standard B280 (ASTM 1997). The test setup violated this ASTM standard by using copper tubes specified for water supply service at a few places; their use is defended by the fact that these copper tubes were sufficient to handle the vibration, pressures, and temperatures encountered during the controlled experiments.

The oil was injected at port-A through a copper tube of 1/8 size [0.2 in. (5 mm) I.D.] into a copper tube of 5/8 size [0.66 in. (16.7 mm) I.D.] carrying the vapor refrigerant, or the oil was injected at port-B through a copper tube of 3/8 size into a copper tube of 3/8 size [0.43 in. (10.9 mm) I.D.] carrying either two-phase or subcooled refrigerant. Similar copper tube dimensions were used elsewhere in the system during the construction of the fluid lines. Special care was taken while designing the fluid lines, so that the dimension and the orientation of the copper tubes and fittings avoided any pressure drops or liquid traps in the lines. Larger tube diameters (5/8 size) were preferred for refrigerant vapor flow, while smaller tube diameters (3/8 size) were preferred for liquid refrigerant flow. The oil lines and the pressure equalization lines were always of 1/8 size.

The check valves, ball valves, gate valves, PVC pipes, copper pipes and tubes, and fittings used in the refrigeration system and the hydronic system (water side of the sub cooler, auxiliary heat exchanger and the evaporators) were ordered from Grainger Inc., Lowe's, McMaster-Carr, Locke Supply Co., and United Refrigeration Inc. The needle valves used on the pressure equalization lines and the oil injection line were from Parker Hannifin Corp. [Model #4A-V4LR-B and #6A-V6LR-B], these needle valves required around 5 turns to open completely, which allowed in having a control over the flow rates of the fluid flowing through them.

3.2 Comparison between Vapor Compression Cycle System and Pump-Boiler System

The following section explains the use of the Vapor Compression Cycle System instead of the Pump-Boiler System for measurements of oil retention effects on the microchannel heat exchanger. This section also shows how the operation of the Pump-Boiler System is different from that of the Vapor Compression Cycle System, and the disadvantages of the use of the Vapor Compression Cycle System in the oil retention studies.

3.2.1 Vapor Compression Cycle System

The following section explains the construction of the Vapor Compression Cycle System. The differences in operation between the Pump-Boiler System and the Vapor Compression Cycle System are also presented in *P-h* diagrams.

The schematic of the test facility utilizing a single speed scroll compressor is shown in Figure 19. The R410A scroll compressor (1), manufactured by Copeland [Model #ZF15K4E-PFV] was charged with Emkarate™ RL 32-3MAF, which is an ISO VG 32 grade Mixed-Acid Polyol Ester (POE) lubricant. The secondary condenser (3) was placed in parallel with the microchannel heat exchanger. The metering valves (9-a) and (9-b) enable different mass flow rates through the microchannel heat exchanger-condenser by directing some flow through the secondary condenser. The pressure transducers and inline thermocouples monitor the refrigerant conditions, a differential pressure transducer measures change in the pressure drop across the microchannel heat exchanger during the process of oil retention. The liquid refrigerant from both the condensers then expands in one expansion valve (8) before going to the evaporator (7). The refrigerant oil separator (2) was used at the discharge of the compressor to prevent the entrained oil droplets in the refrigerant from leaving the compressor and flowing to the test section. A metered amount of oil can either be injected upstream (port-A) or downstream (port-B) of the microchannel heat exchanger using appropriate valves (10-a) and (10-b). The oil extraction device/system extracts the oil from the vapor refrigerant for measurement in the oil level tank

using the helical and coalescent separators. The volume of oil extracted by the oil extraction device into its measurement tank was then measured using the calibrated sight glass tube and capacitance probe sensor.

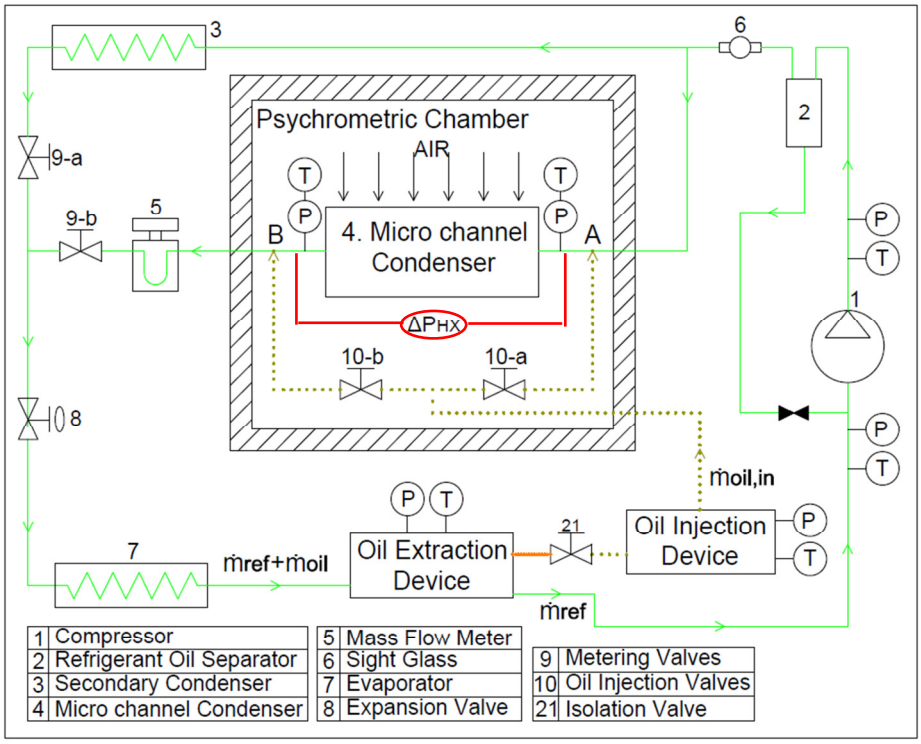

Figure 19: Schematic of the test facility with the Vapor Compression Cycle System.

Figure 20 shows the *P-h* diagram of a sample test with $OCR = 0\%$ (no oil in the test section). The same test was performed in the Pump-Boiler System using a gear pump as well as in the Vapor Compression Cycle System using a scroll compressor. For the test with the Pump-Boiler System, the difference between the maximum and minimum pressures observed was 22 psi (152 kPa), while for the test done with the Vapor Compressor Cycle Systems, a difference of 235 psi (1620.3 kPa) was observed. The expansion valve is absent in the Pump-Boiler System and the fluid experiences only major and minor losses in the tubes, fittings, and components; hence the system operates within a small pressure difference. However, the fluid in the Vapor Compressor Cycle System experiences a large pressure drop in the expansion valve in addition to the minor and major losses.

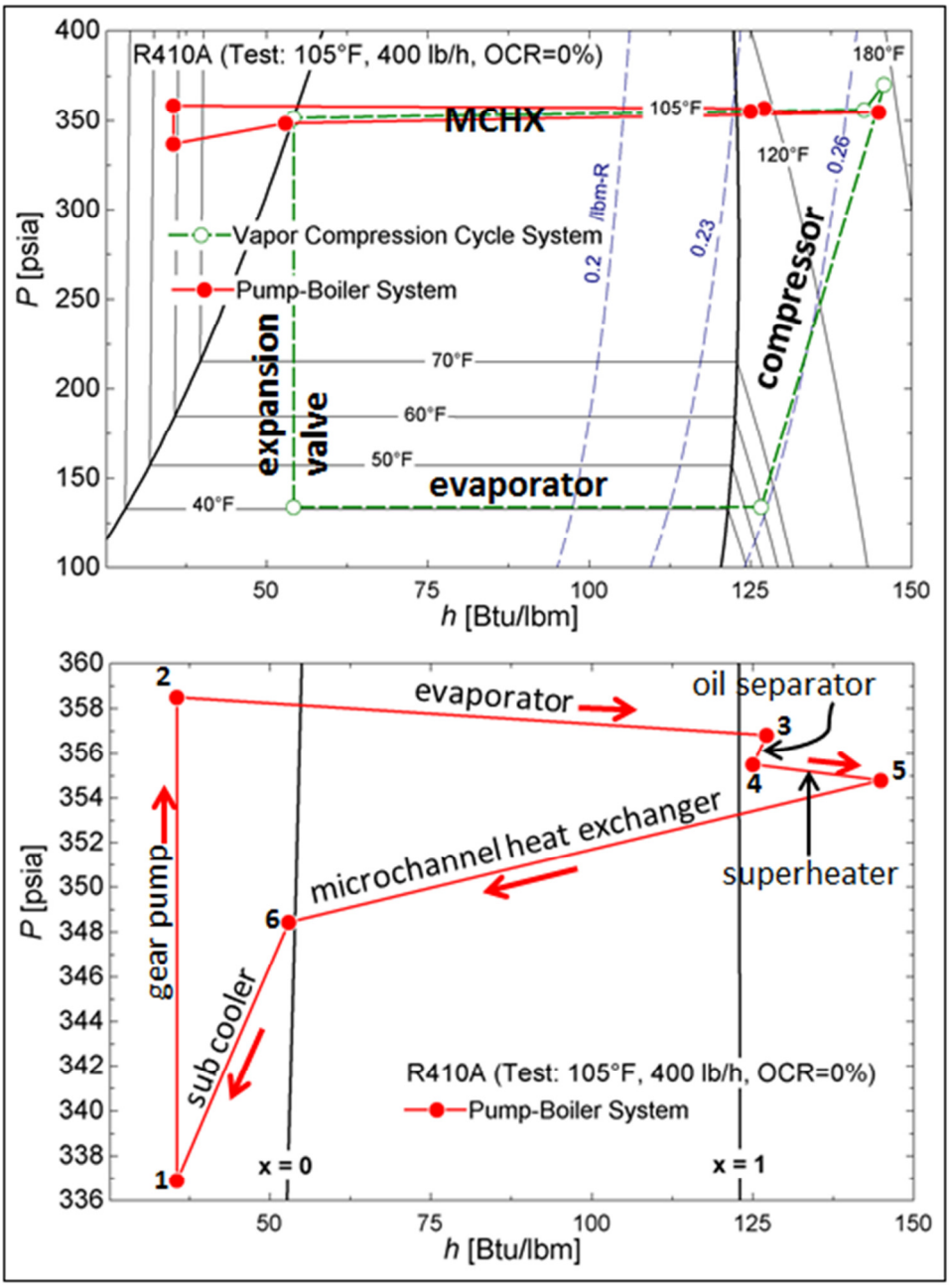

Figure 20: P-h diagram of Pump-Boiler System and Vapor Compression Cycle System.

Initially the system was designed and constructed as a Vapor Compression Cycle System. It was later changed to a Pump-Boiler System because of the difficulties while testing and operating with the compressor, causing its failure. More details about the failure of the scroll compressors are given in later sections.

3.2.1 Oil Management

The following section explains the flow of oil in various components of the system using schematics showing the mass flow rates. This section also presents the problems faced during the oil management in the Vapor Compression Cycle System and the advantages of using the Pump-Boiler System to overcome these problems.

Figure 18 shows the mass flow rates in various circuits of the Pump-Boiler System. It can be observed that once the steady state condition is achieved during the injection test a fractional amount of oil $\delta\dot{m}_{oil}$ cannot be extracted by the oil separator (consisting of helical and coalescent separators in series), as their extraction efficiencies are less than 100%. The oil that is not extracted flows to the test section and returns back to the oil separators at a constant mass flow rate of $\delta\dot{m}_{oil}$. The mass balance shows that the injected mass flow rate of pure oil $\dot{m}_{oil,inj}$ from the oil reservoir into the test section is equal to the mass flow rate of pure oil extracted at the oil level tank by the oil separator. Also, the rate at which the oil-refrigerant mixture is lost from the oil reservoir is equal to the rate at which the oil-refrigerant mixture is collected in the oil level tank, and is given by $\Delta M/\Delta t_{\text{Oil Level Tank}} = -\Delta M/\Delta t_{\text{Oil Reservoir}} = (\dot{m}_{oil,inj} + \dot{m}_{ref,inj})$.

Figure 21 shows the mass flow rates in various circuits of the Vapor Compression Cycle System. In the Vapor Compression Cycle System there are two main circuits within which the oil is circulating. One circuit for the flow of oil is through the test section; the test section circuit consists of the port for oil injection (port-A or port-B), the microchannel heat exchanger, the expansion valve, the evaporator, and the oil separator 2 of the oil extraction device. The oil is injected at the injection port from the oil reservoir using an oil injection gear pump at a mass flow rate of $\dot{m}_{oil+ref,inj}$. Some of the oil is retained in the microchannel condenser and the evaporator; the un-retained oil is then extracted at the oil separator 2 (coalescent oil separator) and transferred to the oil level tank. In the process of oil extraction, the oil separator 2 due to the minor

inefficiency does not extract $(\delta\dot{m}_{oil,1} + \delta\dot{m}_{oil,2})$ amount of oil. Along with the oil retention inside the test section, the other place where the oil is retained is the accumulator on the suction line of the compressor. The other main oil flow circuit consists of a compressor and a discharge oil separator (oil separator 1) operating in a loop. In this loop the unknown amount of oil lost by the scroll compressor, $\dot{m}_{oil,1}$, along with the discharged refrigerant is separated by the discharge oil separator (consisting of helical and coalescent oil separators in series). In the process of oil extraction, the discharge oil separator 1 losses a fractional amount of oil $\delta\dot{m}_{oil,1}$ to the system, as its extraction efficiency is less than 100%. Thus, the compressor acts as an oil source that introduces $\delta\dot{m}_{oil,1}$ amount of oil flow into the test section.

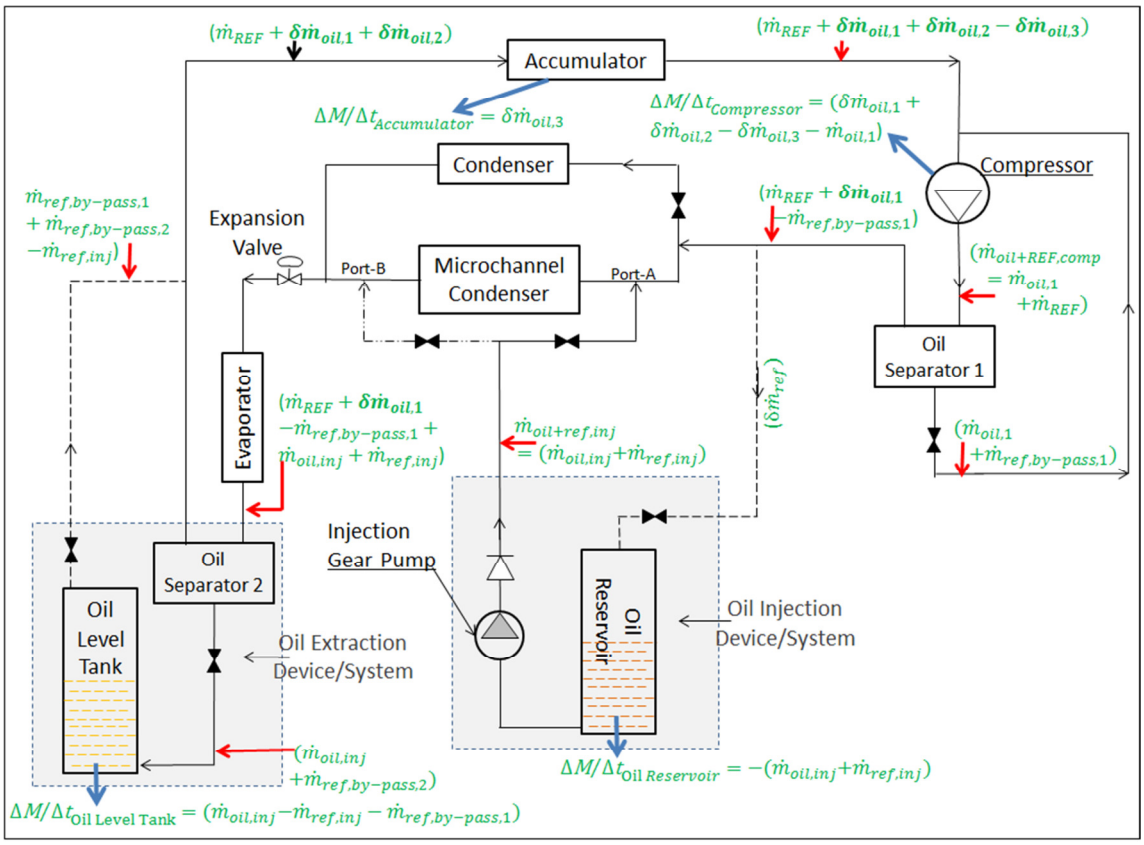

Figure 21: Mass balance on the Vapor Compression Cycle system components.

In the Vapor Compression Cycle System, the presence of the two oil sources (the compressor and the oil reservoir) in the oil flow circuits and the oil separators' having efficiencies

less than 100% make it difficult to keep tract of the amount of pure oil introduced into the test section. A wrong estimation of the oil flow rate in the microchannel heat exchanger introduces error in the calculation of the OCR.

In the Pump-Boiler System, the gear pump does not introduce any oil into the system and the only source for oil introduction is the oil reservoir. The oil is extracted at only one point using the oil separator placed at the end of the test section. In this system it is possible to estimate the amount of oil not extracted by the oil separator, and thus to have a correct measurement of the oil flow through the different components.

3.2.1 Operational Issues with the Vapor Compression System

The Vapor Compresssion Cycle System operated on a single speed scroll compressor. The opening of the metering valves (9-a) and (9-b) facilitates different mass flow rates through the microchannel heat exchanger-condenser by directing some flow through the secondary condenser, refer to Figure 19. Figure 22 shows the comparison of refrigerant mass flow rates, where large fluctuations are seen in the flow rate in the Vapor Compression Cycle System and not in the Pump-Boiler System.

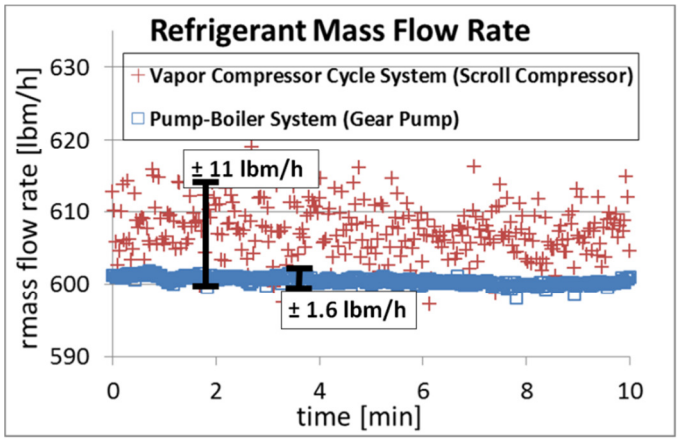

Figure 22: Comparison of the refrigerant mass flow rates in the Vapor Compression Cycle System and the Pump-Boiler System.

For the Vapor Compression Cycle System, the refrigerant mass flow rate (or the oil-refrigerant mixture mass flow rate during the injection test) was measured using the Coriolis mass flow meter placed at the outlet of the microchannel heat exchanger - condenser. The shortcoming of the Coriolis flow meter is that it has errors in measurements if there is a slug flow through its tubes. For error-free reading, care must be taken to have sufficient subcooling at the outlet of the microchannel condenser, which was difficult for the tests performed with the Vapor Compression Cycle System. In the Pump-Boiler System, the Coriolis mass flow meter is placed after the refrigerant gear pump. Becasue the gear pump always supplies subcooled refrigerant, the Coriolis

mass flow meter gives error-free readings as the refrigerant flowing through it is always in a liquid state.

In the Vapor Compression Cycle System, the openings of the metering valves (9-a) and (9-b) determined the refrigerant mass flow rate through the microchannel condenser. The refrigerant mass flow rate also changed with the opening of the expansion valve – needle valve (8) (refer to Figure 19). Closing the expansion valve increased the microchannel condenser pressure and reduced the refrigerant mass flow rate in the system, while opening the expansion valve decreased the condenser pressure and increased the refrigerant flow rate. Optimum openings of the metering valves and expansion valve were needed along with the air conditions at the microchannel condenser to achieve the desired refrigerant mass flow rate, microchannel condenser inlet pressure, and superheated temperature for the particular test.

In the Pump-Boiler System, the mass flow rates through the microchannel heat exchanger can be easily controlled by changing the rotational speed of the refrigerant gear pump. The liquid refrigerant (or oil-refrigerant mixture) transferred by the refrigerant gear pump is then vaporized inside evaporators and the superheater. The boiling of the refrigerant in the evaporator with the help of hot water increases the microchannel condenser pressure. The temperature of the hot water supplied to the superheater is maintained at a few degrees higher than the superheated temperature required at the microchannel condenser inlet. Unlike the Vapor Compression Cycle System, the methods used to maintain the refrigerant mass flow rate, microchannel condenser inlet pressure, and the superheat are independent of each other in the Pump-Boiler System.

Figure 23 shows the control of the condenser pressure in both the systems. Once the temperature of the hot water supplied to the evaporators is set to a constant value in the Pump-Boiler System, the condenser pressure remains constant during the steady state operation of the system. In the Vapor Compression Cycle System, it was difficult to optimize the opening of the

expansion valve and was not always possible to get a steady pressure at the microchannel condenser.

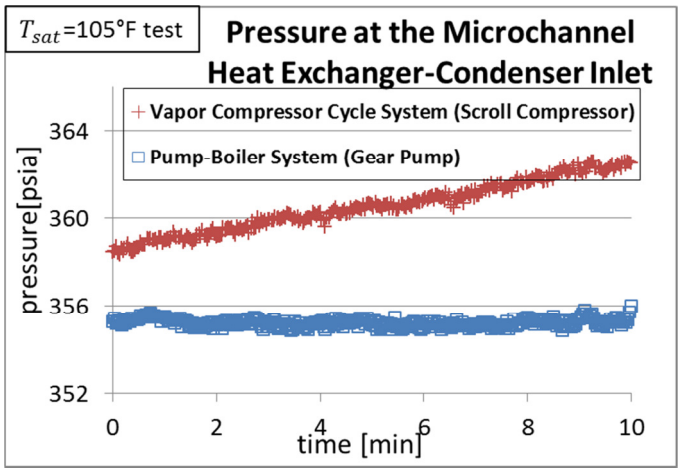

Figure 23: Pressure control in the Vapor Compression Cycle System and the Pump-Boiler System.

In addition to the pressure control problem in the microchannel condenser, the other problem was the control of the superheated temperature at the inlet of the microchannel condenser in the Vapor Compression Cycle system. Figure 24 shows the control of the superheat in both systems. In the Pump-Boiler System, the superheat at the inlet of the microchannel condenser remained steady once the temperature of the hot water supplied to the superheater was maintained at a constant value.

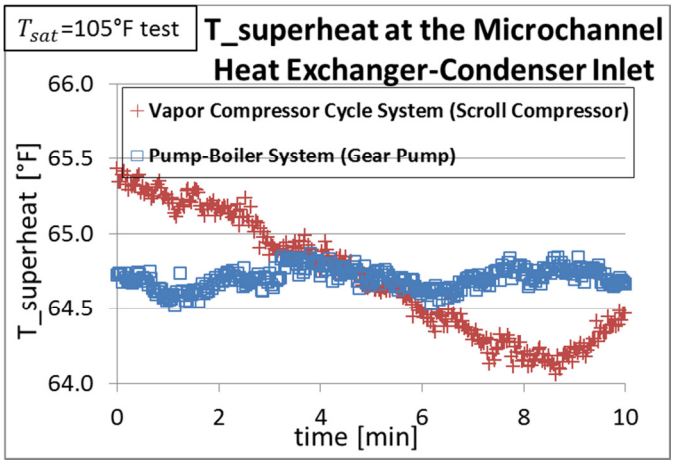

Figure 24: Superheat control of the Vapor Compression Cycle System and the Pump-Boiler System.

3.2.4 Compressor Failure due to Inadequate Lubrication

According to Hall (2012), flooded start, flood back, contamination, improper charging (overcharge and undercharge), and operation of the compressor outside the design envelope are the main factors that can lead to the mechanical failure of the compressor. The failure of the compressor observed during the experiment was due to severe bearing wear. The darkening of the POE oil with contaminants recovered from the failed compressor and the autopsy of the compressor are shown in Figure 25. These symptoms lead to the conclusion that there was a lack of lubricating oil in the compressor housing. The measurements of current indicated that the current consumption increased by 50% before compressor failure. In addition, the discharge temperature increased by 50°F (27.2°C) for similar operational conditions. These effects indicate that oil was carried over with the refrigerant in the test setup and was not returned to the compressor.

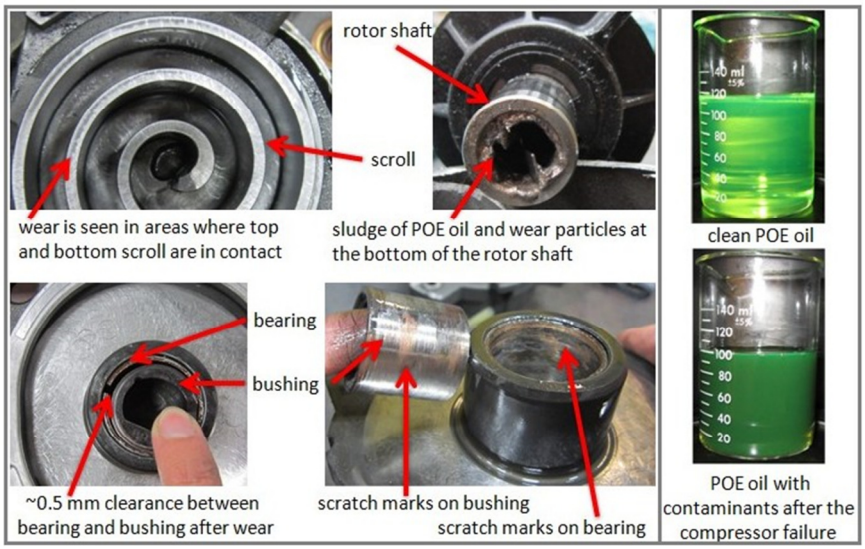

Figure 25: Autopsy of the scroll compressor and the compressor lubricant oil color comparison before and after the compressor failure.

The oil circulation ratio noticed in several tests was as high as 1.7%. Under these conditions, if the compressor operated at 1000 lbm/h (126 g/s), it would take 15 min to drain the

compressor's specified oil charge of 60 oz. (1.77 L). As the oil lost by the compressor did not return, the compressor failed within two weeks of continuous operation.

As shown in Figure 26 (refer to Figure 63 in Appendix A for the schematic), the scroll compressor (A) in the system was replaced and was fitted with a sight glass tube (B), and the compressor sump was supplied with oil from a secondary reservoir (not shown in the figure) whenever a rise in the discharge temperature was observed. A metering valve at the secondary reservoir helped to control the supply of oil to the compressor sump. A suction filter drier (E) was installed to keep foreign particles from the suction line out of the compressor. In addition, to avoid a flooded start, the compressor sump was heated using a band heater (not shown in the figure). However even with all possible precautions, the next failure of the compressor could not be avoided.

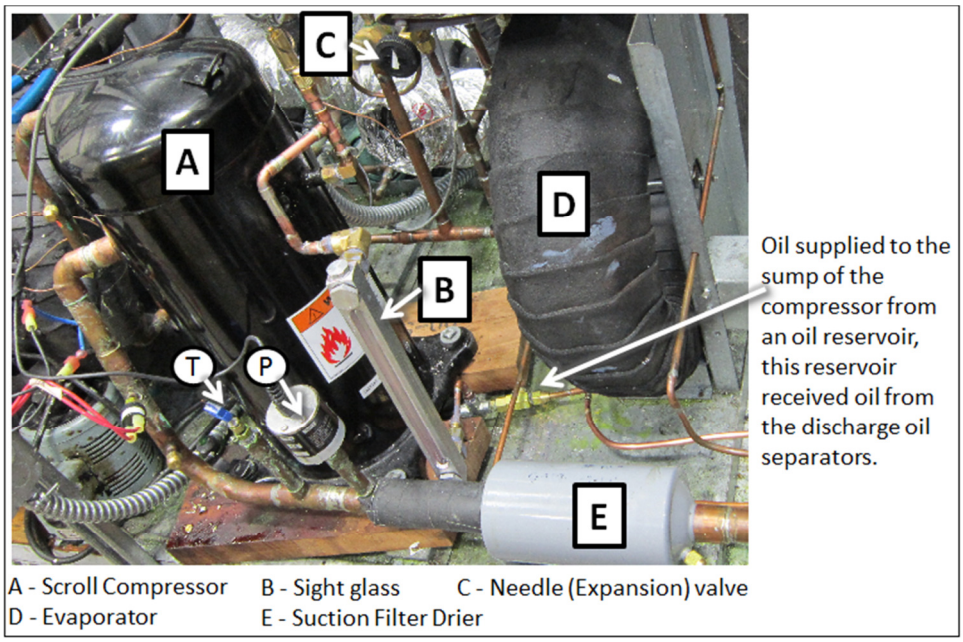

Figure 26: Scroll compressor with a sight glass tube.

The recommended lubricant viscosity for the scroll compressor utilizing the R410A or R134a refrigerant is between 100 SSU (22 cSt) and 300 SSU (68 cSt) at 100°F (37.8°C) (ASHRAE 2010). The scroll compressor in the test setup was lubricated using ISO VG 32 grade

POE (32 cSt). Figure 27 shows that the viscosity is lower than the recommended value when the pressure is above 80 psia (556.3 kPa) and the temperatures are either above 75°F (23.9°C) or below 30°F (-1.1°C). The lubricant is extremely viscous for the application if the temperature and pressure are below 70°F (21.1) and 35 psia (246.1 kPa), respectively.

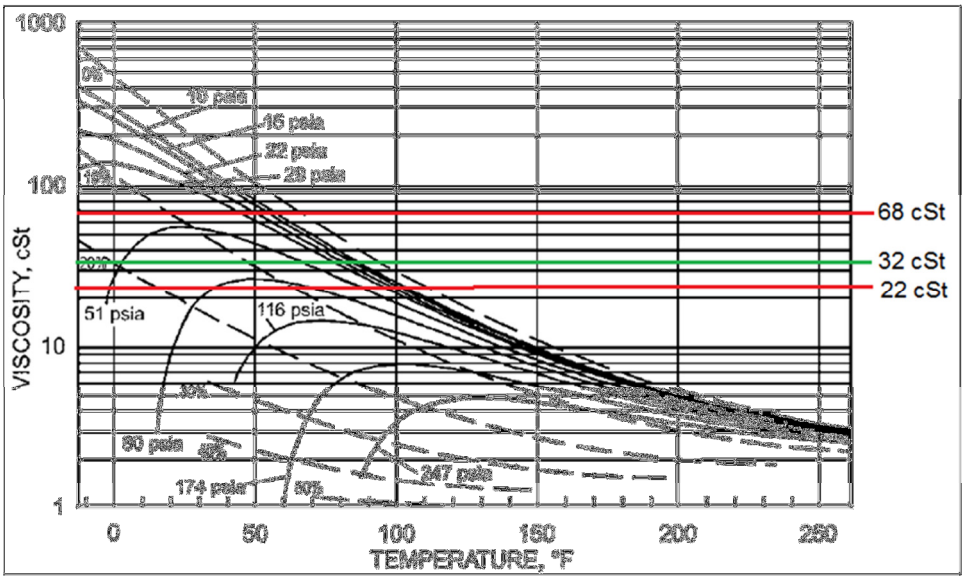

Figure 27: Viscosity/Temperature/Pressure plot for mixture of R-410A and ISO 32 Mixed-Acid Polyol Ester lubricant. Image reproduced from ASHRAE (2010)

The discharge oil separator supplied the extracted oil to the secondary oil reservoir. The pressure inside the secondary reservoir was always above 80 psia (556.3 kPa), therefore the oil had large amounts of refrigerant dissolved in it. When this oil-rich solution at high pressure from the secondary reservoir was transferred to the compressor sump, which was at a lower pressure, there might be a time lag for the refrigerant to un-dissolve from the oil. By the time the refrigerant is un-dissolved, the diluted oil may have already reached the bearings and damaged them.

3.3 Instrumentation and Errors

Qualitative analysis of a system is possible only if the techniques and instruments used to obtain the measurements of system parameters are so close to perfect that the uncertainties and their propagation in further investigations are reduced to a tolerable limit. Errors in any experimental measurements are inevitable. Although these errors cannot be avoided or eliminated, they can be kept to a minimum value if extreme care is taken or exact procedures are followed to get the readings.

These experimental errors or uncertainties propagate when used in calculation, and if large, will skew the results to make them impractical, and no conclusions can be drawn from the expensive and time-consuming experiments. At the same time, one should not strive to get extremely small uncertainties that only increase the cost of the instrumentation in the experimental facility. The goal is to estimate reliably all the possible uncertainties so that the final results of the experiments are convincing. The methods of error analysis and uncertainty propagation outlined in Taylor (1996) are used in this study.

The experimental system in the project uses multiple sensors to measure the temperatures, pressures, mass flow rates, volume flow rates, and other properties of air, refrigerant, and oil. These sensors are discussed in brief in the following sections. Along with the description of the instruments/sensors, this section also discusses the errors or uncertainty in their measured outputs. It is important to note that this report uses the terms “error” and “uncertainty” interchangeably.

Any measured parameter, such as the mass flow rate of the refrigerant $\dot{m}_{ref}$ during the experiment, can be represented as Equation (3.1).

$$\dot{m}_{ref} = \dot{m}_{ref,best} \pm \delta\dot{m}_{ref} = \dot{m}_{ref,best}\left(1 \pm \frac{\delta\dot{m}_{ref}}{|\dot{m}_{ref,best}|}\right) \tag{3.1}$$

where, $\dot{m}_{ref,best}$ is the best estimate of the measured value $\dot{m}_{ref}$ and has an absolute uncertainty of $\pm\delta\dot{m}_{ref}$. The precise quality of the measurement is given by the relative or fractional uncertainty $\frac{\delta\dot{m}_{ref}}{|\dot{m}_{ref,best}|}$ or $\frac{\delta\dot{m}_{ref}}{|\dot{m}_{ref}|}$.

Fractional uncertainty can be explained best using the concept of significant figures. Taylor (1996) defines it as follows: the number with N significant figures has an uncertainty of about 1 in the Nth digit. If a temperature of 25°C is read on a digital thermometer and it is said that the thermometer is accurate up to two significant figures, then it means that the uncertainty is 25±1°C. If the digital thermometer reads 0.25°C then the uncertainty is 0.25±0.01°C. These two values measured at the thermometer have different absolute uncertainties but have the same fractional uncertainty of 4%, as shown in Equation (3.2).

$$\frac{\delta T}{|T|} = \frac{1}{25} = \frac{0.01}{0.25} = 0.04 \; or \; 4\% \tag{3.2}$$

Manufacturers usually provide relative uncertainty at the full scale reading of their instruments. For example, if a differential pressure transducer measures static pressure before the nozzle bank ($P_{air,N,i}$) with an accuracy of ±0.25% of its full scale reading and its scale ranges ±1.5 in. W.C., then the uncertainty in the measured readings is calculated as shown in Equation (3.3) and Equation (3.4).

$$P_{air,N,i} = P_{air,N,i,measured} \pm \delta P_{air,N,i} \tag{3.3}$$

$$\delta P_{air,N,i} = \pm 0.0025 \cdot \big(+1.5 - (-1.5)\big) = \pm 0.0075 \text{ in. W. C} \tag{3.4}$$

3.3.1 Data Acquisition System

All the sensors used on the system are connected to the National Instruments - Data Acquisition (NI-DAQ) system, which has a sampling rate of 1 millisecond. The acquired data are displayed in real time by LabVIEW software graphic interface.

3.3.2 Resistance Temperature Detectors on Air Side

The Resistance Temperature Detector (RTD) works on a simple principle: the resistance of the sensor material, which is platinum in this case, changes with the temperature. This new resistance value is used to get the current temperature from the known temperature-resistance relation. Platinum material is chosen in place of nickel or copper because of its inertness, and also because its temperature and resistance relation is repeatable over a large temperature range.

The RTDs are used to measure the dry bulb temperatures and wet bulb temperatures of the air flowing across the microchannel heat exchanger. An RTD is also used to measure the temperature of the air at the inlet of the nozzle bank. Figure 6 shows the air side instrumentation using RTDs for dry bulb and wet bulb temperature measurements. These temperatures are required in order to calculate the density of the air, Reynolds number, humidity ratio, enthalpy, etc. The specifications of the RTDs are shown in Table 1.

Table 1: Specifications of Resistance Temperature Detector.

Item	**Item Specification**
Model	P-M-1/3-1/8-6-0-T-3
Type	Pt100
Range	-148 to 752°F (-100 to 400°C)
Accuracy	Accuracy 1/3 DIN (-50 ±0.18°C, 0 ±0.1°C, 100 ±0.27°C); ±0.1°F (±0.05°C) after calibration.
Description	100 Ω at 0°C; temperature coefficient of resistance = 0.00385 Ω/Ω/°C; 6" length, 1/8" diameter
Manufacturer	Omega Engineering, Inc.

3.3.3 Thermocouples on Air Side, Oil Side and Refrigeration Side

A thermocouple (TC) works on the principle of the thermoelectric effect, more precisely the Seebeck effect; where a junction (TC) of two dissimilar metals produces voltage when there is a temperature difference between the junction and the voltmeter. The voltage generated across the TC is then calibrated with the help of a reference cold junction to produce an accurate temperature reading. The specifications of the TCs are shown in Table 2.

Table 2: Specifications of the Thermocouple.

Item	Item Specification
Type	T-type (copper - constantan)
Model: Inline Thermocouple	TMQSS-125G-6
Model: Thermocouple Wire	TT-T-24-SLE-1000, the wire needs to be welded.
Range	-40 to 130°F (-40 to 54°C)
Accuracy	±0.5°F (0.3°C); ±0.1°F (±0.05°C) after calibration.
Manufacturer	Omega Engineering, Inc.

Inline thermocouples are installed to measure the temperatures at the refrigerant gear pump inlet ($T_{pump,i}$), the microchannel condenser inlet ($T_{mchx,i}$), the microchannel condenser outlet ($T_{mchx,o}$), and the evaporator outlet ($T_{evap,o}$). They are also used to measure the temperature of the extracted oil-refrigerant mixture from the oil extraction device ($T_{oil-ref,o}$), and the temperature of the injected oil-refrigerant mixture ($T_{oil-ref,i}$). These inline thermocouples are placed in the stream of oil and refrigerant using compression fittings to prevent any possible leaks.

A grid of 18 welded TCs is used on the air supply side of the microchannel heat exchanger. This grid helps in calculating the heat transfer to the air on selected sections of the microchannel heat exchanger slab. A TC is also placed at the inlet of the nozzle in parallel with the RTD, for cross-referencing.

Several welded TCs are attached to external surfaces of the copper fluid line at particular locations where the measurement of temperature is required. The attachment is done with a layer

of thermal grease between the tip of a welded TC and the surface to reduce the contact resistance. The readings from these surface TCs are not used in the data analysis but they help to provide a better and more predictive control over the system. For example, the TCs used to measure the water temperatures in and out of the secondary condenser/sub cooler helped the system operator maintain a definite refrigerant subcooling at the gear pump inlet, or, the measurement of hot water temperatures at the evaporator helped in maintaining the superheat and the pressure of the system. TCs also help in activating the shut-off limits of the pumps; a two-phase flow or no flow will shut down the pump, preventing further damage. A welded TC is attached to the fin of the microchannel heat exchanger when capturing the infrared images in order to calibrate the camera.

Calibration of the TCs and the RTDs is done in a temperature bath with reference to a NIST (National Institute of Standards and Technology) traceable thermometer having an accuracy of $\delta T_a = \pm 0.36°F$ ($\pm 0.2°C$). The software by National Instruments, Measurement & Automation Explorer (MAX) is used along with the NI-DAQ to record the data points at a sampling rate of 1 millisecond (1 kHz) during the calibration. These TCs and RTDs are calibrated to an uncertainty of $\delta T_b = \pm 0.05°F$ ($\pm 0.03°C$) with respect to the thermometer. Adding the errors in the thermometer and the calibrated TCs or RTDs in quadrature (Taylor 1996), Equation (3.5), gives the net error or uncertainty δT in temperature measurements.

$$\delta T = \sqrt{(\delta T_a)^2 + (\delta T_b)^2} \tag{3.5}$$

$$\delta T = \sqrt{(0.36)^2 + (0.05)^2} = 0.36°F\ (\pm 0.2°C). \tag{3.6}$$

Temperature measurements using the RTDs and TCs followed and exceeded the ANSI/ASHRAE Standard 41.1 (ASHRAE 1986).

3.3.4 Relative Humidity of Air

The relative humidity (φ or RH) values of the ambient air and the air supplied by the microchannel heat exchanger are measured and then used along with the dry bulb temperatures to determine the density of the air flowing across the heat exchanger. The specifications are shown in Table 3.

Table 3: Specifications of the Relative Humidity Sensor.

Item	**Item Specification**
Model	HX71-MA
Operating temperature range	-13 to 185°F (-25 to 85°C)
Accuracy	±3.5% from φ =15% to φ = 85%; ±4% below φ = 15%; and ±4% above φ = 85% when measured at 73.4°F (23°C).
Manufacturer	Omega Engineering, Inc.

3.3.5 Air Flow Nozzles

The airflow nozzles are arranged in parallel at the nozzle bank to have a pressure drop in the airflow path. Pressure drop measurements are used to calculate the air flow rates (CFM). This CFM value is then used for the air side calculations, to check the heat balance with the refrigerant side calculations. All the air flow measurements are done according to the ANSI/ASHRAE Standard 41.2 (ASHRAE 1987). The specifications of the nozzles are shown in Table 4.

Table 4: Specifications of the Air flow Nozzles.

Item	**Item Specification**
Model	Elliptical nozzle
Metal	Aluminum
Bore Diameter	8” (203 mm), 7” (178 mm), and 0.5” (12.7 mm)
Operating range	150 to 2,000 cfm (0.07 to 1 m^3/s)
Accuracy	±0.4% of flow rate (using Setra 264 pressure transducer and precise calculation of uncertainty propagation); Tightest Tolerance ±0.001” (±0.0254 mm) = error in bore diameter.
Manufacturer	Helander Metal Spinning Company

3.3.6 Very Low Differential Pressure Measurement of Air

The unidirectional differential pressure transducers, 2641-003WD, measure the air pressure drop across the nozzle bank ($\Delta P_{air,N}, \Delta P2$) and the microchannel heat exchanger ($\Delta P_{air,mchx}, \Delta P1$), while 2641-2R5WD measures the static pressure of the Psychrometric test room ($P_{air,amb}, P1$) in which the microchannel heat exchanger is placed. The bidirectional differential pressure transducer, 2641-1R5WB, measures the static pressure before the nozzle bank ($P_{air,N,i}, P2$). The specifications are shown in Table 5. Simple Pitot tubes are used to measure the pressure inside the air ducts; they are either purchased or constructed from small size copper tubes. As recommended, these Pitot tubes have holes of 1/16 in. (1.6 mm) diameter perpendicular to the direction of the air flow.

Table 5: Specifications of the Very Low Differential Pressure Transducers.

Item	**Item Specification**
Model	264
Manufacturer	Setra System, Inc.
1.)Unidirectional Transducer	2641-003WD
Pressure Range	0 to 3 in. W.C. (0 to 747 Pa)
Accuracy	±0.25% of full scale; ±0.0075 in. W.C.
Output	24 VDC Nominal
Excitation	0-5 VDC
2.)Unidirectional Transducer	2641-2R5WD
Pressure Range	0 to 2.5 in. W.C. (0 to 623 Pa)
Accuracy	±0.25% of full scale; ±0.00625 in. W.C.
Output	0-5 VDC Nominal
Excitation	9-30 VDC
3.) Bidirectional Transducer	2641-1R5WB
Pressure Range	±1.5 in. W.C. (±373 Pa)
Accuracy	±0.25% of full scale; ±0.0075 in. W.C.
Output	24 VDC Nominal
Excitation	0-5 VDC

3.3.7 Absolute Pressure Transducers

Absolute pressure transducers are installed to measure the pressures at the refrigerant gear pump inlet ($P_{pump,i}$), the microchannel condenser inlet ($P_{mchx,i}$), the microchannel condenser outlet ($P_{mchx,o}$), and the evaporator outlet ($P_{evap,o}$). They are also used to measure the pressure of the extracted oil-refrigerant mixture between the oil extraction device and the oil level tank ($P_{oil+ref,o}$), and to measure pressure of the injected oil-refrigerant mixture ($P_{oil+ref,i}$) using the transducer at the oil reservoir. The specifications of the absolute pressure transducer are shown in Table 6. The absolute pressure transducers measuring the refrigerant's vapor pressures at the evaporator outlet and at the oil separators have a sufficient draft of air flowing over them to prevent a high temperature at their circuitry that might damage the sensor or drift the readings. For refrigerant and oil lines having less than 5/8 in. (15.8 mm) outer diameter, the tubing to the pressure transducers is of the same size, while for higher diameter copper lines, the tubing are kept as small as possible to avoid turbulence at the sensor, which could measure total pressure instead of static pressure. Bourdon tube gauges are also used at the oil level tank and the oil reservoir to visually check the pressures while controlling it through the needle valves on the pressure equalization lines. All the pressure measurements on the refrigerant, oil, and air side are done according to ANSI/ASHRAE Standard 41.3 (ASHRAE 1989).

Table 6: Specifications of the Absolute Pressure Transducer.

Item	**Item Specification**
Model	206
Pressure Range	7 to 500 psia (50 to 3450 kPa)
Accuracy	±0.65 psi (±4.5 kPa)
Output	24 VDC Nominal
Excitation	0-5 VDC
Manufacturer	Setra System, Inc.

3.3.8 Differential Pressure Measurement of Refrigerant

A differential pressure transducer is placed between the inlet and the outlet lines connecting the microchannel heat exchanger slab. It measures the pressure drop experienced by the refrigerant or the oil-refrigerant mixture when flowing through the resisting ports of the micro-channels. Figure 9 shows the position of the transducer. The specifications of the differential pressure transducer are shown in Table 7.

Table 7: Specifications of the Differential Pressure Transducers.

Item	**Item Specification**
Model	P55D-4-N-4-40-S-4-A
Pressure Range	8 to 12.5 psi (55 to 86 kPa), actually it can measure as low as 0 psi.
Accuracy	±0.25% of full scale; ±0.03 psi
Output	4 to 20 mA
Excitation	9-55 VDC
Manufacturer	Validyne Engineering

3.3.9 Mass Flow Meter for Refrigerant and Oil

The mass flow rate of the refrigerant ($\dot{m}_{ref}$), the injected oil-refrigerant mixture ($\dot{m}_{oil-ref,inj}$), and the extracted oil-refrigerant mixture ($\dot{m}_{oil-ref,ext}$) are measured using the Coriolis flow meter. The mass of the oil injected at the microchannel heat exchanger ($m_{oil,in}$) is measured by integrating the value of the mass flow rate of injected oil with the time-period of the test. The Coriolis meter can be used to measure either liquid or gas mass flow rate, but it is only employed to measure liquid mass flow rates. The specifications for the mass flow meters are shown in Table 8 and Table 9 respectively. The mass flow meter CMF025 is placed between the refrigerant gear pump and the evaporator to measure the pumped refrigerant mass flow rate. One mass flow meter CMF010M is placed at the oil outlet/drain of the oil separator to measure the

extracted oil-refrigerant mixture, while the other is placed after the injection gear pump on the injection line to measure the injected oil-refrigerant mixture's mass flow rate. (Refer to Figure 11)

Table 8: Specifications of the Refrigerant Mass Flow Meter.

Item	**Item Specification**
Model	(CMF025) CMF025M319NRAAEZZZ
Type	Coriolis Flow and Density Meter
Transmitter	2700C12BBAEZZZ
Flow rate range	4800 lbm/h (2180 kg/h)
Flow rate accuracy	±0.10% of the flow rate
Zero stability	0.06 lbm/h (0.027 kg/h)
Density range	312 lbm/ft^3(5000 kg/m^3) or (5 g/cm^3)
Density accuracy	±0.0312 lbm/ft^3 (±0.5 kg/m^3)
Temperature range	300°F (148°C)
Temperature accuracy	±2°F (±1°C)
Output	4 to 20 mA
Pressure rating for sensor	1500 psig (10.4 MPa)
Manufacturer	Micro Motion Inc.

Table 9: Specifications of the Oil-Refrigerant Mixture Injection and Extraction Mass Flow Meter.

Item	**Item Specification**
Model	(CMF010M) CMF010M323NRAAEZZZ
Type	Coriolis Flow and Density Meter
Transmitter	2700C12BBAEZZZ
Flow rate range	240 lbm/h (108 kg/h)
Flow rate accuracy	±0.10% of the flow rate
Zero stability	0.0045 lbm/h (0.002 kg/h)
Density range	312 lbm/ft^3(5000 kg/m^3) or (5 g/cm^3)
Density accuracy	±0.0312 lbm/ft^3 (±0.5 kg/m^3)
Temperature range	300°F (148°C)
Temperature accuracy	±2°F (±1°C)
Output	4 to 20 mA
Pressure rating for sensor	1813 psig (12.6 MPa)
Manufacturer	Micro Motion Inc.

According to the manufacturer, the rated accuracy of the mass flow meter is ±0.10% of the flow rate. But, if the actual flow rate is less than $\frac{\text{zero stability}}{0.001}$, then the accuracy is $\pm\left(\frac{\text{zero stability}}{\text{flow rate}}100\right)\%$ of the flow rate. The oil-refrigerant mass flow rate in the system varied from 3 to 20 lbm/h. The $\frac{\text{zero stability}}{0.001} = \frac{0.0045}{0.001} = 4.5$ lbm/h, which means that the flow rate from 3 to 4.5 lbm/h has the uncertainty greater than ±0.10% of the flow rate. If calculated, the uncertainty at 3 lbm/h is ±0.15% of the flow rate. Comparing the percentage of the net region of 4.5 to 20 lbm/h with the region of 3 to 4.5 lbm/h it will be reasonable to choose the uncertainty as ±0.10% of the flow rate. This is illustrated in Figure 28. The refrigerant mass flow rate in the system is always greater than 300 lbm/h, while the $\frac{\text{zero stability}}{0.001} = \frac{0.06}{0.001} = 60$ lbm/h, which is very small compared to the flow rate of the refrigerant in the system. Hence, the uncertainty in the refrigerant flow rate is ±0.10% of the flow rate.

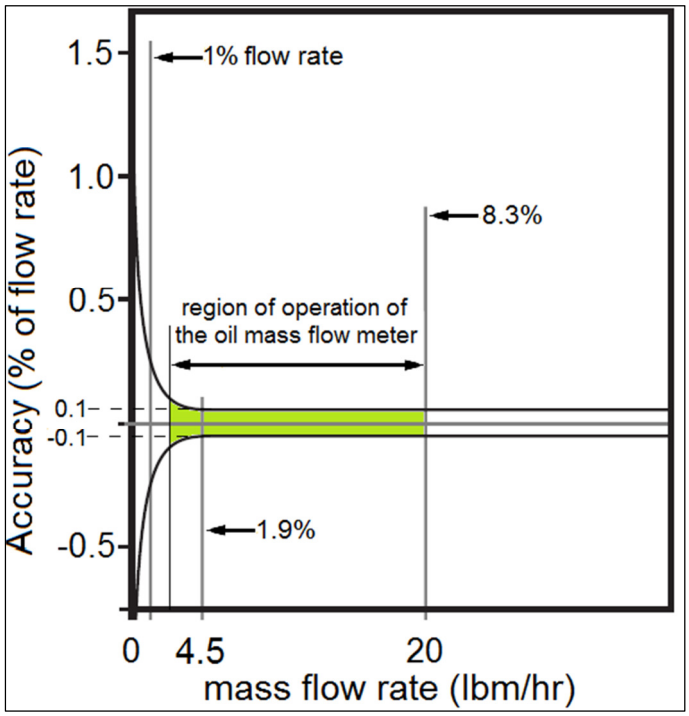

Figure 28: Relation between the flow meter accuracy and the mass flow rate.

3.3.10 Weighing Scale

A weighing scale is used to measure the weight of the oil-refrigerant samples collected at the end of each injection test to determine the solubility of the refrigerant in the oil using the gravimetric method. The specifications of the weighing scale are shown in Table 10.

Table 10: Specification of the Weighing Scale.

Item	**Item Specification**
Model	SAW-L
Capacity	50 lb (22 kg)
Resolution	0.0005 lb (0.2 g)
Accuracy	±0.01% of full scale; ±0.005 lb (±2.2 g)
Manufacturer	Arlyn scales

3.3.11 Oil Level Measurement Sensor

In the Vapor Compression Cycle System, the volume of oil extracted at the oil level tank was measured using a graduated sight glass tube at regular intervals during the test, and it was assisted by the oil level sensor – capacitance probe (specifications are presented in Table 11). The graduated sight glass and the capacitance probe were capable of measuring only the volume of oil extracted at the oil level tank over time. The temperature and the pressure of the extracted oil were used to measure the density and the solubility, which in turn were used to calculate the mass of oil extracted.

Table 11: Specifications of Oil Level Measurement Probe.

Item	**Item Specification**
Sensor model	LV3114-24
Transmitter model	LVCN411
Material covering the probe	PTFE
Length of the probe	24” (60.96 cm)
Maximum operating pressure	290 psig (2 MPa)
Temperature range	14 to 248°F (-10 to 120°C)
Accuracy	±0.5% of full scale
Output	4-24 VDC Nominal
Excitation	24 VDC to the Transmitter
Manufacturer	Omega Engineering,Inc.

3.4 Specification of the Components used on the Test Facility

Table 12: Specification of the Components.

Component	Manufacturer [Model]	Specifications and description of use.
Ball Valves, Gate Valves, PVC pipes, Copper pipes and tubes, and fittings	Grainger Inc., Lowe's, McMaster-Carr, Locke Supply Co, United Refrigeration Inc.	Refrigeration system and Hydronic system (water side of the sub cooler, auxiliary heat exchanger and the evaporators).
Bladder Accumulator	McMaster-Carr [59595K12]	Capacity of 1 gallon; used to stabilize the flow of the refrigerant in the Pump-Boiler System.
Centrifugal pump	Taco [1400 – 50 –A]	Input: 230 V, 60 Hz, 1 phase, 2.4 A, 3450 rpm; used to provide necessary head at the sub cooler and the superheater's inline heater.
Check valve	McMaster-Carr [7775K12,7768K14]	One is used on the oil injection line and the other on the pressure equalization line.
Coalescent Separator	Temprite [925R]	Separates up to 0.05 microns particles, height: 28.6 in. (0.73 m), diameter: 4 in. (10.2 cm). The bottom 16.4 in. (41.6 cm) serves as a reservoir, which has sight glass for monitoring purpose. Internal float valve absent.
Compressor's oil level indicator	McMaster-Carr [1106K27]	Designed for maximum pressure of 290 psi, 9 in. in length; connected at the bottom of the compressor to check its oil/lubricant level.
DAQ wire	Olympic Wire and Cable Corp. [2824]	Multi-conductor 24 AWG cable; used to connect the sensors to the DAQ system.
Expansion Tank	Bell and Gosset [HFT- 15]	It has a total volume of 3 gallons and an acceptance volume of 1 gallon, the shell and diaphragm are made up of carbon steel and heavy duty butyl rubber respectively. It is pre charged to 12 psi, designed to handle 100 psi and 240°F, weight is 5 lbs.
Flow Switch - water flow circuits	Mcdonnell & Miller [FS6-3/4]	Allows minimum flow rate of 0.12 gpm and maximum flow rate of 2.5 gpm.
Gear Pump Motor	Baldor.Reliance Super-E motors [CEM3545]	Input: 230/460 V, 2.8/1.4 A, 60 Hz, 3 phase, usage: 0.75 kW, 1 hp, 3450 rpm; used for refrigeration and injection gear pumps
Helical separator	Henry Technologies Inc. [S-5188]	Designed for 10 cfm for 10 tons refrigeration capacity, height: 19 in. (48.3 cm), diameter: 4 in. (10.2 cm). Internal float valve absent.

Component	Manufacturer [Model]	Specifications and description of use.
High Temperature Heater Tapes	OMEGA Engineering Inc. [FWH171-060]	Input: 120 V, usage: 624 W with 5.2 W/in^2, resists up to 900 °F (480 °C); used to heat the oil-refrigerant mixture in the oil reservoir and the oil level tank.
High-Pressure Safety Valves	McMaster-Carr [5825T21]	The brass safely valve is placed after the refrigerant gear pump (not shown in any figures), and is designed to relieve the pressure from the system if it exceeds 500 psig (34.5 bar).
Inline Water Heater	Chromalox [NWHSRG 06-024PE1]	Heating capacity of 2 KW, 480V, 1 phase, INCOLOY® Sheath Element; used on the hot water loop having the refrigerant superheater.
Injection Gear Pump	Micropump	
Injection Oil Reservoir (Blue Tank), Oil Reservoir #1	Emerson Climate Technologies [AOR-4]	Capacity: 4 gallon (15.1 L), 2.5 ft. (0.88 m) tall; stores the oil to be injected using the injection gear pump.
In-Line Centrifugal Fan	Suncourt inc. Centrax [TF104-CRD 4"]	Input: 120 V, 0.53 A, 60 Hz, 1 phase, usage: 60 W, 4 in. (10.2 cm) air inlet and outlet, 200 cfm, in-line centrifugal fan; used as a fan/blower on the air sampling device.
Needle Valve 1/4"	Parker Hannifin Corp. [4A-V4LR-B]	Opens 10% per 1/2 turn - total 5.125 turns; used on the pressure equalization and the oil injection lines.
Needle Valve 3/8"	Parker Hannifin Corp. [6A-V6LR-B]	Opens 10% per 1/2 turn - total 5.5 turns; used for refrigerant mass flow rate control.
Oil Level Tank/Cylinder	Swagelok [304L-HDF8-1GAL]	Capacity: 1 gallon (3.79 L); oil level tank is made up of two of these cylinders.
Oil Reservoir #2	Parker Hannifin Corp. Sporlan Division [POR-3]	Capacity: 3 gallon (11.4 L), stores the oil separated from the vapor refrigerant and then supply it back to the suction line of the compressor.
Plate Heat Exchanger	GEA [GB400L-14]	14 plates, heat transfer area of 16 ft^2, and minimum heat transfer capacity of 15750 Btu/h
Refrigerant Filter-Dryer	Parker Hannifin Corp. Sporlan Division [C-032]	Size of 3 in^3, removes moisture, dirt, acid, and sludge; initially was used on the refrigerant liquid line, then was transferred on oil line to filter it.
Refrigerant Filter-Dryer	Parker Hannifin Corp. Sporlan Division [C-083-S-HH 3/8]	Size of 8 in^3, removes moisture, dirt, acid, and sludge; used after the refrigerant gear pump.
Refrigeration Gear Pump	Micropump [GC-M25.JVS]	0.48 gallon/1000-rev (1.82 ml/rev), maximum differential pressure: 125 psi (862 kPa)

Component	Manufacturer [Model]	Specifications and description of use.
Remote gas bulb control thermostat	Honeywell [L4008A]	Control thermostat with high temperature limit of 150°F (66°C); used on the Vapor Compression Cycle System.
Scroll Compressor	Copeland [ZF15K4E-PFV]	Used on the Vapor Compression Cycle System.
Service Manifold	Ritchie Engineering Co., Inc. YELLOW JACKET product division [Series 41]	Used to charge and recover the refrigerant from the system.
Sight glass	McMaster-Carr [1138K64]	Pipe size - 1/2 in; used to monitor the oil-refrigerant extraction at the oil separators, and also to ensure that liquid refrigerant enters the refrigerant gear pump (not shown in any figures)
Sight Glass Tube/ Level Indicator	McMaster-Carr [1106K76]	Designed for maximum pressure of 240 psi, viewing glass of 18 in. length; it is graduated and connected to oil level tank to measure the volume of the extracted oil-refrigerant mixture.
Suction Line Accumulator	Grainger Inc. [6AXD3]	Placed on the suction line to prevent any liquid refrigerant to enter the compressor.
Suction line Filter-Dryer	Parker Hannifin Corp. Sporlan Division Catch-All [C-417-S-T-HH]	Separates moisture, dirt, acid, sludge doing to the compressor
Variable frequency Drive	Baldor Electric Company [VS1SP21-1B]	Input: 230 V, 4.2 A, 60 Hz, 3 phase, usage: 0.75 kW, 1hp; Configured for the motors of the refrigerant gear pump and the injection gear pump.
Variable Transformer	Superior Electric [3PN116C]	Input: 120 V, 50/60 Hz, 1 phase, 1.4 KVA, output: 0 - 120V; variac for the heater tapes.

3.5 Dimensions of the Microchannel Heat Exchanger

The manufacturer did not provide the dimensions of the microchannel heat exchanger used in the test section. The dimensions are calculated so that they could be used for analyzing the geometry effects on the results obtained and for modeling purposes. The dimensions are presented in Table 13. The position of the partition inside the header was not known, this partitions inside the header make possible the two passes in the heat exchanger. The position of the partition was found by using an infrared image of the header, Figure 29; the superheated temperature of the refrigerant vapor in the first pass can be easily differentiated at the partition from the saturated temperature of the two-phase refrigerant at the outlet of the second pass.

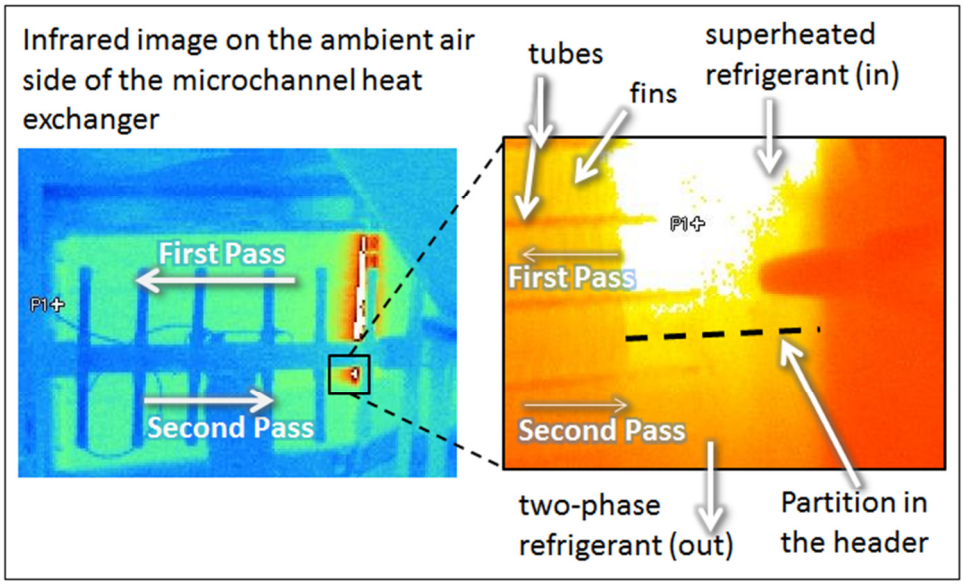

Figure 29: Use of an infrared image to locate the partition inside the header of the microchannel heat exchanger.

Table 13: Dimensions of the Microchannel Heat Exchanger

Description	**Measurement***
Tube and Fin Material	Aluminum
Fin Type	Louvered
Number of pass	two
Number of tubes in the first pass	69
Number of tubes in the second pass	32
Outer diameter of each Header	1.18 in. (30 mm)
Height of each Header	36 in. (0.91 m)
Distance of the inlet copper tube from the bottom of the coil	21.25 in. (0.54 m)
Outer diameter of the inlet copper tube.	5/8 in. (15.88 mm)
Distance of the outlet copper tube and the bottom of the coil	1.5 in. (38.1 mm)
Outer diameter of the outlet copper tube	3/8 in. (9.53 mm)
Length of each microchannel tube between the headers	48 in. (1.22 m)
Overall Coil height measured between the extreme microchannel tubes	35.75 in. (0.91 m)
Number of channels in each tube	4
Hydraulic diameter of each channel	~0.067 in. (1.7 mm)
Aspect ratio of each channel (width/height)	6.125
Tube depth in the direction of air flow, thickness of the microchannel heat exchanger slab	1. in (25.5 mm)
Microchannel tube spacing, space between adjacent tubes	0.291 in. (7.4 mm)
Microchannel tube thickness	0.055 in. (1.4 mm)
Fin density or pitch	17.25 fin per inch
Fin spacing, free space between adjacent fins	~0.039 in. (1 mm)
Fin thickness	~0.002 in. (0.07 mm)
number of louvers on the fin	18
Louver length	~0.252 in. (6.4 mm)
louver height from the fin plane	~0.008 in. (0.2 mm)
Louver pitch	0.889 louvers per mm
Louver angle measured from fin plane	~30°

*Note: The dimensions of the microchannel heat exchanger sample were not provided by the manufacturer. The dimensions were estimated by conducting a limited number of measurements on the sample in Oklahoma State University – Laboratory.

3.6 Test Procedure

AHRI standard 210 (AHRI 2005) is used as a guideline to determine the operating parameters for the tests performed on the microchannel condensers for air-conditioner applications. The microchannel heat exchanger is also tested at additional operating conditions not mentioned in this standard because the objective of this project is to study the working of the microchannel heat exchanger with the oil. AHRI standard 520 (AHRI 2004) for refrigeration positive displacement condensing unit applications was also used as a guideline for the initial tests, which were performed on the Vapor Compression Cycle System. The following experimental test procedure describes the steps used each time the tests were performed; these procedures are adapted from the methods used by Cremaschi et al. (2005).

3.6.1 Pre-injection Test

The pre-injection test is the test just before the injection test when the system is operating at a steady state. Once a steady state is achieved in the system, the system is made to run for an hour so that any oil in the test section gets flushed by the refrigerant, which is then extracted at the extraction point. The DAQ records the sensor's data for 10 min, after which the injection test starts. The following paragraphs explain how the steady state in the system is achieved.

The mass flow rate of the refrigerant in the system is controlled by adjusting the speed of the refrigerant gear pump and opening the by-pass valve across the gear pump; similarly, the speed of the injection gear pump is adjusted to control the oil-refrigerant mixture injected mass flow rate. The pressure in the system is attained by having the temperature of the hot water flowing through the evaporator slightly higher than the saturation temperature at the microchannel heat exchanger. The temperature of the hot water supplied at the superheater determines the superheat at the inlet of the microchannel heat exchanger. The system pressure can

also be changed by altering the temperature of the air inside the psychrometric chamber, which changes the saturated pressure at the microchannel condenser. The volume flow rate of air is always maintained at a constant value using the blower placed after the nozzle banks.

The heating of the oil-refrigerant mixture in the oil level tank and the oil reservoir causes a decrease in the solubility of the oil-refrigerant mixture, which causes the refrigerant to separate from the oil by un-dissolving. This separated refrigerant is in either vapor or two-phase condition. The vaporized refrigerant then enters the system through the pressure equalization line. This process causes the charge inside the system to increase, which increases its pressure and mass flow rate.

To summarize the pre-injection test, the necessary system conditions are achieved by:

1.) Controlling vaporization of the refrigerant at the evaporator using the hot water, and also controlling vaporization of the refrigerant in the oil level tank using the electric heater.

2.) Adjusting the temperature of the hot water at the superheater to have the necessary superheat at the inlet of the microchannel heat exchanger.

3.) Adjusting the speed of the refrigerant gear pump to have the necessary mass flow rate.

4.) Controlling the Psychrometric Chamber's air temperature and flow rate across the microchannel heat exchanger.

5.) Heating the oil-refrigerant mixture in the oil reservoir by electric heater so that the mixture temperature is close to the superheated temperature at the inlet microchannel heat exchanger.

6.) Once the system is running at a steady state condition without any oil in the test section, recording data for 10 min for the pre-injection test.

3.6.2 Method to get required OCR during the Injection Test

The difficulty faced while performing the initial tests was to pre-determine the oil-refrigerant mixture's injection mass flow rate to have the preferred OCR. It was not possible by estimating the injected mass flow rate. A method for knowing the solubility of the oil-refrigerant mixture inside the oil reservoir was required, and this solubility value was used to calculate the injection mass flow rate to have the test results at the expected OCR. The following paragraphs briefly explain the importance of the solubility consideration, how its value is obtained, and its use to get the injection flow rate.

The large oil reservoir holding the injected oil-refrigerant mixture is maintained at a constant condition by using an electric heater and pressure from the pressure equalization line. The pressure equalization line exposes the oil inside the oil reservoir to the refrigerant vapor. The refrigerant vapor, because of its solubility with the oil, gets absorbed in it; this solubility varies with the pressure and the temperature of the mixture at the oil reservoir. The solubility of this mixture at the present temperature and pressure needs to be determined to know the quantity of oil that needs to be injected inside the test section to have the desired OCR.

The data of solubility for R-410A and Mixed Acid POE is taken from Cavestri and Schafer (2000) and extrapolated (refer to section on 4.2 Solubility and Density Determination for more details), while that for R-134a and ISO VG 32 grade Mixed Acid POE (EMKARATE RL32S) is taken from Cavestri (1993, 1995). The Generalized Least Squares method is used to get the surface fit equation for the solubility as a function of the mixture's temperature (T) and the pressure (P). VBA codes are also written to get the solubility value as a function of the mixture's temperature (T) and pressure (P) from the available map (Cavestri (1993, 1995) and extrapolated Cavestri and Schafer (2000) data). The solubility was then used to predict the mass flow rate of injected oil-refrigerant mixture, which in turn helped in adjusting the speed of the

injection gear pump before the actual test started. Figure 30 shows the formulas and the function in the Excel sheet cells, which are solved iteratively to determine the injected oil-refrigerant mass flow rate. This method estimates the injection mass flow rate for the required OCR, when the exact OCR for the test is recalculated during the data reduction; it is within ±0.71 units (with a confidence of 95.45%) of the value used for this method.

R410A	Input		Apply following condition		
OCR =	5	%	inject at MFR =	33.14	lb/h
inlet P of MCHX =	354.5	psia	Actual MFR Ref =	406.21	lb/h
inlet T of MCHX =	111.08	°F			
MFR Ref =	402.45	lb/h	superheat =	6.06	°F
injection P =	358.38	psia	Solubility =	52.55	% w/w
injection T =	112.26	°F	injection pure oil =	21.38	lb/hr
predicted solubility	55	% wt/wt	injected pure ref =	11.76	
extraction P =	354	psia	Solubility =	63.72	% w/w
extraction T =	104.32	°F	Extracted pure ref =	3.11	lb/h
extraction MFR =	8	lb/h	extracted subcool =	0.39	°F

Predicted injection flow rate of the oil-refrigerant mixture

Current system condition

a.) Sample calculation to know the required oil-refrigerant mixture injection mass flow rate to get desired 5% *OCR* at the system's operating condition.

R410A	Input		Apply following condition		
OCR =	5	%	inject at MFR =	=F9+F10	lb/h
inlet P of MCHX =	354.5	psia	Actual MFR Ref =	=C6-C14+F10	lb/h
inlet T of MCHX =	111.08	°F			
MFR Ref =	402.45	lb/h	superheat =	=C5-temperature_PT_g(C4)	°F
injection P =	358.38	psia	Solubility =	=solubility_R410A_POE(C9,C8)	% w/w
injection T =	112.26	°F	injection pure oil =	=F4*C3/100/(1-C3/100)	lb/hr
predicted solubility	55	% wt/wt	injected pure ref =	=F3/(1+100/C10)	
extraction P =	354	psia	Solubility =	=solubility_R410A_POE(C13,C12)	% w/w
extraction T =	104.32	°F	Extracted pure ref =	=C14/(1+100/F12)	lb/h
extraction MFR =	8	lb/h	extracted subcool =	=temperature_PT_l(C12)-C13	°F

b.) Formulas/Functions used in Microsoft Excel's cells are solved iteratively.

Figure 30: Predictive calculation to determine the injection mass flow rate of the oil-refrigerant mixture to have desired *OCR* for the test.

3.6.3 Injection Test

The injection test begins directly after the pre-injection test. During the injection test, the injection gear pump to injects the oil-refrigerant mixture into the test section; the mixture is injected either at port-A or port-B of the microchannel heat exchanger depending on the test. The injection continues at a steady rate until a steady state of operation is observed in the test section. The data recorded during the steady operation is used for the $HTPF$, $PDPF$, and OCR calculation. This section describes the procedure followed during the injection test in the Pump-Boiler System. The Vapor Compression Cycle System requires similar test operations.

During the pre-injection test, the system is already operating in a steady state condition, and the amount of oil in the test section is negligible (refer to section 4.3 Assumptions for Calculations for the reason). Ball valve B10-a is opened and B10-b is closed if the mixture needs to be injected at port-A, and vice versa if the mixture is to be injected at port-B of the test section (refer to Figure 11). The injection test lasts for 30 min. During this period, the system is again in a steady state. To stop the injection test, valve B7 is opened to start recirculating the mixture in the oil reservoir and valve B8 is then closed to stop the flow of the mixture to the test section.

The end of the injection test is followed by the test to measure the solubility of the injected mixture and is discussed in later sections.

3.6.4 Extraction Test

The extraction test took place along with the oil injection test. The oil injected into the test section during the injection tests starts to separate at the helical and coalescent separators at the end of the test section. The extracted oil needs to be measured to calculate the amount of oil retained in the microchannel heat exchanger. This section describes the methods used for measuring the extracted oil.

Method-1: (Used for the Vapor Compression Cycle System) This method was used on the Vapor Compression Cycle System. The oil level tank was fitted with a sight glass tube and calibrated to measure the volume of oil in the oil level tank system. The level sensor on the tank also helped to track the level of the fluid. Figure 65 (refer to Appendix A) gives the schematic of the oil extraction circuit showing the position of the sight glass tube and the level sensor in the oil level tank.

The time and the level on the sight glass were noted as the oil-refrigerant mixture level increased in the oil level tank. These were used to determine the volume extracted. The density and the solubility values were used during the data reduction to determine the mass of pure oil extracted for each time step as the injection test proceeded. The averaged difference between the mass of oil injected and the mass of oil extracted was calculated after the steady state was reached (after time t_2) to get the oil retained for that particular test (refer to Figure 31).

Method-1 was discontinued in the Pump-Boiler System because the oil level tank was at a high pressure and always filled with the condensed refrigerant, thus eliminating any possibility of using the graduated sight glass tube. This was not the case when the tests were performed on the Vapor Compression Cycle System because the pressure equalization line to the oil level tank was connected on the low pressure side of the compressor. The pressure equalization line provided very low pressure at the oil level tank, which was exposed to the ambient condition of

the laboratory. The low pressure at the tank allowed the vaporization of the refrigerant even at the ambient temperature. The vapor refrigerant returned to the system through the pressure equalization line and the oil level tank was always empty for the oil extraction tests.

Method-2: (Used for the Pump-Boiler System.) The Coriolis mass flow meter is used to measure the mass flow rate of the oil-refrigerant mixture extracted at the helical and coalescent separators. The reading from the Coriolis mass flow meter, though constant, showed excess noise during the steady state injection test. The absence of float valves inside the separators continuously exposed the Coriolis meters to local pressure changes inside these separators due to turbulence, and in addition, the fluttering operation of the check valve over the pressure equalization line led to noise in the mass flow rate.

Determining the mass of oil extracted is simplified by taking the difference between the time (t_1) at which the oil is observed in the sight glass and the time (t_0) at which the injection starts. Figure 11 shows the position of the sight glass placed between nodes k and l, and Figure 32 shows the actual image of the extracted oil in the sight glass. The time difference ($t_1 - t_0$), when multiplied by the constant mass flow rate of the pure oil injected in the test section, gives the mass of oil retained.

It is feasible to calculate the oil mass extraction using the above method. Section on 4.3 Assumptions for Calculations explains why the mass flow rate of the injected pure oil is equal to the mass flow rate of the extracted pure oil, while section 4.7 Oil Retention Calculation gives the details of the oil retention calculations for both Methods.

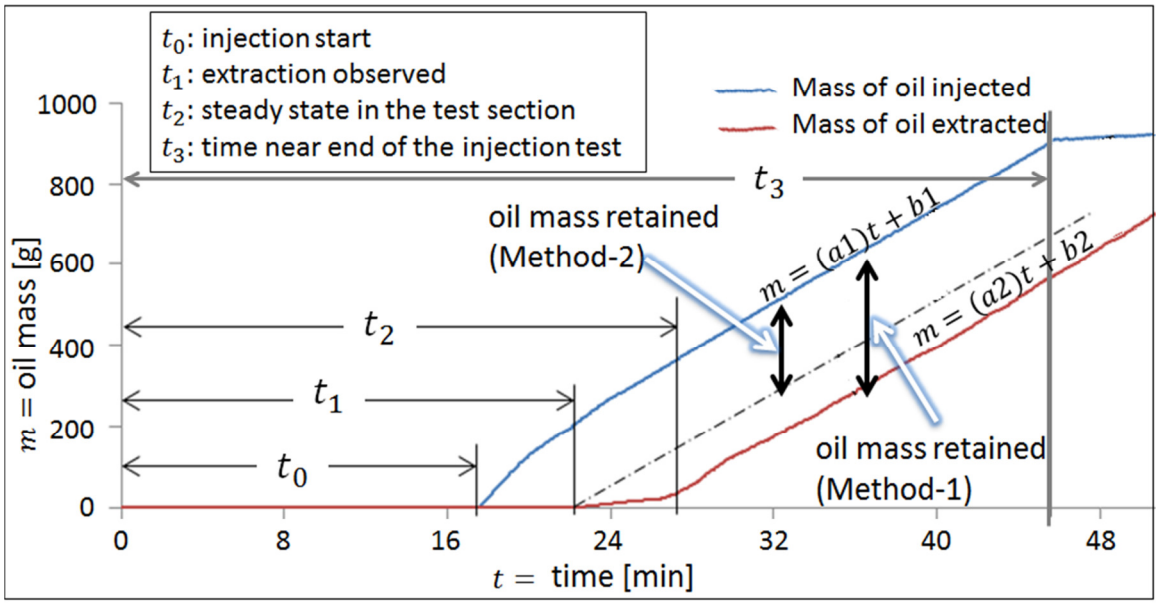

Figure 31: Oil mass retained in a test section during the injection test.

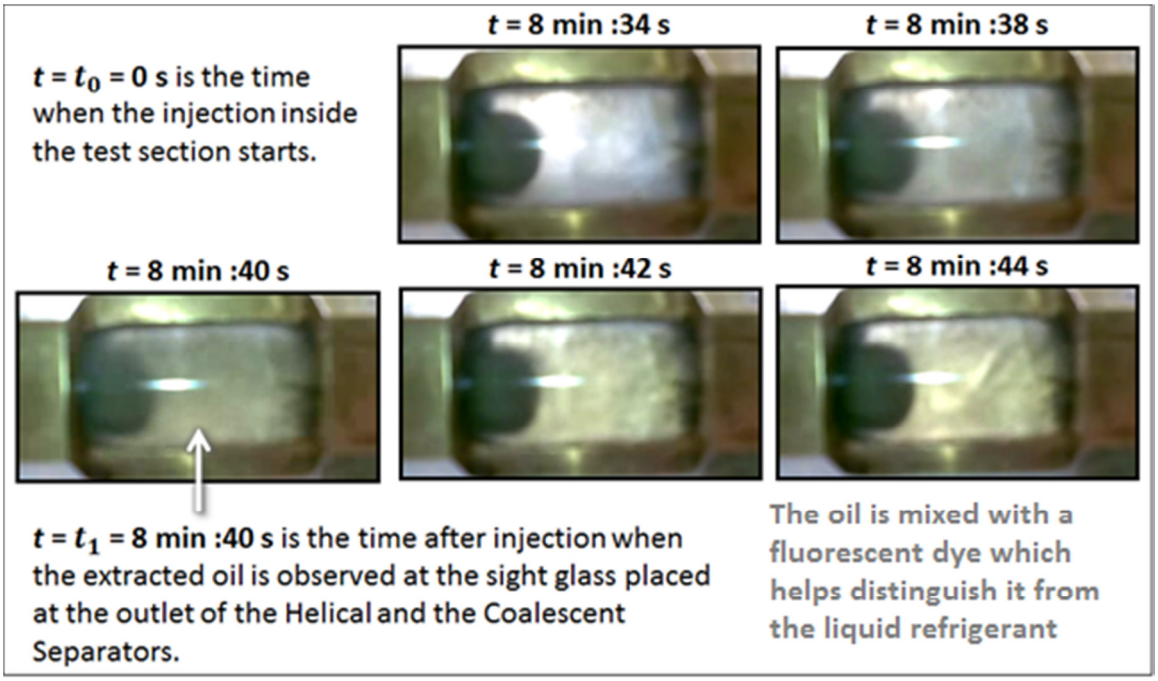

Figure 32: Oil extraction as seen through the sight glass.

3.6.5 Solubility Measurement by Gravimetric Method – Post-injection Test

Cavestri and Schafer (2000) provide R-410A and ISO 32 Mixed Acid POE mixture solubility data for pressures below 247 psia. While performing the experiments, the oil-refrigerant mixtures were subjected to pressures above 247 psia; thus, the literature data from Cavestri and Schafer could not provide the solubility values for the current project. Hence, the solubility of the refrigerant in the injected oil-refrigerant mixture is measured for every injection test.

Measurements of the actual solubility followed the procedure of gravimetric analysis as mentioned in ANSI/ASHRAE Standard 41.4 (ASHRAE 1996). Contrary to the standard's recommendation, a 16.8 in^3 (275 mL) sampling cylinder made of copper was used. The construction of the sampling cylinder is shown in Figure 33. This figure also illustrates the steps used during the sample's weight measurement.

Step1: The sampling cylinder is cleaned by blowing air through it at a high flow rate to remove oil particles. It is then placed in a hot water bath at 104°F (40°C) and evacuated using a vacuum pump until the gauge measures below 10 in Hg for five minutes. This evacuated cylinder is then weighed on a scale ($W1$) capable of measuring 0.0005 lb (0.2 g) with an uncertainty of ±0.005 lb (±2.2 g).

Step2: The sampling cylinder is connected at the ball valve B9 of the system (refer to Figure 11 and Step 2 in Figure 33) on the oil injection line. The oil-refrigerant mixture sample is drawn into the cylinder by opening B9 and ball valve-D in sequence. The valves are then closed and the cylinder is isolated and weighed ($W2$).

Step3: The sampling cylinder is always kept in a vertical position with the capillary side on top after drawing the sample to let the liquid mixture settle at the bottom.

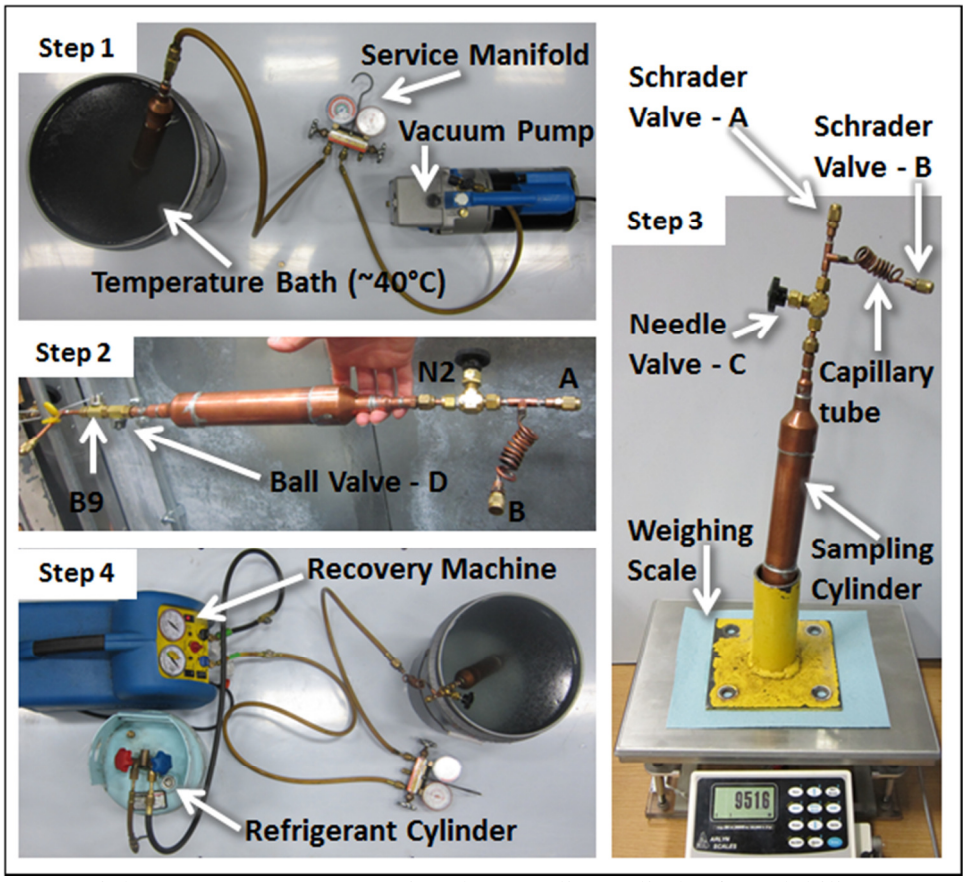

Figure 33: Weight measurement steps using the sampling cylinder for solubility measurement.

Step4: The sampling cylinder is again placed in the hot water bath and after ten minutes the recovery machine is used to recover the refrigerant from the capillary line. The capillary tube and needle valve-C create a pressure drop so that the vapor refrigerant is removed from the cylinder at a very slow rate without having any oil entrained in it. Any traces of the refrigerant are further removed using the vacuum pump and the cylinder is weighed ($W3$). Further, the injected oil-refrigerant solubility is calculated as shown in Equation (3.7).

$$S = \frac{(W2-W3)}{(W3-W1)} \times 100 \tag{3.7}$$

3.6.6 Mapping Test

All the tests had a transient behavior during their oil injection tests. The pre-injection (steady condition) tests provided data for the heat transfer and pressure drop in the absence of oil (OCR =0%). The heat transfer and pressure drop in the absence of oil (OCR =0%) were available for the multiple conditions observed during the transient operation, and were needed to compare the actual heat transfer and pressure drop in the presence of oil (OCR >0%) It was decided to perform a steady state test, also called a mapping test, at "no oil" conditions, at various possible conditions, then use these mapping points to interpolate the "no oil" condition heat transfer ($Q_{air@OCR=0}$) and pressure drop ($\Delta P_{@OCR=0}$) for any system conditions observed during the oil injection test.

For every test, at least two mapping tests were performed to get the mapping points;

a.) One mapping test was the pre-injection test.

b.) The other mapping test was performed at conditions $T_{mchx,i}$, $P_{mchx,i}$, and $\dot{m}_{oil+ref,total}$ observed at the end of injection test, but without injecting oil in the test section (OCR =0%).

c.) If the mapping test did not cover the operating region of the test, then more tests were performed to get the necessary mapping points.

During the mapping tests, every effort was made to ensure that no oil was in the microchannel heat exchanger; very small traces of oil may be present in the fluid lines or trapped in pockets of the header. Figure 34 shows the mapping points covering the operating region of a set of tests. In the figure, the ordinate represents the pressure at the inlet of the microchannel heat exchanger and the abscissa represents the total amount of fluid flowing through the microchannel heat exchanger. For the oil injection tests, both oil and refrigerant flow through the microchannel

heat exchanger and for the mapping test, only pure refrigerant flows through the microchannel heat exchanger.

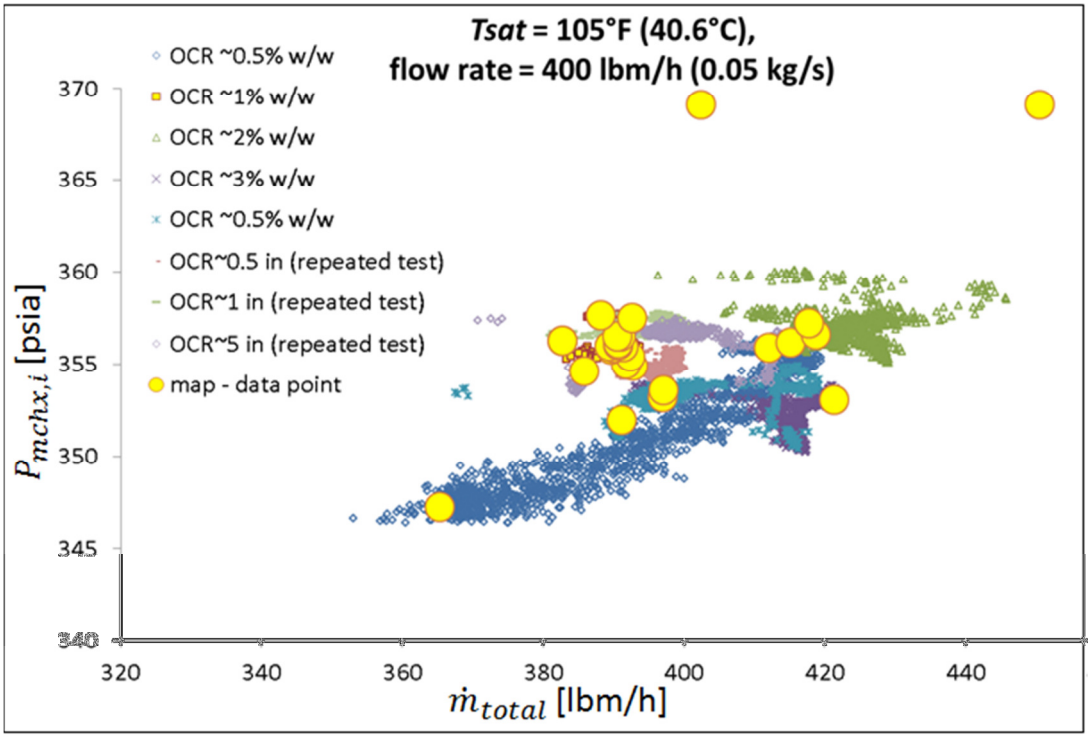

Figure 34: Mapping data along with the operating condition of the test.

CHAPTER IV

IV. DATA REDUCTION

Chapter IV describes the methods and formulas used for the data reduction. The first section 4.1 Refrigerant Lookup Table and its Errors explains the method of selection of the refrigerant properties from the lookup tables and the procedure for their uncertainty calculation. The 4.2 Solubility and Density Determination section explains the use of the data from the literature and its extrapolation to get the solubility value of the oil-refrigerant mixture as a function of the temperature and the pressure.

The 4.3 Assumptions for Calculations section explains important assumptions done for the calculation of the OCR, $HTPF$, $PDPF$, and oil retention. This section, after enumerating the assumptions, gives the actual equations used in the calculations.

The 4.4 OCR Calculation section shows calculation steps for OCR and the 4.7 Oil Retention Calculation section explains the method used to estimate the oil retention, for the Pump-Boiler System as well as for the Vapor Compression Cycle System.

The sections 4.5 Heat Transfer Calculation provides the information of the standards used to calculate the air volume flow rates and the heat transferred from the microchannel heat exchanger to the air. The 4.6 HTPF and PDPF Calculation section presents the calculation procedures for $HTPF$ and $PDPF$, which remain same for both the systems.

4.1 Refrigerant Lookup Table and its Errors

This section explains the method used to create the lookup tables for R-410A and R-134a, and use of the pressure and the temperature values to get the pure refrigerant properties. The properties of the refrigerant selected from the lookup table are further used in analyzing the experimental data. The error propagation from the uncertainties in the measurement sensors to the data selected from the lookup table is also explained. The EES (Engineering Equation Solver) software was used to create the R-410A and R-134a lookup tables to be used in a Microsoft Excel - data reduction and analysis spreadsheet as shown in Appendix F, by running the codes presented in Appendix E. The codes in EES get the refrigerant properties directly from their respective equation of state. The refrigerant properties can also be calculated using the correlations from the literature, but the method that gets the properties directly from their equation of state is chosen as it introduces fewer errors. As the errors are very small in the properties calculated from EES, which should be reflected in the lookup table, their uncertainties are neglected while calculating the propagated errors.

The codes are written in VBA to create functions, shown in Appendix G, to get the refrigerant properties in the sub-cooled and the superheated region as functions of the input pressure and temperature. For the input pressure, the code checks the two consecutive rows in the lookup table between which this pressure value lies. It recovers the saturated liquid or the saturated vapor properties of temperature, specific heat, and enthalpy by interpolating between the two selected rows. The interpolated enthalpy value is either increased in the superheated region or decreased in the sub-cooled region based on the input temperature, interpolated saturated temperature, and interpolated specific heat values. The same approach is used to determine the entropy of the refrigerant at the measurement. By slight modification to these codes, other properties like viscosity or surface tension can be found by interpolation; however these properties should be from the lookup table from EES. These codes can easily be modified to

calculate the refrigerant properties in the two-phase region, if the quality of the refrigerant is known.

The refrigerant or oil pressure calculated using an absolute pressure transducer has some uncertainty; this uncertainty is further reflected when choosing the points from the lookup table. Table 14 demonstrates the method used to get the error propagated from the pressure readings to the temperature readings, when the temperature values are picked from the lookup table of R-410A (Appendix F). The absolute pressure transducer has an error of ±0.65 psi. Columns 1 and 5 of the table are the values from the lookup table for the saturated pressure and the corresponding saturated liquid temperature respectively. Columns 2 and 3 give the high and low pressure by adding and subtracting the pressure errors respectively. The temperature values in column 6 are interpolated corresponding to the high pressure values in column 2, while the temperature values in column 7 are interpolated corresponding to the low pressure values in column 3. Column 8 gives the error in the temperature values corresponding to the high and low temperature values in columns 6 and 7, respectively.

Figure 35 shows a beautiful normal distribution curve of the errors in the saturated liquid temperature from column 8. The standard deviation in the temperature value is σ = 0.11°F. This standard deviation value is calculated using Equation (4.1) and Equation (4.2). The n in the equation is the number of rows in the error column, which is simply the number of data points.

$$\sigma = \sqrt{\frac{1}{n-1}\sum_{i=0}^{n}(T_f error, avg - T_f error_i)^2} \tag{4.1}$$

$$T_f error, avg = \frac{1}{n}\sum_{i=0}^{n}(T_f error_i) \tag{4.2}$$

With a confidence of 95.45%, the error in the saturated liquid temperature reading can be noted as $\delta T_f = \pm 2\sigma = \pm 0.22$°F.

Table 14 Error Propagation from Pressure to Temperature in the Lookup Table.

P_{sat} psia	P_{sat}+ 0.65	P_{sat}- 0.65	P_{sat} error	T_f °F	T_f+ error	T_f- error	T_f error
65.54	66.19	64.89	±0.65	1.83	2.32	1.34	±0.49
66.87	67.52	66.22	±0.65	2.83	3.31	2.34	±0.48
68.23	68.88	67.58	±0.65	3.83	4.30	3.35	±0.48
69.61	70.26	68.96	±0.65	4.83	5.30	4.36	±0.47
71.00	71.65	70.35	±0.65	5.83	6.28	5.36	±0.46
72.42	73.07	71.77	±0.65	6.83	7.28	6.37	±0.45
73.86	74.51	73.21	±0.65	7.83	8.27	7.38	±0.45
75.33	75.98	74.68	±0.65	8.83	9.27	8.39	±0.44
76.81	77.46	76.16	±0.65	9.83	10.26	9.39	±0.43
78.32	78.97	77.67	±0.65	10.83	11.25	10.40	±0.43
79.85	80.50	79.20	±0.65	11.83	12.25	11.41	±0.42
81.40	82.05	80.75	±0.65	12.83	13.24	12.41	±0.42
483.40	484.05	482.75	±0.65	128.70	128.81	128.59	±0.11
489.40	490.05	488.75	±0.65	129.70	129.81	129.59	±0.11
495.50	496.15	494.85	±0.65	130.70	130.80	130.59	±0.11
501.70	502.35	501.05	±0.65	131.70	131.80	131.60	±0.10
507.90	508.55	507.25	±0.65	132.70	132.80	132.60	±0.10
514.20	514.85	513.55	±0.65	133.70	133.80	133.60	±0.10
520.50	521.15	519.85	±0.65	134.70	134.79	134.60	±0.10
526.90	527.55	526.25	±0.65	135.60	135.70	135.51	±0.10
533.40	534.05	532.75	±0.65	136.60	136.70	136.50	±0.10
539.90	540.55	539.25	±0.65	137.60	137.70	137.50	±0.10
546.50	547.15	545.85	±0.65	138.60	138.70	138.50	±0.10
553.10	553.75	552.45	±0.65	139.60	139.70	139.50	±0.10
559.80	560.45	559.15	±0.65	140.60	140.70	140.50	±0.10

	Average	±0.23
	Maximum	±0.49
Confidence	Minimum	±0.10
68.27%	σ	0.11
95.45%	2σ	0.22
99.70%	3σ	0.33

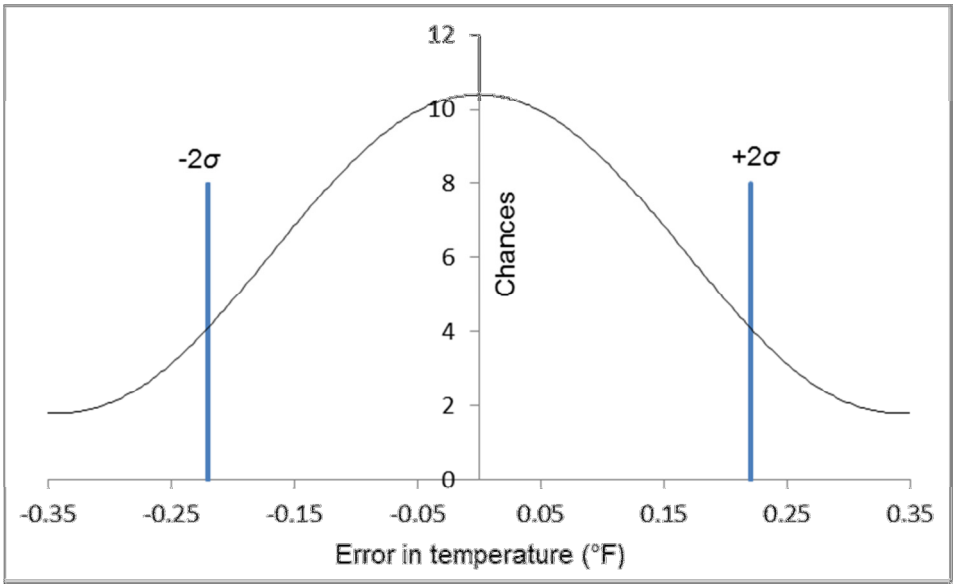

Figure 35: Normal distribution curve of error in temperature.

Table 15 shows the uncertainties calculated using the above procedure for R-410A and R-134a – saturated liquid and saturated vapor temperatures, enthalpies, and specific heats.

Table 15: Uncertainties in properties of R-410A and R-134a obtained from the Lookup Table

Error with confidence of 95.45%	**R-410A**	**R-134a**	**units**
P_{sat}	±0.65	±0.65	psi
T_f	±0.22	±0.24	°F
T_g	±0.22	±0.24	°F
h_f	±0.066	±0.066	Btu/lbm
h_g	±0.034	±0.052	Btu/lbm
$c_{p,f}$	±0.0004	±0.002	Btu/lbm-R
$c_{p,g}$	±0.0003	±0.003	Btu/lbm-R

4.2 Solubility and Density Determination

The refrigerant vapor is dissolved in the oil because of its soluble nature. This solubility varies with the pressure and the temperature. During the experiment, the oil-refrigerant mixture was injected in the test section; the solubility value indicates what percentage of oil is present in the injected mixture.

The solubility (S) is defined as the percentage by weight of refrigerant soluble in oil or lubricant, Equation (4.3), and its unit is expressed as % w/w.

$$S = \frac{m_{ref}}{m_{oil}} \times 100 = \frac{\dot{m}_{ref}}{\dot{m}_{oil}} \times 100 \tag{4.3}$$

The data of solubility for R-410A and ISO VG 32 grade Mixed Acid POE (EMKARATE RL32S) is taken from Cavestri and Schafer (2000) (Figure 36). The future tests of the same project will be done with R-134a and ISO VG 32 grade Mixed Acid POE, and will use the data from Cavestri (1993, 1995).

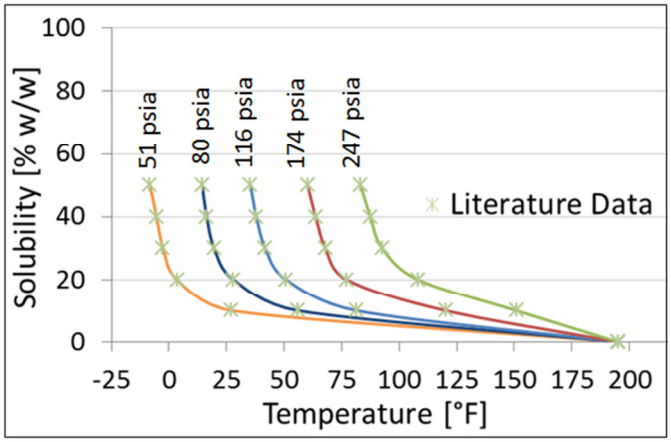

Figure 36: Solubility data for R-410A and ISO 32 Mixed Acid POE, from Cavestri and Schafer (2000).

Cavestri and Schafer provide R-410A and ISO 32 Mixed Acid POE mixture solubility data for pressures below 247 psia. While performing the experiments, the oil-refrigerant mixtures were subjected to pressures above 247 psia; thus, the literature data from Cavestri and Schafer

could not provide the solubility values for the current project. In Figure 37, the region in green is the actual temperature and the pressure of the oil-refrigerant mixture observed while testing, the region in grey consists of the solubility curves plotted using the data provided by Cavestri and Schafer, and the curves in the grey region are same as in Figure 36. The solubility curves outside the grey region are drawn by extrapolating the literature data.

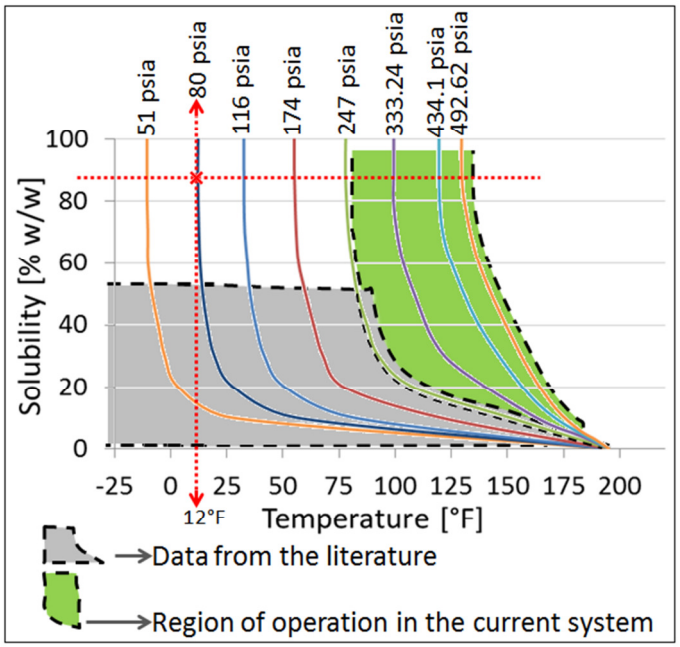

Figure 37: Extrapolation of the solubility data

No research project done in the past, except for Cavestri and Schafer (2000), provides the solubility data for the particular mixture of R-410A and ISO 32 Mixed Acid POE. Hence, it was decided to extrapolate the solubility data of Cavestri and Schafer by applying simple Gibbs' Phase Rule. The extrapolated data was needed to predict the injected mass flow rate of the oil-refrigerant mixture. To account for correct solubility of the injected mixtures, the mixture samples were taken for every oil injection test, whose solubility values were determined using the gravimetric method.

The Gibbs' Phase Rule is shown in Equation (4.4).

$$F = C - P + 2 \quad (4.4)$$

where, F is the degree of freedom or the number of intensive properties, C are the number of components in the mixture, and P are the phases in the mixture at equilibrium. (Note, P is not a pressure in Equation (4.4))

The oil-refrigerant mixture is injected from the oil reservoir, and there are only two components in the mixture, $C = 2$, which are the oil and the refrigerant, the impurities if present are negligible. The two phases that exists in the reservoir are the completely miscible oil-rich solution (which is oil and some amount of refrigerant soluble in it) and the vapor refrigerant. As there are two phases at equilibrium, $P = 2$, and thus, $F = 2$ in Equation (4.4), that is the solubility, S, is a function of two intensive properties, the temperature and the pressure, $S = f(T, P)$.

If the temperature decreases at a constant pressure, the solubility of the refrigerant in the oil increases. Figure 2 (page no.19) shows that for a constant pressure if the temperature decreases, a temperature is reaches when the oil-refrigerant mixture no longer remains completely miscible, and change into a partially miscible mixture, and there exists three phases, $P = 3$, in equilibrium: refrigerant vapor, refrigerant-rich solution, and oil-rich solution. Refer to Figure 3 (page no.20), which shows the three phases existing in equilibrium inside the oil reservoir. For $P = 3$ phases, $F = 1$ in Equation (4.4), that is the solubility is a function of one intensive properties, either temperature or pressure.

The extrapolated curves are shown in Figure 37. The extrapolation was done by extending the solubility curves by hand, after extending the curves manually it was observed that at 86% w/w of the solubility value the slope of the curves became infinite, that is above 86% w/w, the solubility was a function of either temperature or pressure, which followed the Gibbs' Phase Rule. While drawing (extrapolating) the constant pressure curves manually, adjustments

were made to the curves, so that when the slopes of the curves reached infinity the temperature of the mixture were equal to the saturated temperature of R-410A at the particular pressure of the mixture.

For example, consider the solubility curve at constant pressure of 80 psia in Figure 37. For solubility values below 86% w/w, the solubility is a function of temperature and pressure, that is it follows the Gibbs' Phase Rule and there exists two phases, with F = 2. For solubility values above 86% w/w, the solubility is a function of either temperature or pressure, that is it follows the Gibbs' Phase Rule and there exists three phases, with F = 1, and the temperature is $T_{sat,R-410A}$ = 12°F which corresponds to the $P_{sat,R-410A}$ = 80 psia. Similar extrapolation was done to the density data of the R-410A and ISO 32 Mixed Acid POE mixture, which is provided by Cavestri and Schafer (2000), but is not provided in details in this report.

The Generalized Least Squares method is used to get the surface fit Equation (4.5) for the density and solubility data as a function of the mixture temperature (T) and pressure (P). The coefficients for this equation are presented in Table 16.

$$S\ (or\ \rho) = C1 + C2(T) + C3(T^2) + C4(T^3) + C5(P) + C6(P^2) + C7(P^3) + C8(T^2 \cdot P) + C9(T \cdot P^2) + C10(T \cdot P) \tag{4.5}$$

where, T is the temperature of the oil and refrigerant mixture (°F),

P is the pressure of the oil and refrigerant mixture (psia),

ρ is the density of the oil-refrigerant mixture (g/ml), and

S is the solubility, which is the percentage of refrigerant in oil (% w/w).

Table 16: Coefficients for Density and Solubility of R-134a / ISO 32 Mixed Acid POE and R-410A / ISO 32 Mixed Acid POE Mixtures.

Coefficients	R-134a**		R-410A***	
	ρ (g/mL)	S (% w/w)	ρ (g/mL)	S (% w/w)
C1	8.9997E-01	8.1547E-02	1.0768E+00	-2.6992E-03
C2	-2.8311E-03	-5.1411E-01	-1.3292E-03	-1.0631E+00
C3	5.0959E-05	1.4122E-02	1.1477E-05	1.7155E-02
C4	-3.1592E-07	-7.9573E-05	-3.9485E-08	-6.6241E-05
C5	2.5435E-03	8.3344E-01	5.0528E-04	8.1683E-01
C6	1.1428E-06	1.6751E-03	2.2792E-06	1.4166E-03
C7	2.7461E-09	-2.3558E-07	-3.3620E-09	-2.6131E-07
C8	3.2129E-07	1.1493E-04	4.0496E-08	5.4828E-05
C9	-3.1501E-08	-1.2536E-05	-3.4687E-09	-7.0633E-06
C10	-5.2546E-05	-2.0734E-02	-1.1541E-05	-1.4010E-02
Error*	±0.0405 g/ml	±6.2% w/w	±0.005 g/ml	±4.2% w/w
T range	-30 to 125°F	-30 to 125°F	15 to 200°F	15 to 300°F
P range	10 to 495 psia	10 to 495 psia	15 to 245 psia	50 to 500 psia
Data range	0.76 to 1.18 g/mL	3 to 58 % w/w	0.95 to 1.22 g/mL	0 to 86% w/w

*Error is with the confidence of 95.45%.
** Density and Solubility of R-134a / ISO 32 Mixed Acid POE are not extrapolated.
*** Density and Solubility of R-410A / ISO 32 Mixed Acid POE are extrapolated.

VBA codes are also written to interpolate the solubility value as a function of the mixture temperature (T) and pressure (P) from the lookup table created in a Microsoft Excel spreadsheet from the available map (Cavestri (1993, 1995), and extrapolated data from (Cavestri and Schafer 2000)). The solubility values are then used to predict the mass flow rate of the injected oil-refrigerant mixture.

4.3 Assumptions for Calculations

1.) Solubility of the refrigerant in the injected oil was measured immidiately after every injection test, and this solubility is considered to be constant for the complete duration of the oil injection.

Reason: The oil reservoir holding the injected oil-refrigerant mixture (the oil and the refrigerant soluble in it) has a capacity of 4 gallons (15.1 L). The injection gear pump continuously circulates the oil in the 2.5 ft (0.88 m) tall oil reservoir. During the injection test the circulation is stopped because the same injection gear pump is used to inject the oil-refrigerant mixture from the bottom of the oil reservoir into the test section. Before the injection test, the temperature and pressure in this reservoir are maintained constant by using an electric heater at the bottom of the oil reservoir and using a pressure equalization line. The stratification of the oil-refrigerant mixture column inside the oil reservoir starts as the vapor refrigerant, which separates from the oil in the equilibrium condition, tends to rise due to buoyancy. The solubility should also decrease with the decrease in the hydrostatic pressure along the height of the tank. As the rate of rise of the refrigerant vapor due to the buoyancy effect is small, and also the change in the hydrostatic pressure from the bottom to the top of the tank is less than 1.5 psi (10.3 kPa), thus, the rate of change in the solubility values at different levels in the oil reservoir is very low. That is, during the ~30 min of injection test the solubility in the oil reservoir remains constant. It is ascertained that there is no significant change in the temperature and pressure of the injected mixture at the bottom of the oil reservoir where it is measured. This finding supports the assumption that the solubility is constant throughout the test.

2.) The helical and coalescent separator's efficiencies are very small, are neglected.

Reason: Once the steady state condition during the injection test is achieved, the fraction of the entrained oil in the vapor refrigerant cannot be extracted at the separators, as the extraction efficiency is less than 100%. The oil which is not extracted flows to the test section and returns to the oil separators at a constant mass flow rate of $\delta\dot{m}_{oil}$. The mass balance shown in Figure 18 explains how a small amount of oil always circulates though the test section at a constant mass flow rate of $\delta\dot{m}_{oil}$ during the steady state of the injection test.

3.) Once the steady state in the injection test is achieved, the amount of pure oil injected is equal to the amount of pure oil extracted.

Reason: The mass balance in Figure 18 shows that the mass flow rate of the pure oil ($\dot{m}_{oil,inj}$) which is injected from the oil reservoir into the test section, is equal to the mass flow rate of the pure oil extracted to the oil level tank by the helical and coalescent separators. Also, the rate at which the oil-refrigerant mixture that is lost from the oil reservoir is collected in the oil level tank is given by $\Delta M/\Delta t_{\text{Oil Level Tank}} = -\Delta M/\Delta t_{\text{Oil Reservoir}} = (\dot{m}_{oil,inj} + \dot{m}_{ref,inj})$.

4.) The mass flow rate of the refrigerant ($\delta\dot{m}_{ref}$) received by the oil reservoir from the pressure equalization line is negligible.

Reason: Refer to Figure 11 and Figure 18, Valve N4 is always closed, and the opening to the needle valve, N5, is very small. The small opening allows a few molecules of vapor refrigerant to enter the oil reservoir to pressurize it, so that the amount of refrigerant received by the massive oil reservoir is negligible. Hence the mass flow rate ($\delta\dot{m}_{ref}$) is neglected during the data reduction when calculating the refrigerant flow rate through the test section.

4.4 *OCR* Calculation

The oil-refrigerant mixture is injected into the test section at a mass flow rate of $\dot{m}_{oil+ref,inj}$, shown in Equation (4.6). This mixture can be either oil-rich or refrigerant-rich based on the solubility at that condition. The solubility (S) value is determined by the Gravimetric Test performed after every injection test using the sampling cylinder. This solubility is expressed as the percentage of the amount of pure refrigerant injected to the amount of pure oil injected in the mixture shown in Equation (4.7). The amount of pure refrigerant present in the oil-refrigerant mixture is given by Equation (4.8), and the amount of pure oil in the same injected mixture is given by Equation (4.9).

$$\dot{m}_{oil+ref,inj} = \dot{m}_{ref,inj} + \dot{m}_{oil,inj} \tag{4.6}$$

$$S = \left(\dot{m}_{ref,inj}/\dot{m}_{oil,inj}\right) \times 100 \tag{4.7}$$

$$\dot{m}_{ref,inj} = {\dot{m}_{oil+ref,inj}}\Big/{\left(1 + \frac{100}{S}\right)} \tag{4.8}$$

$$\dot{m}_{oil,inj} = {\dot{m}_{oil+ref,inj}}\Big/{\left(1 + \frac{S}{100}\right)} \tag{4.9}$$

In the Pump-Boiler System, the liquid refrigerant is pumped by the refrigerant gear pump at a mass flow rate of $\dot{m}_{oil+REF,gp}$. This refrigerant rich mixture has injected oil present in it, which can be inferred through the mass balance shown in Figure 18. The helical and coalescent separators placed after the gear pump extract this injected oil and some amount of refrigerant, and transfer the remaining pure refrigerant ($\dot{m}_{ref,test-section}$) to the test section. Equation (4.10) shows the mass balance equation at the separators.

$$\dot{m}_{ref,test-section} = \dot{m}_{oil+REF,gp} - \dot{m}_{oil,inj} - \dot{m}_{ref,by-passed} \tag{4.10}$$

The oil-refrigerant mixture, when injected before the microchannel, has refrigerant present in it. This injected refrigerant flow rate ($\dot{m}_{ref,inj}$) added to the pure refrigerant flow rate entering the test section gives the total pure refrigerant mass flow rate through the microchannel heat exchanger, as shown in Equation (4.11).

$$\dot{m}_{ref,mchx} = \dot{m}_{ref,test-section} + \dot{m}_{ref,inj} \tag{4.11}$$

The oil circulation ratio is the ratio of the mass flow rate of the pure oil to the net mass flow rate through the microchannel heat exchanger as shown Equation (4.12).

$$OCR = \left(\dot{m}_{oil,inj} \Big/ \left(\dot{m}_{oil,inj} + \dot{m}_{ref,mchx} \right) \right) 100 \tag{4.12}$$

The OCR calculation for the test in the Vapor Compression Cycle system was relatively simple. The Coriolis mass flow meter placed after the microchannel heat exchanger measured the total flow rate of the fluid ($\dot{m}_{oil,inj} + \dot{m}_{ref,mchx}$) flowing through it. The solubility value was used to calculate the amount of pure oil ($\dot{m}_{oil,inj}$) injected into the test section. These values, when substituted into Equation (4.12), gave the OCR for the test.

It is to be noted that the investigators refer to the amount of oil circulating in the system as either “oil mass fraction” (OMF), “oil concentration,” or “oil circulation ratio” (OCR).

4.5 Heat Transfer Calculation

The volume flow rate of the air through the microchannel heat exchanger is calculated using the formulas given in ANSI/ASHRAE Standard 41.2 (ASHRAE 1987). These equations require the properties of air, which are calculated from ASHRAE Handbook – Fundamentals (ASHRAE 2001). The equations to calculate the air properties and CFM are used to create the VBA functions and are presented in Appendix D. The dry bulb temperature of the ambient air ($T_{air,amb}$), the dry bulb temperature of the supply air ($T_{air,supply}$) of the microchannel heat exchanger, the CFM value calculated at the nozzle bank, the density of the air (ρ_{air}) at the heat exchanger, and a constant value of specific heat (c_p= 0.2405 Btu/lbm-°F, as it does not vary in the operating range), are used to calculate the heat transferred by the microchannel heat exchanger – condenser to the air (Q_{air} in Btu/h), as shown in Equation (4.13).

$$Q_{air} = \rho_{air} \cdot CFM \cdot 60 \cdot c_p \cdot (T_{air,supply} - T_{air,amb}) \tag{4.13}$$

4.6 *HTPF* and *PDPF* Calculation

The heat transferred by the microchannel to the air during a steady state oil injection test ($OCR > 0\%$) is termed $Q_{air@OCR}$. If a test is performed without injecting any oil ($OCR = 0\%$),"no oil injection test," having the same inlet pressure, inlet temperature, and total refrigerant flow rate as that given in the former test conditions, then the heat transferred to the air in the absence of oil is termed $Q_{air@OCR=0}$. It is important to note that the pure refrigerant mass flow rate in a "no oil injection test" is equal to the total (refrigerant and oil) mass flow rate through the microchannel heat exchanger during a similar oil injection test.

The heat transfer penalty factor ($HTPF$) is calculated by taking the ratio of heat transferred by the microchannel to the air in the presence of oil to the heat transferred in the absence of oil under the same operating conditions, as shown in Equation (4.14).

$$HTPF = {Q_{air@OCR}}\Big/{Q_{air@OCR=0}} \tag{4.14}$$

As the oil injection test and the "no oil injection test" are performed under the same operating conditions, the density, the CFM, and the specific heat of the air remain constant; thus, the $HTPF$ can also be calculated by taking the ratios of $\Delta T_{air} = (T_{air,supply} - T_{air,amb})$ as shown in Equation (4.15).

$$HTPF = {\Delta T_{air@OCR}}\Big/{\Delta T_{air@OCR=0}} \tag{4.15}$$

The pressure drop penalty factor ($PDPF$) is calculated by taking the ratio of the pressure drop in the microchannel in the presence of oil to the pressure drop in the absence of oil under the same operating conditions, as shown in Equation (4.16). The pressure drop values are measured using a differential pressure transducer placed between the inlet and the outlet lines of the microchannel heat exchanger.

$$PDPF = {\Delta P_{@OCR}}\Big/{\Delta P_{@OCR=0}} \tag{4.16}$$

When the oil injection test is performed, the pressure drop ($\Delta P_{@OCR}$) is measured and the heat transferred ($Q_{air@OCR}$) is calculated for every time step of two seconds. The $HTPF$ and the $PDPF$ are then calculated at every time step and averaged over the entire time period when the steady state is observed. For every time step, a heat transfer ($Q_{air@OCR=0}$) and pressure drop ($\Delta P_{@OCR=0}$) value is required, as they represent a "no oil" test with similar operating conditions at that time step. It is difficult and time consuming to perform the "no oil injection tests" under exactly the same operating conditions. To overcome this difficulty, mapping tests are performed over the operating region. These mapping tests also include the data from the pre-injection test, from which the data for the heat transferred and the pressure drop are obtained for the "no oil" condition. This mapping data is used to interpolate the heat transferred ($Q_{air@OCR=0}$) and pressure drop ($\Delta P_{@OCR=0}$) for every time step.

4.7 Oil Retention Calculation

Method-1 describes the steps used to get the amount of oil mass retained in the microchannel heat exchanger when the tests were performed on the Vapor Compression Cycle System, while Method-2 describes the steps when tests were performed on the Pump-Boiler System. Method-1 also describes the steps to get the oil retention volume and the normalized oil retention volume in the microchannel heat exchanger.

Method-1: (used for the Vapor Compression Cycle System)

The oil-refrigerant mixture was first injected downstream or after the microchannel heat exchanger at port-B with the help of the injection gear pump at a definite mass flow rate of $\dot{m}_{oil+ref,inj}$. This mass flow rate depended on the OCR requirement for the test and the solubility at the oil reservoir. The solubility value was used to get the mass flow rate of the pure oil injected at port-B ($\dot{m}_{oil,inj,port-B}$). This value was measured for every time step (t) and is shown in the third column of Table 17. The Trapezoidal Rule described in Equation (4.17) gives the mass of pure oil injected ($\hat{m}_{oil,inj,port-B,t}$) at each time step as in column 4. The cumulative amount of oil mass injected ($m_{oil.inj,port-B,t}$) by the gear pump in the test section from the beginning of the injection process to the current time step (k) as shown in column 5 is calculated using Equation (4.18).

Table 17: Measurement of Oil Injected into the Test Section.

k	time = t [s]	$\dot{m}_{oil,inj,port-B,t}$ [lb/h (g/s)]	$\hat{m}_{oil,inj,port-B,t}$ [lb (g)]	cumulative $m_{oil.inj,port-B,t}$ [lb (g)]
1	t1=0	0	0	0
2	t2	$\dot{m}_{oil,inj,port-B,2}$	$\hat{m}_{oil,inj,port-B,2}$	$m_{oil.inj,port-B,2}$
3	t3	$\dot{m}_{oil,inj,port-B,3}$	$\hat{m}_{oil,inj,port-B,3}$	$m_{oil.inj,port-B,3}$
4	t4	$\dot{m}_{oil,inj,port-B,4}$	$\hat{m}_{oil,inj,port-B,4}$	$m_{oil.inj,port-B,4}$
5	t5	-	-	-
6	-	-	-	-

$$\hat{m}_{oil,inj,port-B,t} = \left(\dot{m}_{oil,inj,port-B,t} + \dot{m}_{oil,inj,port-B,(t-1)}\right) \cdot \left(t_t - t_{(t-1)}\right) \cdot (1/2) \tag{4.17}$$

$$m_{oil.inj,port-B,t} = \sum_{t=1}^{k} \hat{m}_{oil,inj,port-B,t} \tag{4.18}$$

The oil injected in the test section is then extracted, stored, and measured at the oil level tank for a unit time interval. The volume measured through the sight glass is converted to mass extracted using the density at the measured time steps ($m_{oil,ext-B}$). The temperature and pressure of the extracted oil are used to get the density and the solubility from literature data, which in turn are used to calculate the mass of pure oil extracted.

The steps explained above help in plotting the mass of oil injected and extracted on the mass vs. time graph. (Refer to Figure 31.) In the steady state injection tests, two straight lines are obtained, one for the injected oil mass, $m = (a1)t + b1$, and the other for the extracted oil mass, $m = (a2)t + b2$. If the steady state oil injection test is observed between time t_2 and time t_3, then the averaged difference between the injection and the extraction lines in the steady state period $(t_3 - t_2)$ gives the amount of oil mass retained (ORM) in the test section, as shown in Equation (4.19). Solving the integral gives Equation (4.20). (Note, the definition and subscript of time in Figure 31 and Table 17 are different.)

$$ORM = time\ averaged\ \Delta m = {\int_{t_2}^{t_3}\left((a1)t + b1 - (a2)t - b2\right)dt}\Big/{(t_3 - t_2)} \tag{4.19}$$

$$ORM = time\ averaged\ \Delta m = (a1 - a2) \cdot {(t_3 - t_2)}/{2} + (b1 - b2) \tag{4.20}$$

The injection test explained above was used when the oil was injected at port-B of the microchannel heat exchanger. Thus, the amount of oil retained in the connecting lines of the test section after the microchannel heat exchanger and before the extraction point is OR_{line}. When

another test is performed under the same operating conditions using port-A of the micro-channel heat exchanger for the injection of oil, the amount of oil retained in the microchannel heat exchanger and the connecting lines is $OR_{mchx+line}$. The difference between the two gives the amount of mass of oil retained in the microchannel heat exchanger (ORM_{mchx}), as shown in Equation (4.21).

$$ORM_{mchx} = OR_{mchx+line} - OR_{line} \tag{4.21}$$

Method-2: (used for the Pump-Boiler System)

With the modification of the system, a few problems were encountered while measuring the oil extracted, as explained in section 3.6.4 Extraction Test. Thus, the oil retention measurement was simplified.

The section 4.3 Assumptions for Calculations, explains why the injected oil mass flow rate was equal to the extracted oil mass flow rate. This makes $a1 = a2 = \dot{m}_{oil,inj}$, in Equation (4.20), because $a1$ is the rate at which oil is injected and $a2$ is the rate at which oil is extracted. Time t_0 is the time when the injection starts, and t_1 is the time when the extraction is observed in the sight glass. Then the intercepts on the ordinate become, term $b1 = -\dot{m}_{oil,inj} \cdot t_0$ and $b2 = -\dot{m}_{oil,inj} \cdot t_1$ (refer to Figure 31). This action simplifies Equation (4.20) to Equation (4.22).

$$ORM = (b1 - b2) = \dot{m}_{oil,inj} \cdot (t_1 - t_0) \tag{4.22}$$

The rest of the steps to calculate the oil mass retained in the microchannel heat exchanger are the same as in Method-1.

The mass of oil retained in the microchannel heat exchanger is converted to the volume of oil retained using the density of the pure oil, as shown in Equation (4.24). The density data for the pure POE are obtained from the available maps (Cavestri 1993, 1995, and Cavestri and Schafer 2000), and is expressed as a function of the temperature, Equation (4.23).

$$\rho_{oil} = (-0.0005) \cdot \mathrm{T} + 1.0622 \tag{4.23}$$

$$ORV = ORM/\rho_{oil} \tag{4.24}$$

The oil retention volume is further normalized by dividing it by the internal volume of the microchannel heat exchanger (V_{mchx}); the microchannel heat exchanger used has an estimated internal volume of 0.64 gallon (2.4357 L). The normalized oil retention volume (ORV_N) is shown in Equation (4.25).

$$ORV_N = {ORV}/{V_{mchx}} \tag{4.25}$$

4.8 Uncertainty Propagation in the Calculations

The following section explains the rule of uncertainty propagation outlined in Taylor (1996), which was used extensively to determine the transfer of the sensor and instrumentation errors to the final results of the OCR, $HTPF$, and $PDPF$ calculations. It is important to note that in this report, the terms "error" and "uncertainty" are used interchangeably.

The rule of uncertainty propagation is as follows. If the parameters in Equation (4.13), ρ_{air}, CFM, $\Delta T_{air} = (T_{air,supply} - T_{air,amb})$ have independent and random uncertainties of $\delta\rho_{air}$, δCFM, and $\delta\Delta T_{air}$ respectively, and Q_{air} is a function of these parameters, then the uncertainty δQ_{air} is the quadratic sum of the partial uncertainties due to each of the separate uncertainties, as shown in Equation (4.26).

$$\delta Q_{air} = \sqrt{\left[\left(\frac{\partial Q_{air}}{\partial \rho_{air}}\delta\rho_{air}\right)^2 + \left(\frac{\partial Q_{air}}{\partial CFM}\delta CFM\right)^2 + \left(\frac{\partial Q_{air}}{\partial \Delta T_{air}}\delta\Delta T_{air}\right)^2\right]} \quad (4.26)$$

4.8.1 Uncertainty in Heat Transfer Calculation

Figure 38, Figure 39, and Figure 40 shows the dependence of the calculated heat transfer (Q_{air}) and its uncertainty (δQ_{air}) on the values and uncertainties of the air volume flow rate (CFM), the density of air (ρ_{air}), and the air temperature drop at the microchannel heat exchanger(ΔT_{air}), respectively. The δQ_{air} depends on the values of the CFM and the ρ_{air} used in Equation (4.13); the δQ_{air} increases with increase in the input value of the CFM and the ρ_{air} (Figure 38 and Figure 39). For the same value of the CFM or the ρ_{air} there is no significant change in the δQ_{air} with change in either δCFM or the $\delta\rho_{air}$. Figure 40 shows that the value of Q_{air} increase significantly with increase in the value of ΔT_{air}; while the uncertainty δQ_{air} change is small because of change in the ΔT_{air} compared to change in the uncertainty because of the CFM or the ρ_{air}.

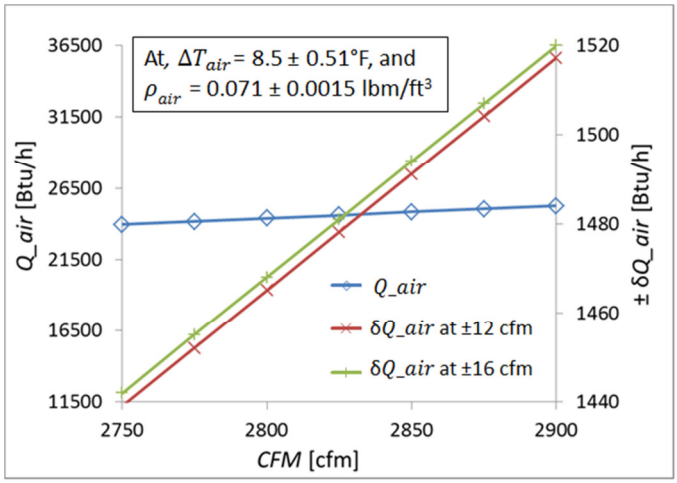

Figure 38: Change in *Q_air* with *CFM*.

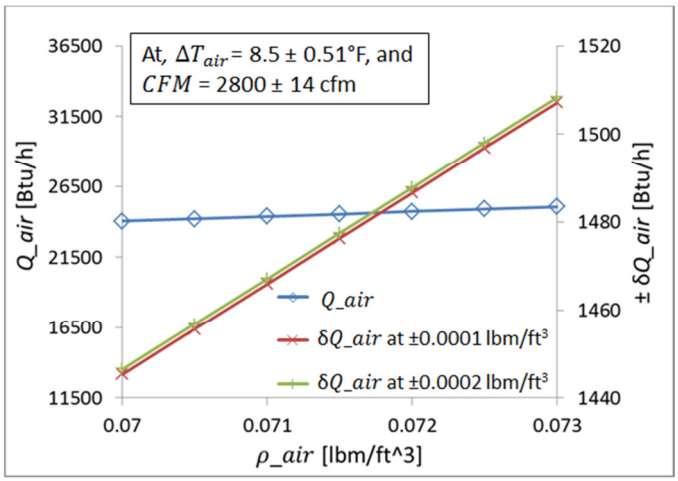

Figure 39: Change in *Q_air* with *ρ_air*.

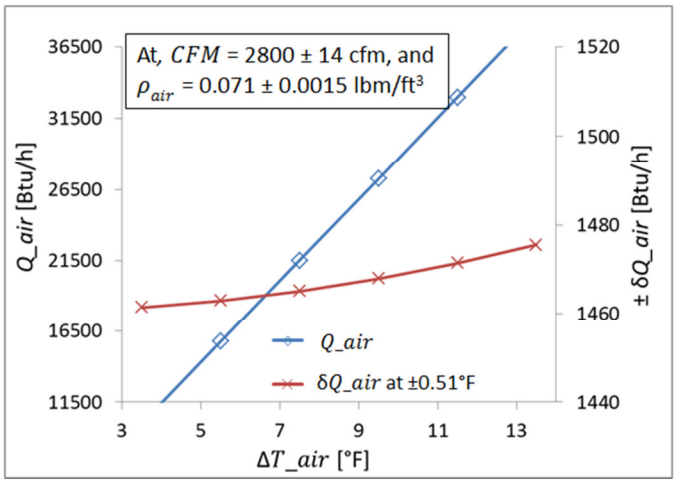

Figure 40: Change in *Q_air* with *ΔT_air*.

The CFM calculated, as explained in section 4.5 Heat Transfer Calculation, is a function of pressure drop across the nozzle bank ($\Delta P_{air,N}$), the density of the air (ρ_{air}), and the nozzles dimension. The dimension of the nozzles in the nozzle bank remains constant and the density of the air changes by small value, thus they have insignificant effect on the change in the CFM value. The CFM value changed significantly with the change in the pressure drop across the nozzle bank (refer to plot (a.) in Figure 41). It was also noticed that the uncertainty propagated in the CFM value depended more on the uncertainty in the calculated air density than others parameters (refer to plot (b.) in Figure 41), thus attempts were always made to measure the air properties accurately to reduce the error in the density calculated.

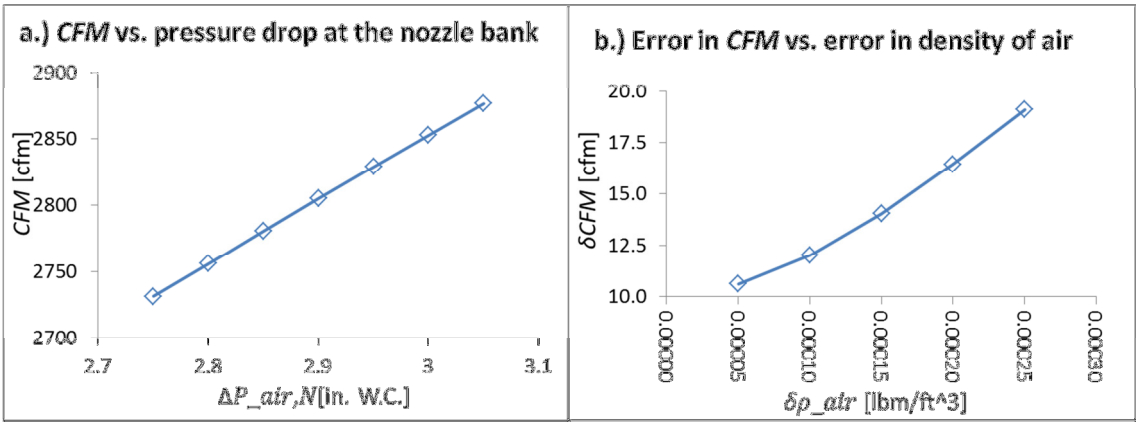

Figure 41: Change in *CFM* and its uncertainties.

4.8.2 Uncertainty in *HTPF* Calculation

Applying the rule of uncertainty propagation by Taylor (1996) to the Heat Transfer Penalty Factor ($HTPF$) Equation (4.14), gives an Equation (4.27) to calculate the uncertainty $\delta HTPF$.

$$\delta HTPF\_Q_{air} = \sqrt{\left[\left(\frac{1}{Q_{air@OCR=0}}\delta Q_{air@OCR}\right)^2 + \left(\frac{-Q_{air@OCR}}{Q_{air@OCR=0}^{\ 2}}\delta Q_{air@OCR=0}\right)^2\right]} \quad (4.27)$$

The uncertainty presented in Equation (4.27) is the uncertainty in $HTPF$based on the heat transfer calculation. The rule of uncertainty propagation can also be applied to Equation (4.15) to calculate the uncertainty in $HTPF$ based on the temperature drop measurement, $HTPF\_\Delta T_{air}$, Equation (4.28).

$$\delta HTPF\_\Delta T_{air} = \sqrt{\left[\left(\frac{1}{\Delta T_{air@OCR=0}}\delta \Delta T_{air@OCR}\right)^2 + \left(\frac{-\Delta T_{air@OCR}}{\Delta T_{air@OCR=0}^{\ 2}}\delta \Delta T_{air@OCR=0}\right)^2\right]} \quad (4.28)$$

While calculating the $\delta HTPF$, the uncertainty $\delta Q_{air@OCR=0}$ was taken equal to the uncertainty $\delta Q_{air@OCR}$. This was done because the $HTPF$, which is the ratio of $\delta Q_{air@OCR}$ and $\delta Q_{air@OCR=0}$, always had its calculated value between 0.85 and 1.5, that is the heat transfer value in the numerator and the denominator in its ratio were always close to each other, hence their uncertainties were same. Equation (4.27) was simplified accordingly to get a new Equation (4.29).

$$\delta HTPF = \sqrt{\left[\left(HTPF\frac{\delta Q_{air}}{Q_{air@OCR}}\right)^2 + \left(HTPF^2\frac{\delta Q_{air}}{Q_{air@OCR}}\right)^2\right]} \quad (4.29)$$

Equation (4.29) simplification leads to Equation (4.30) which expresses the fractional uncertainty of $HTPF$ as a function of the fractional uncertainty of $Q_{air@OCR}$.

$$\frac{\delta HTPF}{HTPF} = \sqrt{1 + HTPF^2}\cdot\frac{\delta Q_{air}}{Q_{air@OCR}} \quad (4.30)$$

The calculated test results of $\frac{\delta HTPF}{HTPF}$ when plotted against $\frac{\delta Q_{air}}{Q_{air@OCR}}$ (refer to Figure 42), shows agreement with Equation (4.30). Each diagonal dotted line in Figure 42 is the slope ($\sqrt{1 + HTPF^2}$) at various $HTPF$ values.

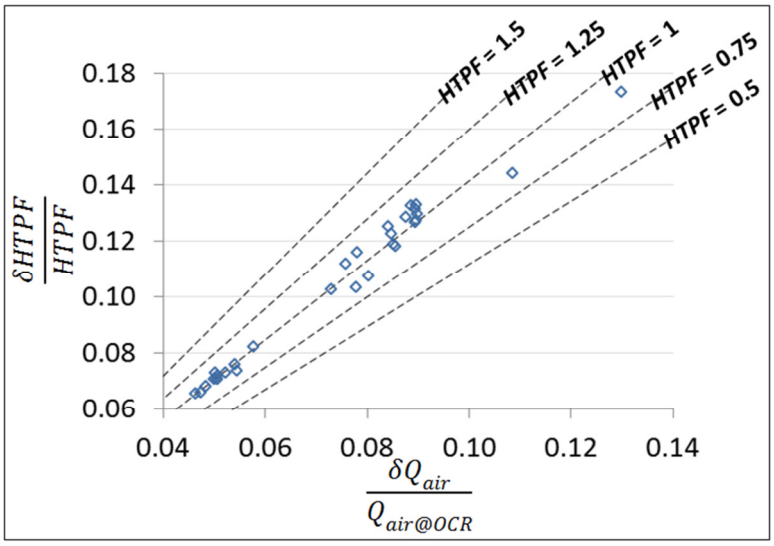

Figure 42: Fractional uncertainty of *HTPF* as a function of the fractional uncertainty of $Q_{air@OCR}$.

4.8.3 Uncertainty in *PDPF* Calculation

Similar to $HTPF$ uncertainty analysis, applying the rule of uncertainty propagation by Taylor (1996) to the Pressure Drop Penalty Factor ($PDPF$) Equation (4.16), gives an Equation (4.31) to calculate the uncertainty $\delta PDPF$.

$$\delta PDPF = \sqrt{\left[\left(\frac{1}{\Delta P_{@OCR=0}}\delta\Delta P_{@OCR}\right)^2 + \left(\frac{-\Delta P_{@OCR}}{\Delta P_{@OCR=0}^{\ 2}}\delta\Delta P_{@OCR=0}\right)^2\right]} \tag{4.31}$$

The uncertainty $\delta\Delta P_{@OCR=0}$ of the mapping data and the uncertainty $\delta\Delta P_{@OCR}$ of the pressure drop for tests with $OCR > 0\%$ were same and equal to ±0.03 psi (according to the specification sheet of the Differential Pressure Transducer provided by the manufacturer). Equation (4.31) was simplified accordingly to get a new Equation (4.32).

$$\delta PDPF = \sqrt{\left[\left(PDPF\,\frac{\delta\Delta P_{@OCR}}{\Delta P_{@OCR}}\right)^2 + \left(PDPF^2\,\frac{\delta\Delta P_{@OCR}}{\Delta P_{@OCR}}\right)^2\right]} \tag{4.32}$$

Equation (4.32) simplification leads to Equation (4.33) which expresses the fractional uncertainty of $PDPF$ as a function of the fractional uncertainty of $\Delta P_{@OCR}$.

$$\frac{\delta PDPF}{PDPF} = \sqrt{1 + PDPF^2}\cdot\frac{\delta\Delta P_{@OCR}}{\Delta P_{@OCR}} \tag{4.33}$$

The calculated test results of $\frac{\delta PDPF}{PDPF}$ when plotted against $\frac{\delta\Delta P_{@OCR}}{\Delta P_{@OCR}}$ (refer to Figure 43), shows agreement with Equation (4.33). Each diagonal dotted line in Figure 43 is the slope ($\sqrt{1 + PDPF^2}$) at various $PDPF$ values.

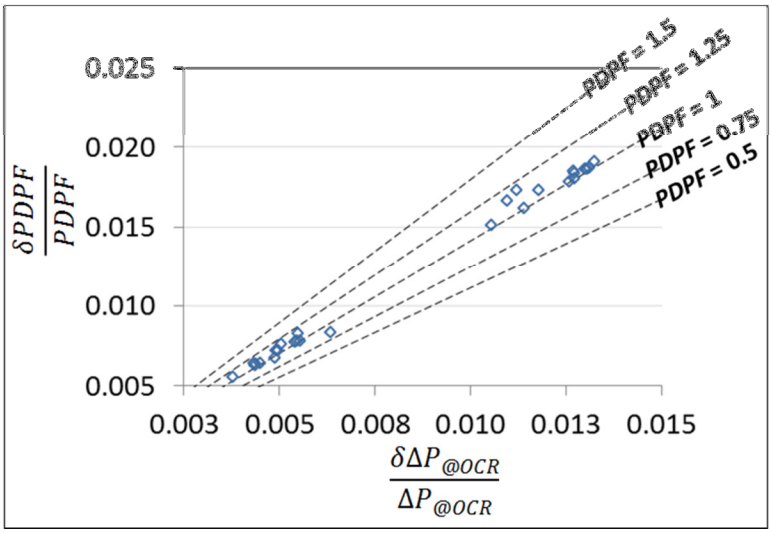

Figure 43: Fractional uncertainty of *PDPF* as a function of the fractional uncertainty of $\Delta P_{@OCR}$

4.8.4 Uncertainty in OCR Calculation

Figure 44 shows uncertainties in the measured solubility values which were calculated according to the method described by Taylor (1996). In $P_{oil\ reservoir} < 365$ psia tests, the uncertainties in the calculated solubility values increased from ±1% w/w (at 20% w/w) to ±2.7% w/w (at 75% w/w) with a quadratic trend. In $P_{oil\ reservoir} \approx 495$ psia tests, the weights of the oil-mixture samples collected in the sampling cylinder were high; this reduced the fractional uncertainties of the weights measured at the weighing scale. Thus, the calculated solubility values had comparatively lower uncertainties.

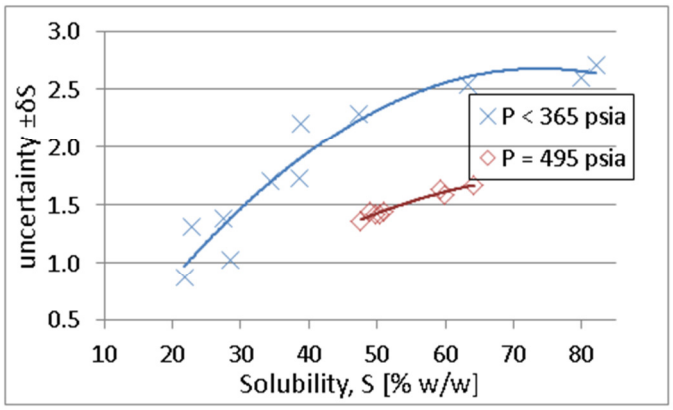

Figure 44: Error in the solubility measured with the gravimetric method.

The uncertainties in the solubility values were propagated to the errors in the OCRs. The errors in the OCRs also depended on the errors in the measured mass flow rates of the refrigerant and the injected oil-refrigerant mixture. The use of the Coriolis mass flow meter resulted in extremely small uncertainties at the measured mass flow rates, which means that the uncertainties in the solubility dominated the errors in the OCRs. Figure 45 shows that the average calculated fractional uncertainties in the OCRs were ±0.1%.

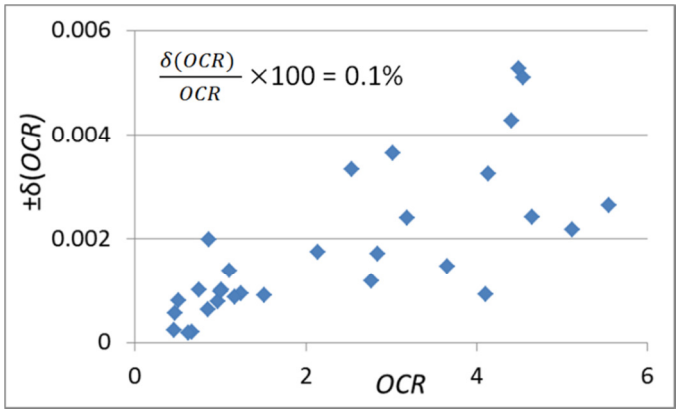

Figure 45: Uncertainties in the calculated OCRs.

Accurate measurement of the solubility values of the injected oil-refrigerant mixture by the gravimetric method instead of relying on the solubility data from the literature considerably reduced the uncertainty propagated to the calculated OCRs.

4.8.5 Correction of the Random Errors

Errors are classified into systematic and random errors. Systematic errors push the results in same direction. To eliminate the statistical uncertainties, which oppose the accurate measurements, the instruments are calibrated against good ones. Random errors are inherent, unpredictable, and unavoidable. The fluctuations in the sensors/instruments output due to mechanical vibration, electric noise, or change in ambient temperature, and the human error in interpretation of the reading are reasons for random errors. The random uncertainties, which oppose precise measurements, can be treated with the statistical analysis. Statistical analysis is good only for the random uncertainties. In the following paragraphs, it is assumed that all the sources of systematic uncertainties are identified and rectified to a tolerable level. Now the remaining sources of errors are random errors.

The OCR, $HTPF$ and $PDPF$ values are calculated for number of times during the steady state injection test, which are then averaged to get their best values. (Refer the graphs in the Appendix B, which shows the calculations of $HTPF$s and $PDPF$s done for every two seconds during the injection test.) For an example, the calculation of $PDPF$ is repeated for n number of times during the steady state injection test, then the best estimate $PDPF_{best}$ is the average or mean $\overline{PDPF}$ of the n measurements, as shown in Equation (4.34).

$$PDPF_{best} = \overline{PDPF} = \frac{\sum_{i=0}^{n} PDPF_i}{n} \tag{4.34}$$

The standard deviation σ_{PDPF} of the n measurements, Equation (4.35), is the estimate of the average uncertainty of the measurements. The standard deviation can be described as Root Mean Square (RMS) deviation of the n measurements.

$$\sigma_{PDPF} = \sqrt{\frac{1}{n-1}\sum_{i=0}^{n}(PDPF_i - \overline{PDPF})^2} \tag{4.35}$$

The results of the n measurements will have a normal (or Gaussian) distribution around the mean value $\overline{PDPF}$ which forms a bell-shaped curve. The uncertainty in the value of $PDPF$ can be represented by:

$PDPF = \overline{PDPF} + 1(\sigma_{PDPF})$, with 68.27% confidence,

$PDPF = \overline{PDPF} + 2(\sigma_{PDPF})$, with 95.45% confidence, and

$PDPF = \overline{PDPF} + 3(\sigma_{PDPF})$, with 99.7% confidence.

Table 18 provides the range of data of the important parameters and their uncertainties calculated using the procedures mentioned above. The uncertainties in the value of OCR, $HTPF$ and $PDPF$ are with 95.45% confidence.

Table 18: Data and Uncertainty Limits of the Important Parameters.

R-410A tests		**Range of Data**		**Range of Uncertainty (±δ)**	
Parameter	**unit**	**min**	**max**	**± δ_min**	**± δ_max**
$P_{mchx,i}$	psia	269.06	494.60	0.65	0.65
$T_{mchx,i}$	°F	99.60	134.08	0.36	0.36
$\dot{m}_{oil+ref,inj}$	lbm/h	3.60	36.12	0.002	0.028
$\dot{m}_{oil,inj} + \dot{m}_{ref,mchx}$	lbm/h	350.34	613.20	0.005	0.033
S	% w/w	21.8	86.0	0.78	2.36
OCR*	%	0.46	5.54	0.0002	0.0061
$\Delta P_{air,N}$	in W.C.	2.8	3.0	0.0075	0.0075
ρ_{air}	lbm/ft^3	0.070	0.073	0.0001	0.0002
CFM	cfm	2750	2900	12	16
$\Delta T_{air@OCR}$	°F	3.84	12.11	0.509	0.509
$\Delta T_{air@OCR=0}$	°F	4.32	12.78	0.509	0.509
$Q_{air@OCR}$	Btu/h	11608	33801	1303	1508
$Q_{air@OCR=0}$	Btu/h	13202	35306	1303	1508
$\Delta P_{@OCR}$	psi	2.27	12.64	0.030	0.919
$\Delta P_{@OCR=0}$	psi	2.19	12.21	0.030	0.919
$HTPF\_Q_{air}$*	-	0.87	1.11	0.057	0.152
$HTPF\_\Delta T_{air}$*	-	0.87	1.61	0.031	0.124
$PDPF$*	-	0.85	1.18	0.020	0.122

*uncertainties are with 95.45% confidence.

An example is presented in Appendix H, which shows the calculations done to obtain OCR, $HTPF$, and $PDPF$ values and the uncertainties propagated in them.

CHAPTER V

V. RESULTS AND DISCUSSION

Section 5.1 Solubility Using the Gravimetric Method presents the measured data of the injected oil-refrigerant mixture solubility that is not available in the literature.

Section 5.2 System Calibration for Heat Balance explains the calibration of the important measurement sensors which were used to get the heat balance within acceptable limits. It also discusses the parameters which have a significant effect on the calculated uncertainty of the heat transfer.

Section 5.3 Preliminary Results compares the analyzed $HTPF$ and $PDPF$ results from the Vapor Compression Cycle System and the Pump-Boiler System. It also explains the reason for the failure of the analysis test procedure if qualitative analyses of the mapping data are not done. A subsection provides HTPF and PDPF results at different testing condition. A few preliminary results of the normalized oil retained volume are provided, but are not discussed in detail.

5.1 Solubility Using the Gravimetric Method

Cavestri and Schafer (2000) provide R-410A and ISO 32 Mixed Acid POE mixture solubility data for pressures below 247 psia. While performing the experiments, the oil-refrigerant mixtures were subjected to pressures above 247 psia; thus, the literature data from Cavestri and Schafer could not provide the solubility values for the current project. No research project done in the past, except for Cavestri and Schafer (2000), provides the solubility data for the particular mixture of R-410A and ISO 32 Mixed Acid POE. Hence, the solubility of the refrigerant in the injected oil-refrigerant mixture was measured for every injection test. Figure 46 and Figure 47 presents the plot of solubility, S, measured using the gravimetric method as a function of the temperature, T, and pressure, P, observed at the oil reservoir.

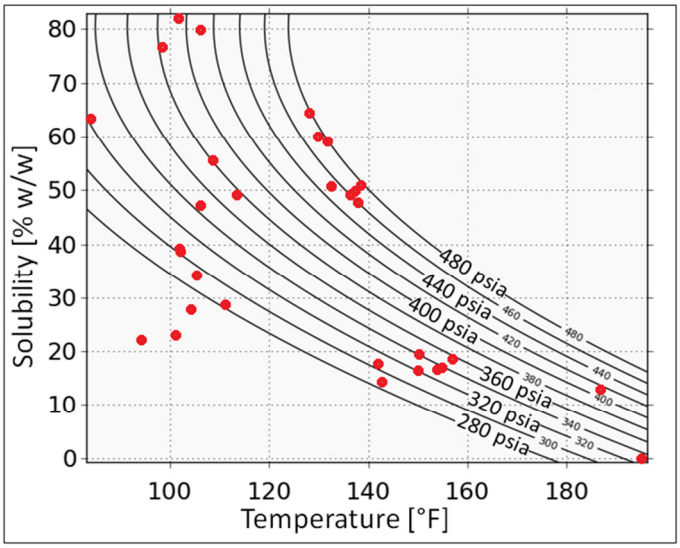

Figure 46: Solubility measured using the gravimetric method, *P=f(T,S)*.

In Figure 46 the constant pressure lines are plotted by fitting the data (from Appendix C) to the surface ($P = f(T,S)$) represented by Equation (5.1).

$$P = 2.52E+47 \times exp\left(-0.5 \cdot \left(\left(\frac{23380.22-\mathrm{T}}{1620.58}\right)^2 + \left(\frac{80.57-S}{56.97}\right)^2\right)\right) \quad (5.1)$$

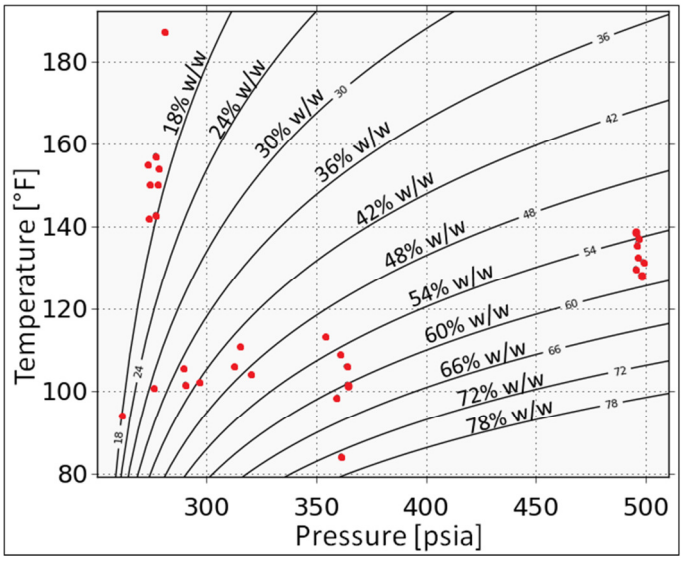

Figure 47: Solubility measured using the gravimetric method, *S=f(P,T)*.

In Figure 47 the constant solubility lines are plotted by fitting the data (from Appendix C) to the surface ($S = f(P,T)$) represented by Equation (5.2).

$$S = 570.7 \times (T^{-0.73}) \times \ln(P - 249.87) - 32.83 \quad (5.2)$$

5.2 System Calibration for Heat Balance

This section explains the calibration of the important measurement sensors, which were used to get the heat balance within acceptable limits. These include the temperature and air pressure measurement sensors. The proper mixing of air on the side of the supply air in the microchannel heat exchanger also played a critical role in balancing the heat transfer.

This section does not includes a description of the absolute and differential pressure transducers used to monitor the refrigerant side pressure and pressure drop, as their uncertainty values used for calculations were as prescribed by the manufacturer.

5.2.1 Modification of the Air Ducts

Figure 48 and Figure 49 show a 2D simulation of the air flow patterns inside the duct on the air supply side of the microchannel heat exchanger. The simulation is done using the online freeware Flowsquare version 3.0 (Minamoto 2012). This section discusses the difficulties faced with the original duct construction and the modification to overcome the problems.

The sharp bend inside the air duct within a few feet of the microchannel heat exchanger created stagnant pockets in the duct, as shown in Figure 48. The microchannel heat exchanger fins temperatures are high near the inlet of the superheated refrigerant; the fins are at their lowest temperatures at the outlet of the heat exchanger, which had a two-phase or subcooled refrigerant. This configuration causes uneven heating of the air flowing across the heat exchanger slab; thus the temperature in the airstream is not uniform. The unconventional construction of the duct and the absence of any mixing device cause this non-uniform airstream temperature to be observed at the inlet of the nozzle bank, which introduces systematic error into the air flow rate measurement. The course construction of the sampling tree placed near the microchannel heat exchanger could not sample the air efficiently because of its high by-pass factor; also it could not cover the whole heat exchanger (refer to Figure 8). As the sampling tree was not effective in sampling the air, it

introduced errors in the calculations of density using the dry bulb temperature and the relative humidity sensors.

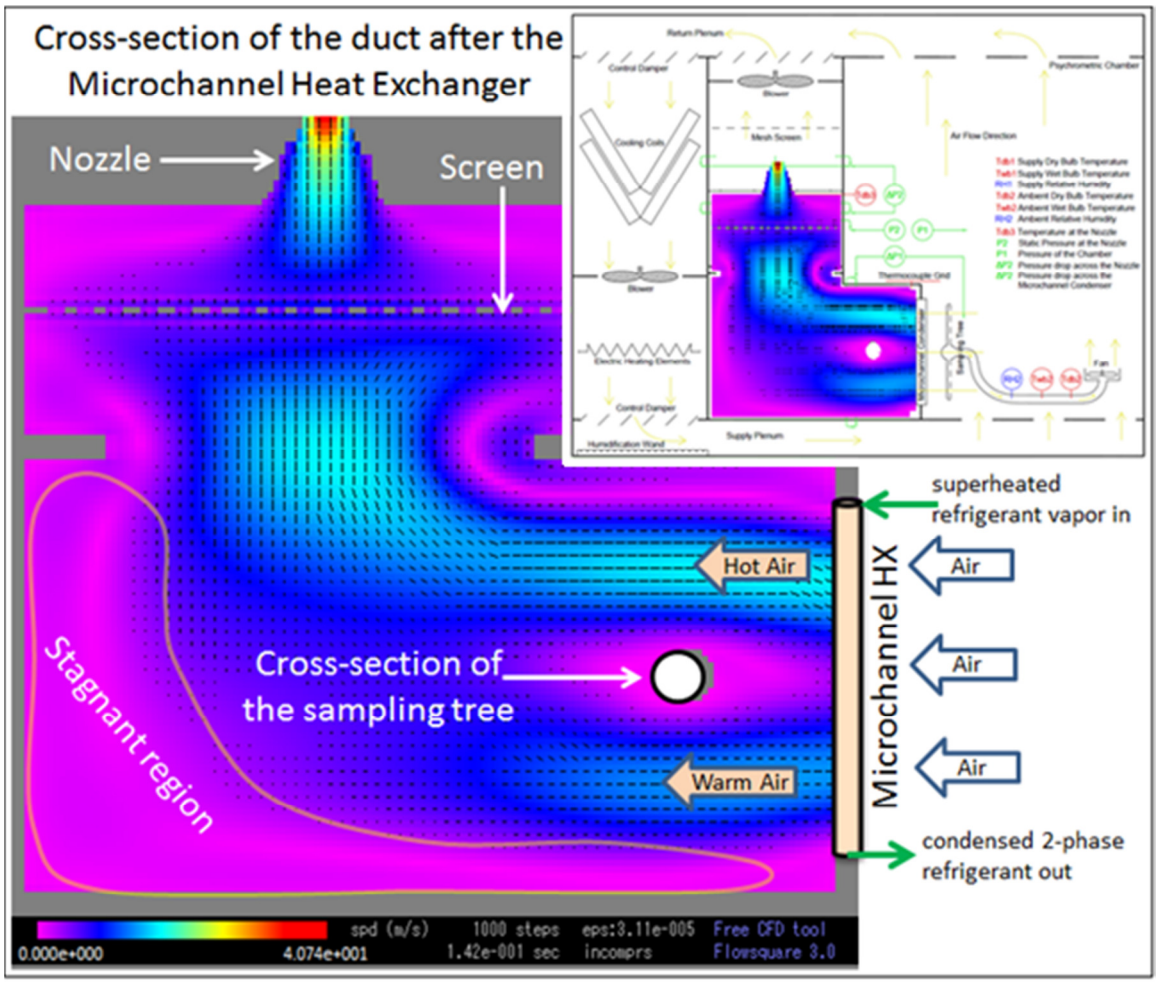

Figure 48: Flow visualization inside the air supply duct of the microchannel heat exchanger.

Modification was done (refer to Figure 49) by covering the stagnant regions inside the duct with Styrofoam boards, thus preventing possible circulations in the stagnant regions. The conduit constructed with the boards helped to mix the air stream before it reached the nozzle bank. The sampling tree was shifted away from the microchannel heat exchanger to a point where the air was completely mixed, thus increasing the effectiveness of the sampling tree to sample the air.

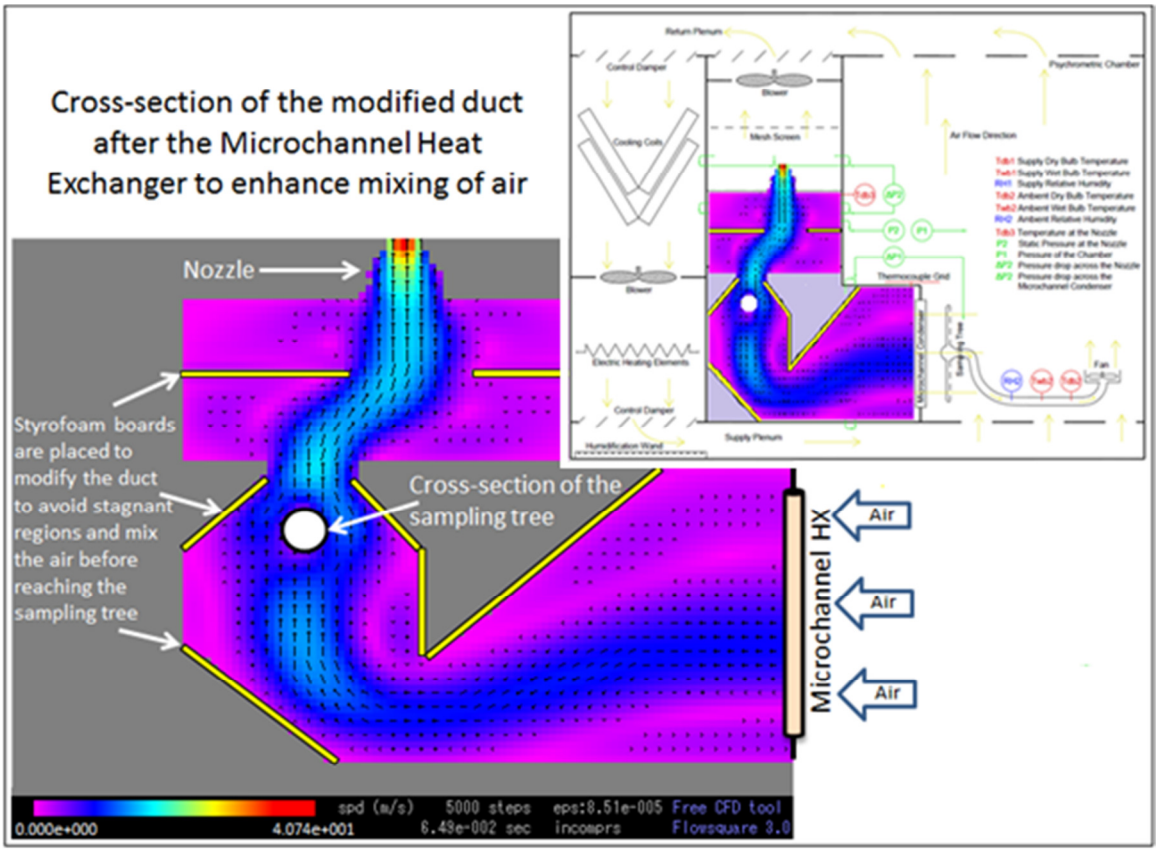

Figure 49: Flow visualization inside the modified air supply duct of the microchannel heat exchanger.

The in-house calibration of the nozzle bank gave a correction for the CFM, Equation (5.1) and Equation (5.2). This correction, when applied to the equations in the ANSI/ASHRAE Standard 41.2 (ASHRAE 1987), gave the correct air flow rate (CFM). The CFM values were further used for the heat transfer calculations.

$$CFM = CFM \times correction \tag{5.1}$$

$$correction = -0.1267 * (1 / \rho_{air}) + 2.9673 \tag{5.2}$$

5.2.2 Calibration of the Temperature Sensors

The thermocouples and the RTDs, though calibrated, needed verification every month to ensure that they have not drifted; the drift causes systematic error in their measurements. Plot (a.) of Figure 50 shows the inconsistency in the air temperature readings of all the temperature sensors (these readings were noted when refrigerant was not flowing through the microchannel heat exchanger). Plot (b.) of Figure 50 shows the percent difference of all the temperature readings from the temperature of the supply air. In this figure, the RTDs measuring the dry bulb temperatures of the ambient air and the supply air were close to each other, but a drift was seen in the temperature sensors placed near the inlet of the nozzle bank. Such conditions required immediate calibration of the thermocouples and the RTDs.

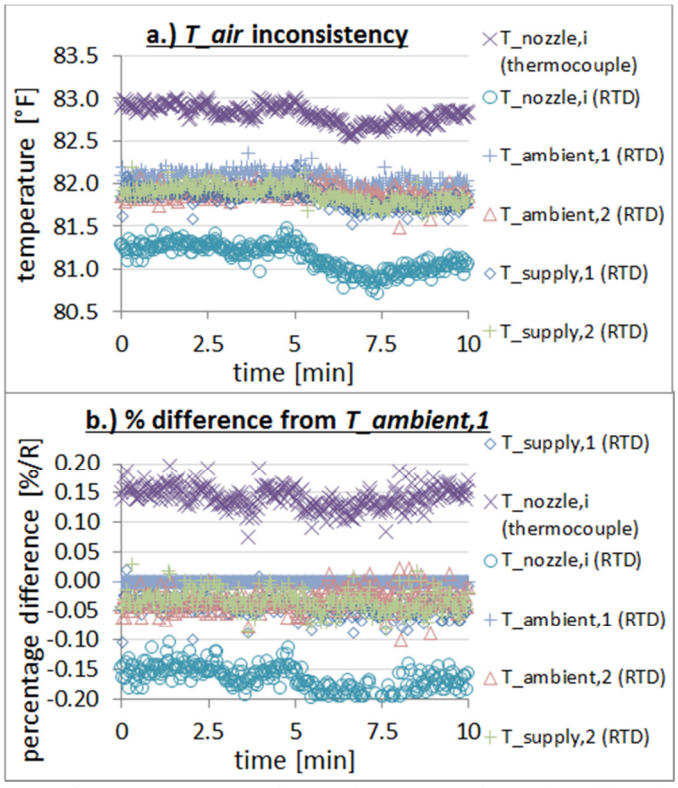

Figure 50: Temperatures inconsistency and needs calibration.

Plot (a.) of Figure 51 shows the consistency in the air temperature readings after calibration of the thermocouples and the RTDs. Plot (b.) of Figure 51 shows the percent difference per rankine of all the temperature readings from the supply air temperature was within ±0.1%.

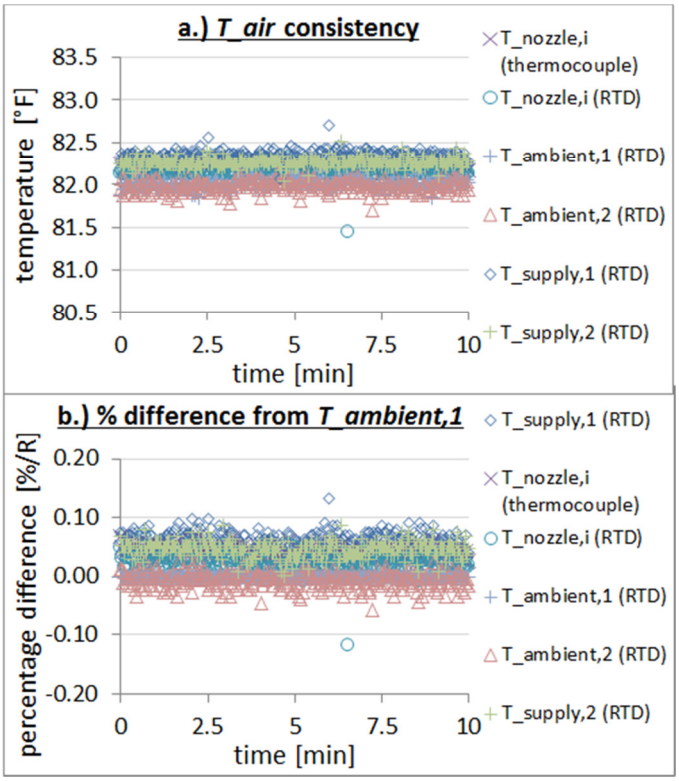

Figure 51: Temperatures showing consistency after calibration.

5.2.3 Correction of the Differential Pressure Transducers

The main reason for not getting the heat balance was traced back to the accuracy of the differential pressure transducer placed inside the air duct. It was observed that the plastic tubes connecting the transducer had developed cracks, which resulted in their failure to read the static pressures. The difference between the DAQ reading and the manometer reading for the differential was huge, and it was corrected by replacing the tubes. Figure 52 and Figure 53 show the corrected pressure reading after fixing the tube.

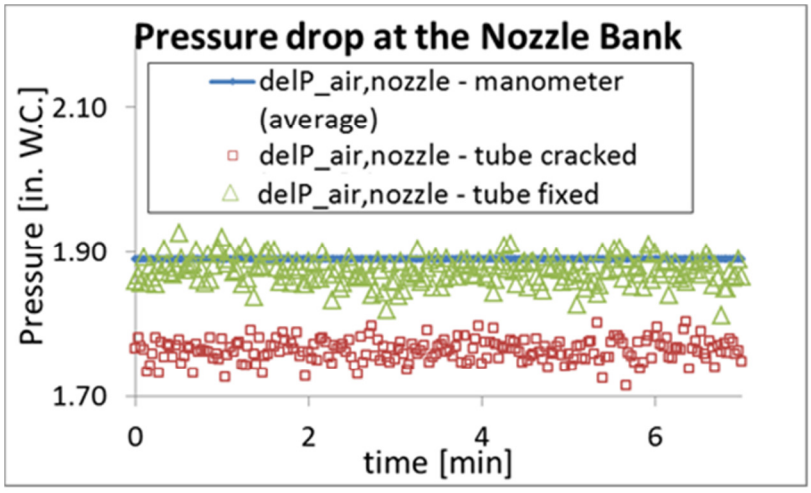

Figure 52: Pressure drop across the nozzle bank.

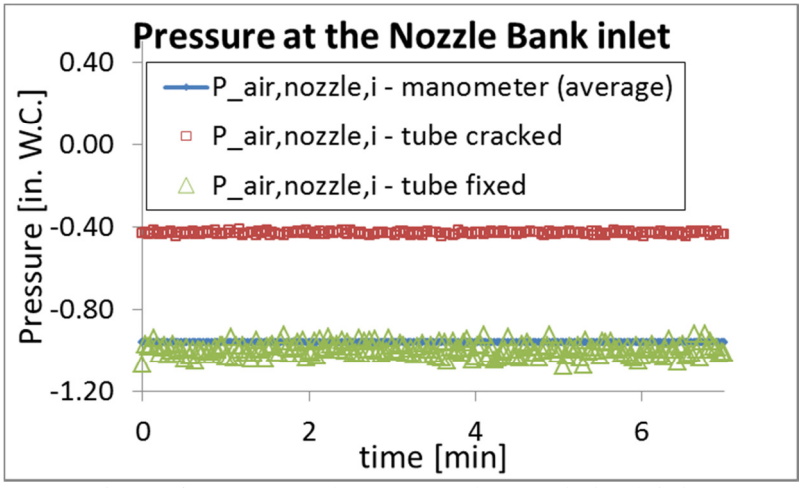

Figure 53: Pressure drop across the nozzle bank inlet.

5.2.4 Heat Balance

The heat transferred from the condensing refrigerant to the air flowing over the microchannel could be calculated within ±5% error. Preliminary tests showed that the problem of getting the heat balance within an acceptable limit was traced back to the drift of the temperature sensors, cracked tubes to the pressure transducers, and improper mixing of the air in the supply duct. The temperature sensors were calibrated with reference to the NIST traceable thermometer, the cracked tubes sensing the static pressure inside the ducts were replaced, and the air supply duct was modified, which reduced the error in the air flow rate measurement at the nozzle bank. Figure 54 shows typical heat balances that were observed. The data in the figure are for the condensing saturated temperatures of 105°F (40.6°C) and 85°F (29.4°C) respectively.

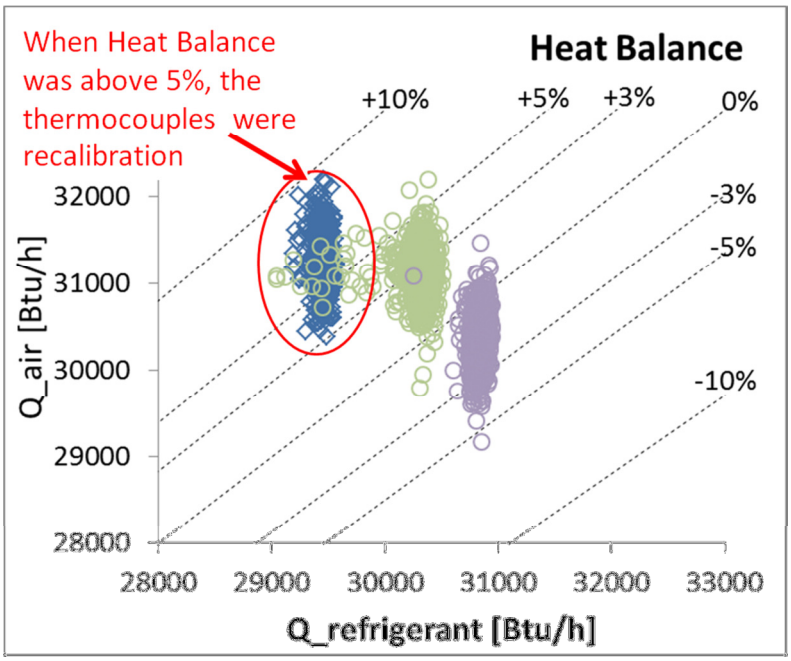

Figure 54: Heat balance on the refrigerant and air side of the microchannel heat exchanger.

No heat balance test was performed at the condensing saturated temperature of 130°F (54.4°C) because for this test, the water temperature at the evaporator needed to be extremely high, which was detrimental to the PVC cement used at the joints of the water pipes. All the tests with saturated temperatures of 130°F (54.4°C) were done consecutively, without stopping, to

prevent the cement from melting and the water from leaking. The calculated heat transferred to the air at the high saturation temperature was considered correct because the uncertainties of the air side instrumentation were within acceptable limits.

The microchannel heat exchanger runs in a two-phase regime at its outlet at the time of the injection test; thus, it is not possible to calculate the heat rejected by the refrigerant because its quality is not known. The oil inside the heat exchanger can be inside the microchannel tubes or trapped in the headers, which makes the calculation of the sensible heat lost by the oil difficult. Hence, during the injection tests, the measurements of the heat transfer at the microchannel heat exchanger had to rely on accurate calculations of the heat gained by the air. The efforts spent on getting the heat balance on the sides of the microchannel heat exchanger exposed to the air and refrigerant during the "no oil injection tests" reflected the accuracy of the calculated results for $HTPF$s and $PDPF$s.

5.3 Preliminary Results

The section compares the analyzed $HTPF$ and $PDPF$ results from the Vapor Compression Cycle System and the Pump-Boiler System. The plots for $HTPF$ and $PDPF$ as a function of OCR are provided under different testing conditions.

5.3.1 Repeatability Test

Figure 55 shows a sample repeatability test for the data obtained from the Pump-Boiler System and the data from the Vapor Compression Cycle System. The blue and red lines and markers represent the tests performed on the Pump-Boiler System for the same saturation temperature and mass flow rate. The orange line and markers shows the test performed on the Vapor Compression Cycle System.

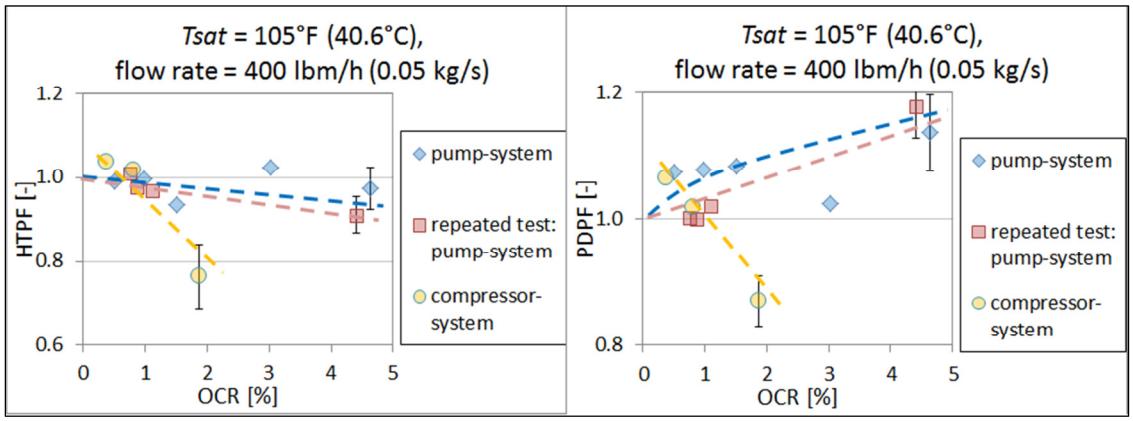

Figure 55: Repeatability test for *HTPF* and *PDPF*

The two sets of tests (blue and red) performed on the Pump-Boiler System showed repeatability within their uncertainty limits. No repeatability was observed in the results (orange) obtained from the Vapor Compression Cycle System.

The accuracy in the $HTPF$ and $PDPF$ results depends on the qualitative analysis of the mapping points. The poor mapping points cannot be used if they were obtained from the test in which there was oil inside the microchannel tubes. In the Vapor Compressor Cycle System, there

were chances for the oil to be present in the microchannel heat exchanger, due to issues with the oil management, while measuring the "no oil" condition heat transfer ($Q_{air@OCR=0}$) and pressure drop ($\Delta P_{@OCR=0}$) values. No mapping tests were performed for the Vapor Compressor Cycle System, the pre-injection test data were used as the mapping points. The less number of mapping data were not efficient to get a good surface fit to calculate the "no oil" condition heat transfer ($Q_{air@OCR=0}$) and pressure drop ($\Delta P_{@OCR=0}$) values. The less number of mapping points and the chance of these mapping points to be of poor quality rendered the $HTPF$ and $PDPF$ results of the Vapor Compressor Cycle System to be not repeatable.

5.3.2 *HTPF* and *PDPF* results

It can be observed from Figure 56 that the heat transfer impact depends on both mass flow rate and OCR. The effect of oil on heat transfer is stronger for higher OCR. The $HTPF$ for the mass flow rate of 400 lbm/h decreases as the OCR increases, while the opposite effects are seen at the higher mass flow rate of 600 lbm/h.

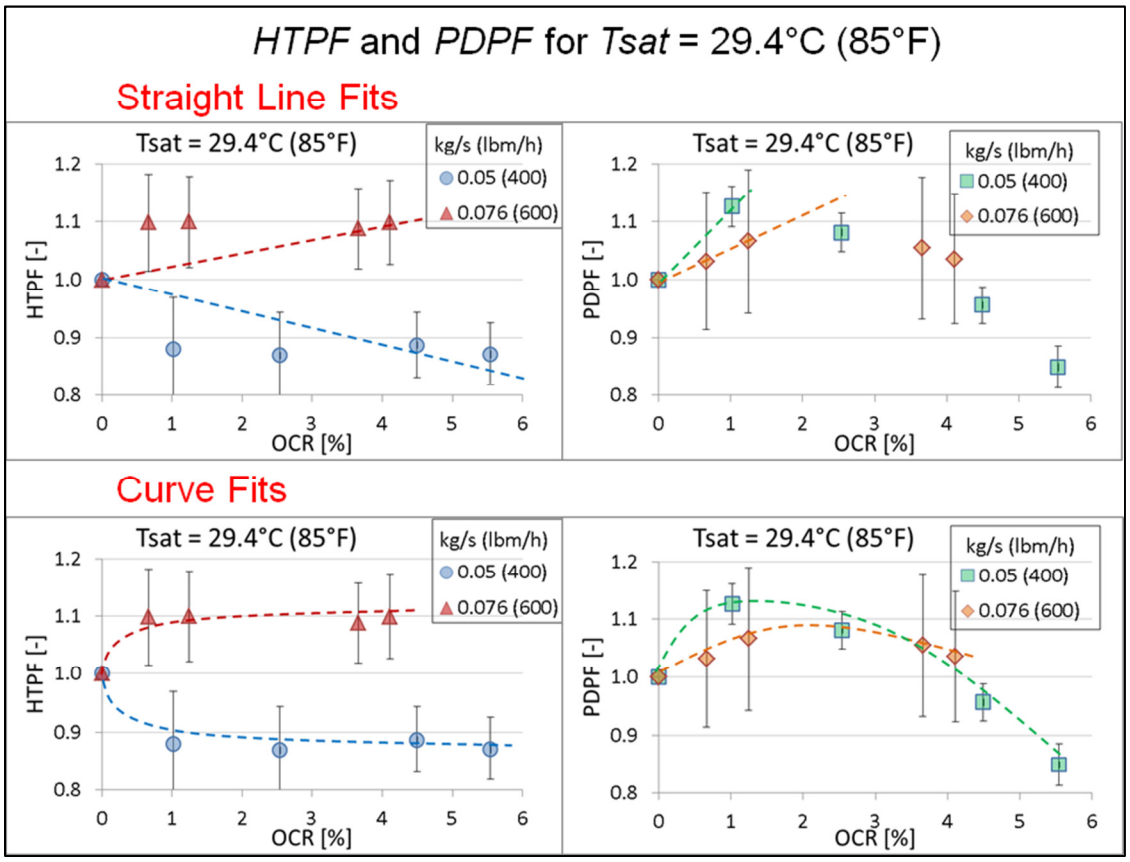

Figure 56: *HTPF* and *PDPF* for T_{sat}=85°F (29.4°C)

The $PDPF$ in Figure 56 is strongly dependent on, and varies non-linearly with, the OCR. As indicated, the $PDPF$ has a peak value at the OCR value of 1.5. The tests with OCR values above 4% had their "no oil" condition pressure drop $\Delta P_{@OCR=0}$ values (obtained from the mapping points' surface fit) higher than the pressure drop $\Delta P_{@OCR}$ values for the oil injection tests, resulting in calculated $PDPF$s below 1.0; refer to Equation (4.15) for the $PDPF$

calculation. The uncertainty measurement of $PDPF$ at 600 lbm/h was high because of the use of absolute pressure transducers to measure the pressure drop instead of the more accurate differential pressure transducer, as the observed pressure drop was higher than the maximum limit of the differential pressure transducer.

Figure 57 shows that the data for $HTPF$ have scattered results with their values lying within the uncertainty limits, resulting in an inconclusive relationship. Better results were indicated in the $PDPF$ relations. As the OCR increases, the $PDPF$ increases and shows a similar trend for both the mass flow rates, with relatively more pressure drop for 400 lbm/h.

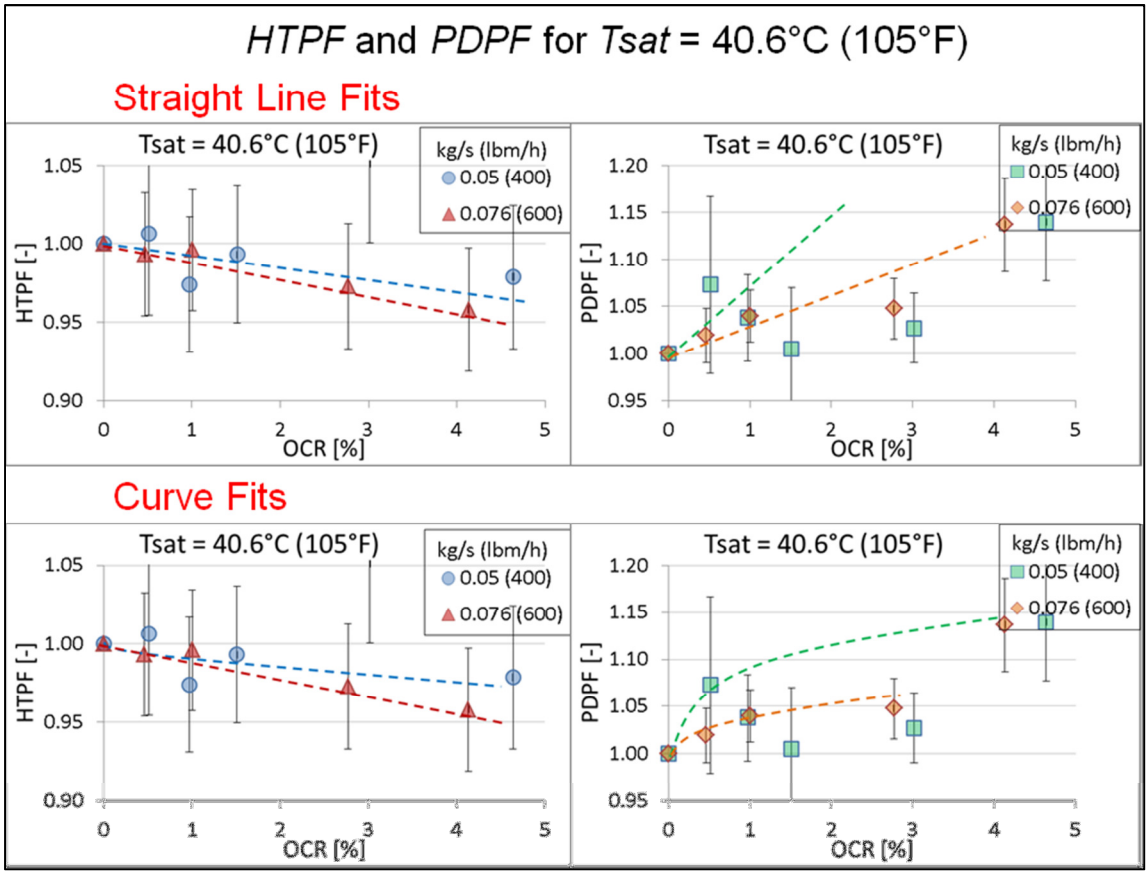

Figure 57: $HTPF$ and $PDPF$ for T_{sat}=105°F (40.6°C)

For a saturation temperature of T_{sat}=130°F (54.4°C), Figure 58, $HTPF$s are observed with patterns similar to those of T_{sat}=85°F (29.4°C), while $PDPF$s are observed with patterns

similar to those of T_{sat}=105°F (40.6°C). The effect of oil on heat transfer is stronger for higher OCRs. The heat transfer for a mass flow rate of 400 lbm/h decreases as the OCR increases, while the opposite effects are observed at the higher mass flow rate of 600 lbm/h. It should be noted that the straight line or the curve fits of $HTPF$ and $PDPF$ data are within their measurement uncertainty.

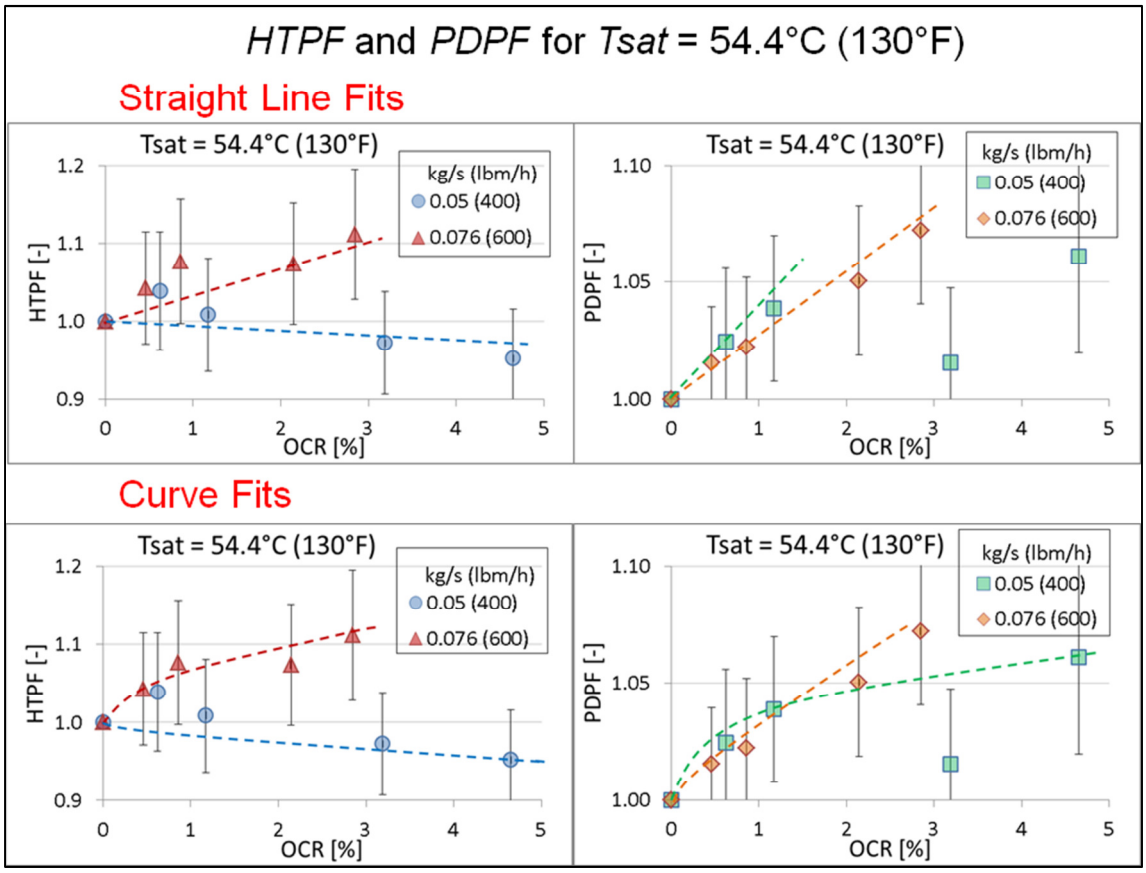

Figure 58: *HTPF* and *PDPF* for T_{sat}=130°F (54.4°C)

5.3.3 Oil Retention Preliminary Results

Although the oil retention in the microchannel heat exchanger-condenser was not the focus of this study, the test facility allowed the measurement of the amount of oil retained in a microchannel condenser.

Figure 59 shows the calibration curve of the oil level tank, which was used to measure the volume of oil extracted, for the test performed with the Vapor Compressor Cycle System. The calibration process involved pouring a measured volume of oil in the tank and marking the oil level on the graduated scale.

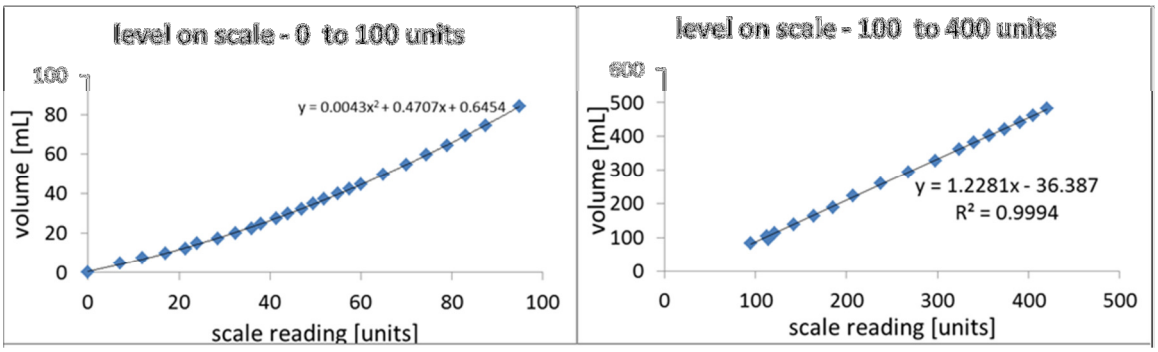

Figure 59: Calibration curve for the oil level tank to measure the volume of oil extracted.

This section further provides the preliminary results for the normalized oil retention volume in the microchannel condenser. The calculations were done using the method described in section 4.7 Oil Retention Calculation.

Figure 60 shows that for a saturated temperature of 85°F (29.4°C), the ORV_N values increase linearly from 0 to 0.08 for the Pump-Boiler System as well as the Vapor Compressor Cycle System, which shows their repeatibility below OCR of 2%. With further increase in OCR value, the trend of the data is no longer linear. The Vapor Compressor Cycle System data at a mass flow rate of 400 lbm/h show the ORV_N to be higher that that of the Pump-Boiler System data at a mass flow rate of 600 lbm/h. Overall, the tests for T_{sat}=85°F (29.4°C) shows that for 1%

OCR, 3% of the total heat exchanger volume is occupied by the oil. And, for 4% OCR, 14% of the total heat exchanger volume is occupied by the oil.

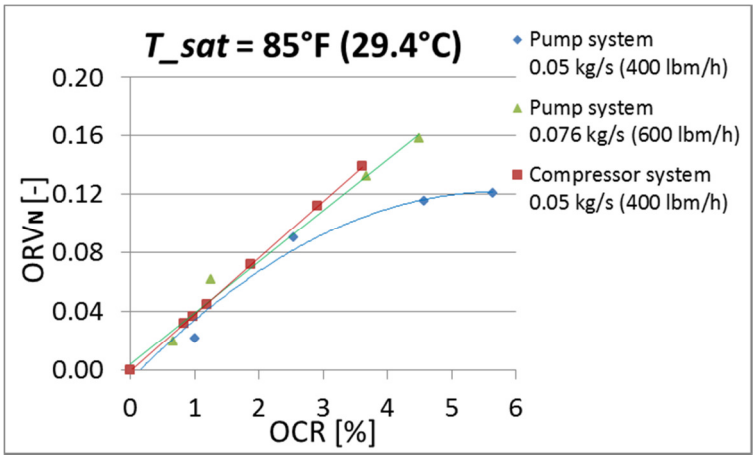

Figure 60: ORV_N for T_{sat}=85°F (29.4°C)

Figure 61 shows that for a saturated temperature of 105°F (40.6°C), the rate of rise of ORV_N is higher for the Pump-Boiler System and the Vapor Compressor Cycle System. Above 0.5% OCR, the methodology used for the Pump-Boiler System measures more retained oil than the Vapor Compressor Cycle System measures. The absence of Vapor Compressor Cycle System data above 2% OCR makes it difficult to compare it with the Pump-Boiler System. These tests for T_{sat}=105°F (40.6°C) show that for 1% OCR, 2% of the total heat exchanger volume is occupied by the oil.

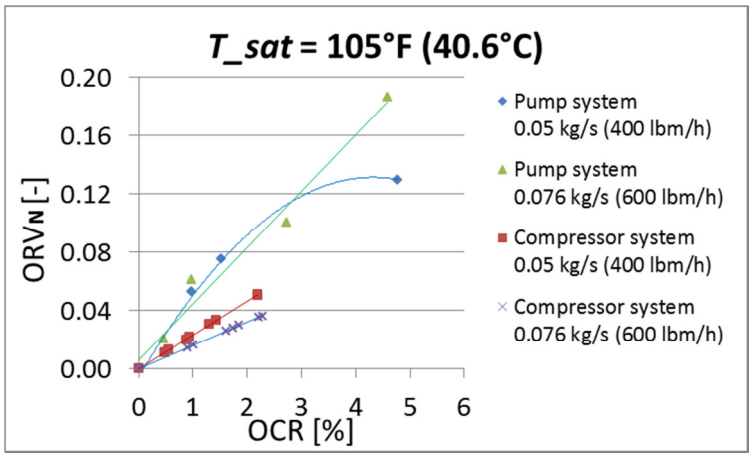

Figure 61: ORV_N for T_{sat}=105°F (40.6°C)

Figure 62 shows the results from the tests with a saturation temperature of 130°F (54.4°C). The rate of rise ORV_N is higher for a mass flow rate of 600 lbm/h than for 400 lbm/h. The Vapor Compressor Cycle System data show repeatibility with the Pump-Boiler System data for a mass flow rate of 400 lbm/h. Overall, the test for T_{sat}=130°F (54.4°C) shows that for 0.5% OCR and mass flow rates of 400 lbm/h and 600 lbm/h, 1% of the total heat exchanger volume is occupied by the oil. At 3% OCR and a mass flow rate of 400 lbm/h, 5% of the total heat exchanger volume is occupied by the oil, while at 3% OCR and a mass flow rate of 600 lbm/h, the volume occupied by the oil increases to 15%.

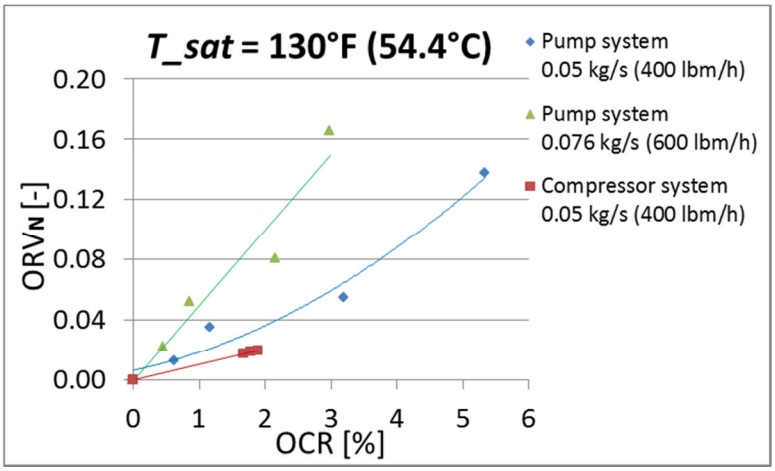

Figure 62: ORV_N for T_{sat}=130°F (54.4°C)

The Vapor Compressor Cycle System oil retension results are should be more accurate than the results from the Pump-Boiler System, which are presented in the figures above, because the volume of oil was actually measured in the Vapor Compressor Cycle System and not in the Pump-Boiler System. (For more information refer to section 3.6.4 Extraction Test.) Further investigation of the uncertainties of oil retention are needed to explain the discrepency between the Vapor Compressor Cycle System results and the Pump-Boiler System results.

CHAPTER VI

VI. CONCLUSION

The design, construction, and calibration of the experimental test facility have been completed. The research and project work done by Cremaschi (2004), Cremaschi et al. (2004), and Cremaschi et al. (2005) formed the basis for this thesis project: the system design and analysis procedures mentioned in these papers were used as a reference. All possible suggestions from advisors, consultants, and the literature were followed to have the best system for measuring the oil retention effects on the performance of the microchannel heat exchanger while working as a condenser.

Although the oil retention in the microchannel heat exchanger-condenser was not the focus of this study, the test facility allowed the measurement of the amount of oil retained in a microchannel condenser. The modification of the system to test the microchannel heat exchanger as an evaporator is possible by changing the layout of a few copper tubes. The microchannel heat exchanger-condenser is the only component placed inside a thermal enclosure of the Psychrometric Room. The rest of the system components are placed outside the room. This design makes it possible for the air temperature and air volume flow rate at the microchannel heat exchanger to be controlled without getting disturbed by the refrigeration system components of the test facility.

Initially a Vapor Compression Cycle System was constructed for experimentation. The system was then converted to a Pump-Boiler System. The time and effort spent on modifying the system is reflected on the quality of the $HTPF$ and $PDPF$ data that were obtained using the Pump-Boiler System. This research project directly compares these two experimental set-ups for the first time and provides a quantitative comparison of the oil retention measurements' experimental methodology

In the oil retention measurements experiments, the use of the Pump-Boiler System, with gear pump, displayed various advantages over the use of the Vapor Compression Cycle System, with a single speed scroll compressor. In the Pump-Boiler System the mass flow rate could be controlled instantaneously by varying the speed of the gear pump, the bladder accumulator dampened the fluctuations in the mass flow rate, control of the superheat at the microchannel heat exchanger inlet was possible with the help of a superheater, and the system required less supervision

Unlike the compressor, which failed in the Vapor Compression Cycle System during the oil retention experiments, the gear pump in the Pump-Boiler System did not face problems such as a flooded start, flood back, contamination, improper charging, heat dissipation, and inefficient lubrication.

In the Vapor Compression Cycle System, the presence of the two oil sources (the compressor and the oil reservoir) in the oil flow circuits and the oil separators in each circuit having efficiencies less than 100% made it difficult to keep track of the amount of pure oil introduced to the test section. A wrong estimation of the oil flow rate in the microchannel heat exchanger can introduce error in the calculation of the OCR. In the Pump-Boiler System, the gear pump did not introduce any oil in the system; the only source for oil introduction was the oil reservoir, and the oil was extracted at only one point, using the oil separator placed at the end of

the test section. In this system it was possible to estimate the amount of oil that escaped from the oil separator to the test section, and thus to have a correct measurement of the oil flow through the test section, consisting the microchannel heat exchanger.

The constructed oil extraction system could extract and measure the volume of oil in the oil level tank in the Vapor Compression Cycle System. In the project's Pump-Boiler System only the difference between the oil injection time and the oil extraction time could be measured, as the oil level tank was always excessively filled with the liquid refrigerant. This disadvantage of the Pump-Boiler System was the only one that was encountered.

No research project done in the past, except for Cavestri and Schafer (2000), provides the solubility data for the particular mixture of R-410A and ISO 32 Mixed Acid POE. Cavestri and Schafer provided R-410A and ISO 32 Mixed Acid POE mixture solubility data for pressures below 247 psia. While performing the experiments, the oil-refrigerant mixtures were subjected to pressures above 247 psia. Hence, the solubility of the refrigerant in the injected oil-refrigerant mixture was measured using the gravimetric method for every injection test. Accurate measurement of the solubility values by the gravimetric method considerably reduced the uncertainty propagated to the calculated OCRs. The average of the calculated fractional uncertainties in the OCRs was ±0.1%.

The Vapor Compressor Cycle System results for $HTPF$ and $PDPF$ showed different trends then the Pump-Boiler System results. The limited and poor quality of the mapping points available for the analysis of the Vapor Compressor Cycle System was the reason for the nature of the non-similar trends and the non-repeatability of the test results. The Pump-Boiler System had good quality mapping points, thus, its results were repeatable and could be trusted.

Summary of the Results:

***HTPF* results**

At the low T_{sat}=85°F (29.4°C) and for the low mass flow rate of 400 lbm/h (0.05 kg/s), the $HTPF$ decreased with the increase in OCR value, but for the high mass flow rate of 600 lbm/h (0.076 kg/s), the $HTPF$ increased with the increase in OCR.

At the T_{sat}=105°F (40.6°C), the $HTPF$ decreased with the increase in OCR.

At the T_{sat} =130°F (54.4°C), the $HTPF$ patterns are similar to those seen in the tests for T_{sat}=85°F (29.4°C).

The maximum increase or decrease in the $HTPF$ values observed for all the tests was ±10% at the $OCR = 5\%$.

***PDPF* results**

The $PDPF$ results were non-linear for all tests performed at different saturation temperatures.

The rate of rise in the $PDPF$ values was higher in the tests with a low mass flow rate of 400 lbm/h (0.05 kg/s) and the rate of rise was lower in the tests with a high mass flow rate of 600 lbm/h (0.076 kg/s).

At the low T_{sat}=85°F (29.4°C), the $PDPF$ increased by 10% at OCR =1.5% then started to drop.

At the T_{sat}=105°F (40.6°C) and OCR =3%, the $PDPF$ increased by 5% and 12% for mass flow rates of 600 lbm/h (0.076 kg/s) and 400 lbm/h (0.05 kg/s) respectively.

At the T_{sat}=130°F (54.4°C), for both the high and low mass flow rate tests, the $PDPF$ values increased by 4% at the OCR =1.7%, after which the rise was continuous.

NOMENCLATURE

c_p	specific heat at constant pressure, Btu/lbm-R (J/kg-K)
CFM	air flow rate, ft^3/min or cfm (m^3/s)
COP	coefficient of performance, - (-)
h	enthalpy, Btu/lbm (J/kg)
$m, \hat{m}, M$	mass, lbm (g)
$\dot{m}$	mass flow rate, lbm/h (g/s)
OCR	oil circulation ratio, %
OMF	oil mass fraction, %
ORM	oil retention mass, lbm (kg)
ORV	oil retention volume, in^3 (mL)
ORV_N	normalized oil retention volume, - (-)
P	pressure, psia (kPa, bar) or in. W.C.
Q	heat transfer, Btu/h (J/s)
s	entropy, Btu/lbm-R (J/kg-K)
S	solubility, % w/w
t	time, s or min
T	temperature,°F (°C)
V	volume, gallon (L)
W	mass, lb (g)
$HTPF$	Heat Transfer Penalty Factor (-)
$HTPF\_Q_{air}$	Heat Transfer Penalty Factor calculated using Q_{air} (-)
$HTPF\_\Delta T_{air}$	Heat Transfer Penalty Factor calculated using ΔT_{air} (-)
$PDPF$	Pressure Drop Penalty Factor (-)
ρ	density, lbm/ft^3 (g/ml)
φ	relative humidity, % (%)
δ	uncertainty or error, or a very small quantity
μ	dynamic viscosity, lbm/ft-h (kg/m-s)
Δ	difference in two quantities
POE	polyol ester
MO	mineral oil
PAG	polyalkylene glycol
AB	alkylbenzen

Subscripts

$A, port-A$	port-A at the inlet of the microchannel heat exchanger
amb	ambient property
air	air, or air property
$B, port-B$	port-B at the outlet of the microchannel heat exchanger
$by-pass$	by-passed refrigerant at the oil separators
db	dry bulb temperature
$evap$	evaporator
$ext-A$	extraction at the oil separator when the injection is at port-A
$ext-B$	extraction at the oil separator when the injection is at port-B
f	saturated liquid condition
g	saturated vapor condition
gp	gear pump
i	inlet
$line$	connecting lines in the test section
$mchx$	microchannel heat exchanger
i	inlet
inj	injection
ext	extraction
max	maximum
min	minimum
N	air flow nozzle/nozzle-bank
$oil+ref$	oil and refrigerant mixture, either oil-rich or refrigerant-rich mixture.
$oil+REF$	oil and refrigerant mixture, refrigerant-rich mixture.
$OIL+ref$	oil and refrigerant mixture, oil-rich mixture.
o	outlet
oil	pure oil, no refrigerant dissolved in the oil
ref	refrigerant
inj	injected
sat	saturated condition
t	time step, or time, s (s)
$test-section$	test section consisting of the microchannel heat exchanger and the connecting lines.
wb	wet bulb temperature

REFERENCES

ASHRAE. 2007. *ANSI/ASHRAE Standard 34-2007, Designation and Safety Classification of Refrigerants*. Atlanta: American Society of Heating, Refrigerating and Air-Conditioning Engineers, Inc.

ASHRAE. 2009. *2009 ASHRAE Handbook—Fundamentals (I-P Edition)*. Atlanta: American Society of Heating, Refrigerating and Air-Conditioning Engineers, Inc. Chapter 29, Refrigerants.

ASHRAE. 2010. *2010 ASHRAE Handbook—Refrigeration (I-P Edition)*. Atlanta: American Society of Heating, Refrigerating and Air-Conditioning Engineers, Inc. Chapter 12, Lubricants in Refrigerant Systems.

ASME. 1996. *ASME Standard B31.9, Building services piping*. New York: American Society of Mechanical Engineers.

ASTM. 2007. *ANSI/ASTM Standard D2422-97, Classification of industrial fluid lubricants by viscosity system.* West Conshohocken, PA: American Society for Testing and Materials.

Bivens, D. B, and A. Yokozeki. 1998. Composition changes during container transfers for multi component refrigerants. *International Refrigeration and Air Conditioning Conference.* Purdue University, West Lafayette, IN. 392:81-86.

Cavestri, R. C. 1993. Measurement of viscosity, density, and gas solubility of refrigerant blends in selected synthetic lubricants. ARTI MCLR Project Number 650-51400: Blends: Quarterly Report, Air-Conditioning and Refrigeration Technology Institute, USA.

Cavestri, R. C. 1995. Measurement of viscosity, density, and gas solubility of refrigerant blends in selected synthetic lubricants. ARTI MCLR Project Number 650-51400: Blends: Final Report, Air-Conditioning and Refrigeration Technology Institute, USA.

Cavestri, R. C., and W. R. Schafer. 2000. Measurement of solubility, viscosity, and density of R-410A refrigerant/lubricant mixtures, (RP-928). *ASHRAE Transactions* 106 (1): 277-285.

Cremaschi, L., H. Yunho., and R. Radermacher. 2005. Experimental investigation of oil retention in air conditioning systems. *International Journal of Refrigeration* 28:1018–1028.

Creux, L. 1905. Rotary engine. US Patent No. 801182.

Crompton, J. A., T. A. Newell, and J. C. Chato. 2004. Experimental measurement and modeling of oil holdup. ACRC TR-226. Air Conditioning and Refrigeration Center. College of Engineering. University of Illinois, Urbana-Champaign, IL, USA.

EPA. 2012. United States Environmental Protection Agency. www.epa.gov

Green, A. 2012. A brief history of air conditioning, *Popular Mechanics*. www.popularmechanics.com/home/improvement/electrical-plumbing/a-brief-history-of-air-conditioning-10720229

Hall, J. R. 2012. Q&A: compressor problems and solutions. *Air Conditioning, Heating & Refrigeration News* vol. 245: 10-12.

Jassim, E. W., and T. A. Newell. 2006. Prediction of two-phase pressure drop and void fraction in microchannel using probabilistic flow regime mapping. *International Journal of Heat and Mass Transfer* 49 : 2446-2457

Jensen, M. K., and D. L. Jackman. 1984. Prediction of nucleate pool boiling heat transfer coefficients of refrigerant-oil mixtures. *Journal of Heat Transfer* 106(1):184-190.

Lee, Jun-Pyo. 2003. Experimental and theoretical investigation of oil retention in a carbon dioxide air-conditioning system. Ph.D. Dissertation, University of Maryland, College Park, MD.

Mehendale, S.S., and R. Radermacher. 2000. Experimental and theoretical investigation of annular film flow reversal in a vertical pipe: application to oil return in refrigeration systems. *HVAC&R Research* 6(1):55-74

Moe, J. 2011. HVAC refrigerants: a balanced approach. *Trane Engineers Newsletter* vol 40–2.

Mohanraj, M., C. Muraleedharan, and S. Jayaraj. 2011. A review on recent developments in new refrigerant mixtures for vapour compression-based refrigeration, air-conditioning and heat pump units. *International Journal of* Energy Research 35:647–669.

Nino, V. G. 2002. Characterization of two-phase flow in microchannels. Ph.D. Dissertation, University of Illinois, Urbana-Champaign, IL.

Roger's Refrigeration. 2012. Refrigeration history. www.rogersrefrig.com/history.html

Scheideman, F. C., and N. A. Macken. 1975. Pressure loss of oil-refrigerant mixture in horizontal pipes. ASHRAE Transactions 81(1):235-249

Scheideman, F. C., M. L. Jacobs, S. Kazem, and N. A. Macken. 1977. Pressure loss of oil-refrigerant mixture in suction and discharge lines. ASHRAE Transactions 83(2):203-221

Sheth, V. P., and T. A. Newell. 2005. Refrigerant and Oil Migration and Retention in Air Conditioning and Refrigeration Systems. ACRC TR-240. Air Conditioning and Refrigeration Center. College of Engineering. University of Illinois, Urbana-Champaign, IL, USA.

Schnur, N. E., P. Popovic, R. L. Shimon, M. Pate. 2000. Effects of lubricant miscibility and viscosity on the performance of an R-134a refrigeration system/Discussion. *ASHRAE transactions: Symposia*:668-678

Sundaresan, S. G., and R. Radermacher. 1996. Oil return characteristics of refrigerant oils in split heat pump system. *ASHRAE Journal* 38(8):57-61.

Taylor, J. R. 1996. *An Introduction to Error Analysis. The Study of Uncertainties in Physical Measurements*, 2nd ed. Chapters 1 to 4, University Science Books.

Yokozeki, A., K. Takigawa, and S.I. Sandler. 2000. Solubility and viscosity of hydrofluorocarbon /alkylbenzene oil mixtures. *International Refrigeration and Air Conditioning Conference.* Purdue University, West Lafayette, IN 488:241-248.

Zoellick, K. F., and P. Hrnjak. 2010. Oil retention and pressure drop in horizontal and vertical suction lines with R410A/POE. *International Refrigeration and Air Conditioning Conference*, Paper 1097. Purdue University, West Lafayette, IN. 2327:1-8.

BIBLIOGRAPHY

AHRI. 2004. *AHRI Standard 520-2004*, *Performance Rating of Positive Displacement Condensing Units*. H. a. R. I. Air-Conditioning. Arlington, VA Air-Conditioning, Heating and Refrigeration Institute.

AHRI. 2005. *AHRI Standard 210/240-2005, Unitary air conditioning and air-source heat pump equipment*. H. a. R. I. Air-Conditioning. Arlington, VA Air-Conditioning, Heating and Refrigeration Institute.

AHRI. 2008. *AHRI Standard 210/240-2008, Performance Rating of Unitary Air-Conditioning & Air-Source Heat Pump Equipment.* H. a. R. I. Air-Conditioning. Arlington, VA Air-Conditioning, Heating and Refrigeration Institute.

ASHRAE. 1986. *ANSI/ASHRAE Standard 41.1-1986, Standard method for temperature measurement*. Atlanta: American Society of Heating, Refrigerating and Air-Conditioning Engineers, Inc.

ASHRAE. 1987. *ANSI/ASHRAE Standard 41.2-1987, Standard methods for laboratory airflow measurement*. Atlanta: American Society of Heating, Refrigerating and Air-Conditioning Engineers, Inc.

ASHRAE. 1989. *ANSI/ASHRAE Standard 41.3-1989, Standard method for pressure measurement*. Atlanta: American Society of Heating, Refrigerating and Air-Conditioning Engineers, Inc.

ASHRAE. 1996. *ANSI/ASHRAE Standard 41.4-1996, Standard method for measurement of proportion of lubricant in liquid refrigerant*. Atlanta: American Society of Heating, Refrigerating and Air-Conditioning Engineers, Inc.

ASHRAE. 2001. 2001 ASHRAE *Handbook—Fundamentals*. Atlanta: American Society of Heating, Refrigerating and Air-Conditioning Engineers, Inc. Chapter 6, Psychrometrics.

ASME. 1992. *ASME Standard B31.5, Refrigeration piping*. New York: American Society of Mechanical Engineers.

ASTM. 1997. *ASTM Standard B280, Standard specification for seamless copper tube for air conditioning and refrigeration field service*. West Conshohocken, PA: American Society for Testing and Materials.

Baustian, J. J., M. B. Pate, and A. E. Bergles. 1986. Properties of oil-refrigerant liquid mixtures with applications to oil concentration measurement: Part I – Thermophysical and transport properties. *ASHRAE Transactions* 92(1a):55-73.

Cremaschi, L. 2004. Experimental and theoretical investigation of oil retention in vapor compression systems. Ph.D. Dissertation, University of Maryland, College Park, MD

Cremaschi, L., Y. Hwang, and R. Radermacher. 2004. Investigation of oil retention in residential heat pump. *International Refrigeration and Air Conditioning Conference*, Paper 636. Purdue University, West Lafayette, IN. R104:1-9.

Cremaschi, L., and E. Lee. 2008. Design and heat transfer analysis of a new psychrometric environmental chamber for heat pump and refrigeration systems testing. *ASHRAE Transactions* 114(2): 619-631.

Garimella, S. 2003. Innovations in energy efficient and environmentally friendly space conditioning systems. *Energy* 28(15):1593-1614.

Graham, D.M., H. R. Kopke, M. J. Wilson, D. A. Yashar, J. C. Chato, and T. A. Newell. 1999. An Investigation of void fraction in the stratified/annular flow regions in smooth, horizontal tubes. ACRC TR-144. Air Conditioning and Refrigeration Center. College of Engineering. University of Illinois, Urbana-Champaign, IL, USA.

Iu, I. 2007. Development of air-to air heat pump simulation program with advanced heat exchanger circuitry. Ph.D. Dissertation, Oklahoma State University, Stillwater, OK.

Jacobi, A. M., Y. Park, Y. Zhong, G. Michna, and Y. Xia. 2005. High performance heat exchangers for air-conditioning and refrigeration applications (non-circular tubes). Final Report. ARI. Arlington, VA, ARTI-21CR/605-20021- 01, Final Report for the Air-Conditioning and Refrigeration Technology Institute, USA.

Jacobs, M., F. Scheideman, S. Kazem, and M. Macken. 1976. Oil transport by refrigerant vapor. *ASHRAE Transactions* 81(2):318-329.

Kandlikar, S., S. Garimella, D. Li, S. Colin, and H. R. King. 2006. *Heat Transfer and Fluid Flow in Minichannels and Microchannels*. Chapter 6, Condensation in minichannels and microchannels. S. Garimella. Elsevier Limited.

Minamoto, Y. 2012. Flowsquare Version 3.0. www.flowsquare.com

Shen, B., and E. A. Groll. 2005. A critical review of the influence of lubricants on the heat transfer and pressure drop of refrigerants – Part II: Lubricant influence on condensation and pressure drop. *HVAC&R Research* 11(4):511-526.

APPENDICES

Appendix A: Schematic of the test facility - Vapor Compression Cycle System.

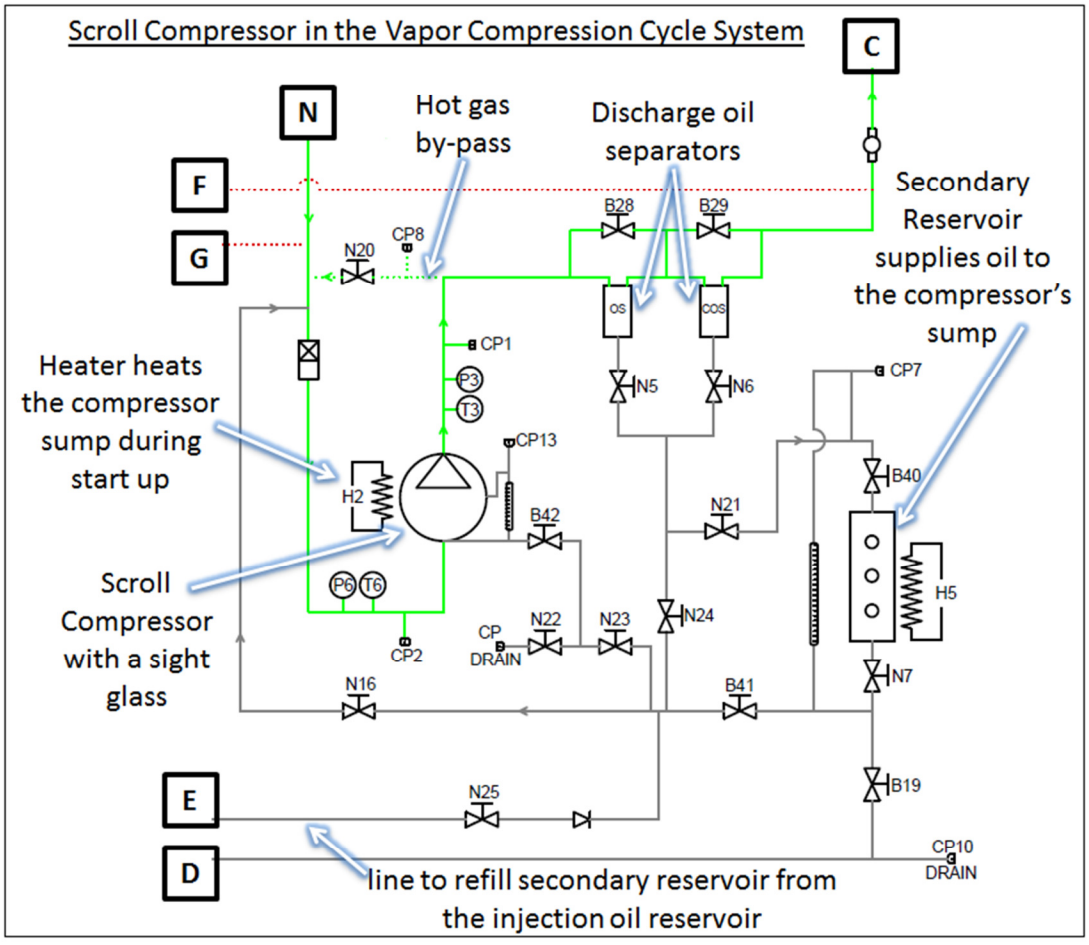

Figure 63: Fluid lines connecting the scroll compressor in the Vapor Compression Cycle System

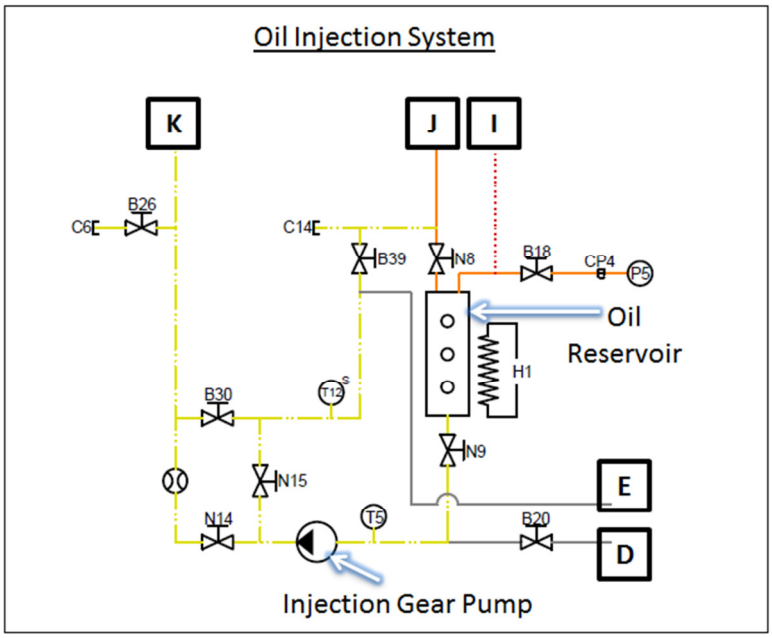

Figure 64: Oil injection system of the Vapor Compression Cycle System

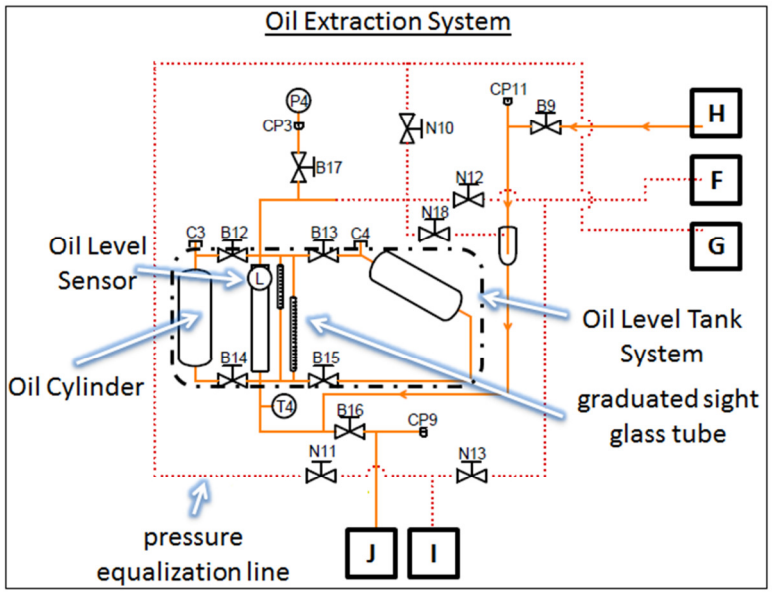

Figure 65: Oil extraction system of the Vapor Compression Cycle System

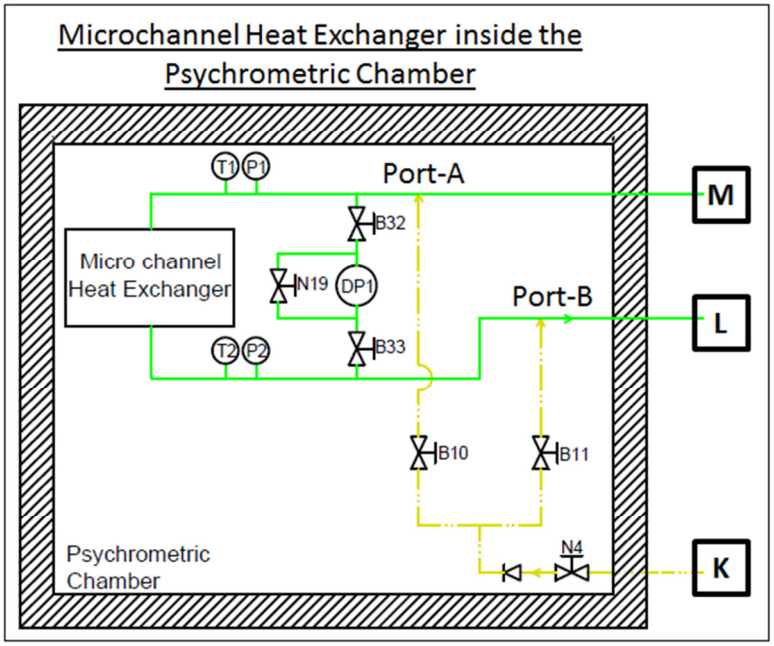

Figure 66: Fluid lines to the microchannel heat exchanger in the Vapor Compression Cycle System

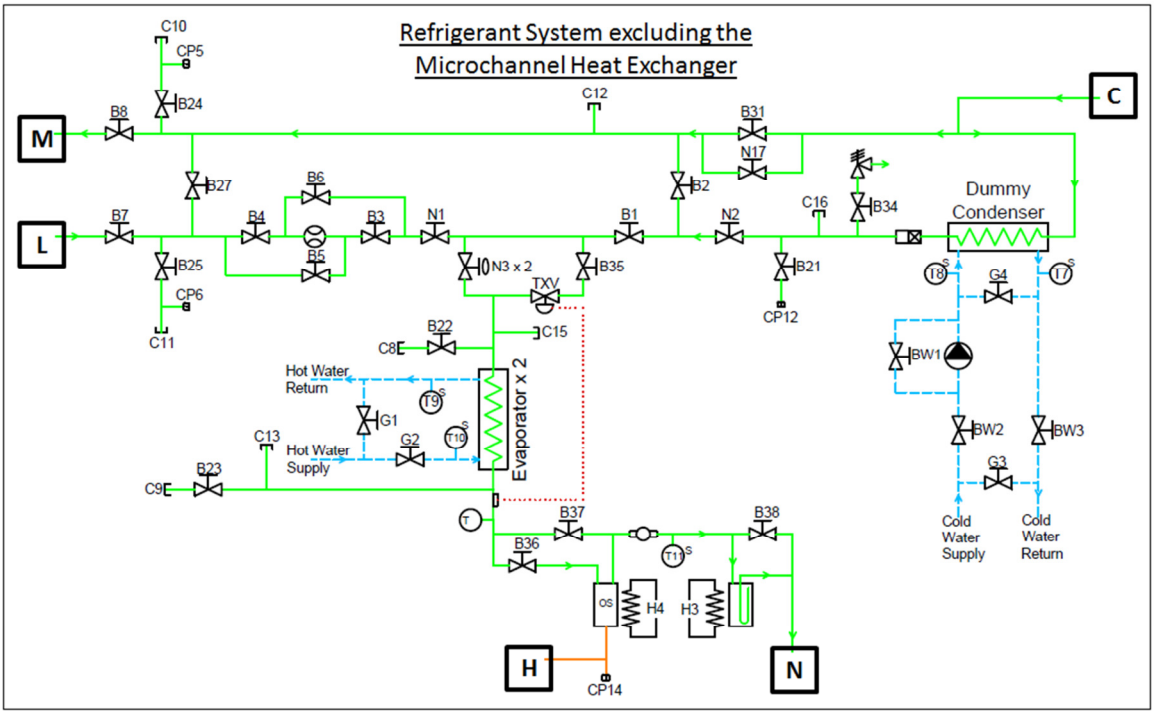

Figure 67: Refrigerant lines of the Vapor Compression Cycle System

Appendix B: Analyzed results of the *HTPF*s and *PDPF*s for all the R-410A/POE32 tests performed on the Pump-Boiler System.

Following graphs presents the translation of the tests from the transient condition to the steady state condition, from the start till the end of the injection test, and shows the change in the *HTPF* and *PDPF* results accordingly. When the green line in the graphs increase from low to high value, it is start of injection test, and when it decrease from high to low value, it is a point where the injection is stopped.

29.4°C (85°F), 0.05 kg/s (400 lbm/h)

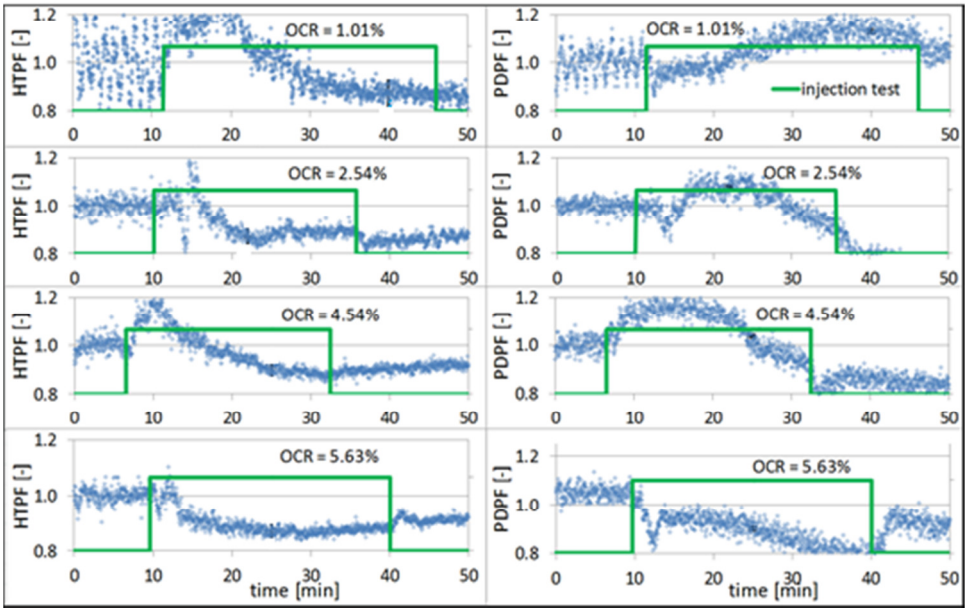

29.4°C (85°F), 0.076 kg/s (600 lbm/h)

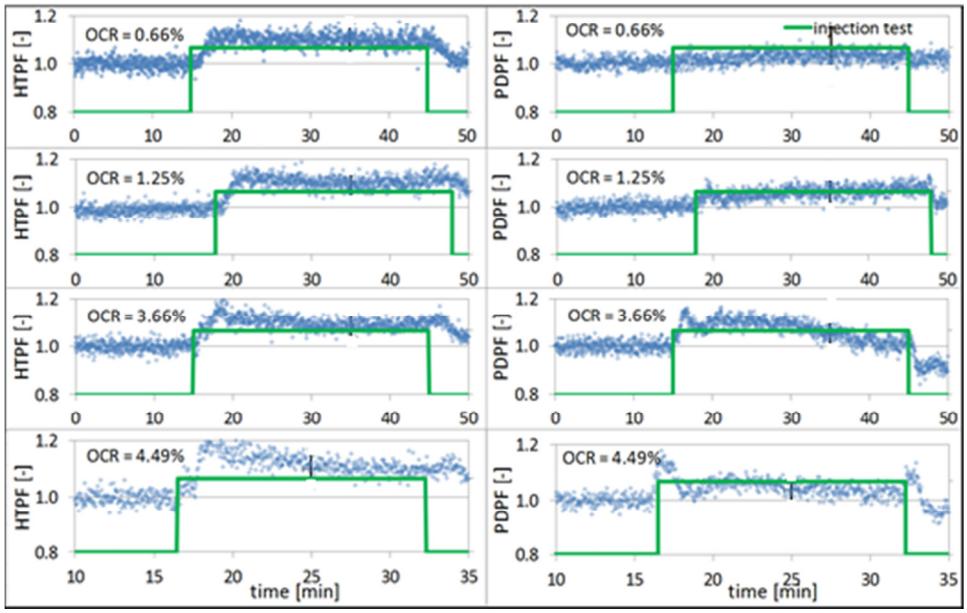

40.6°C (105°F), 0.05 kg/s (400 lbm/h)

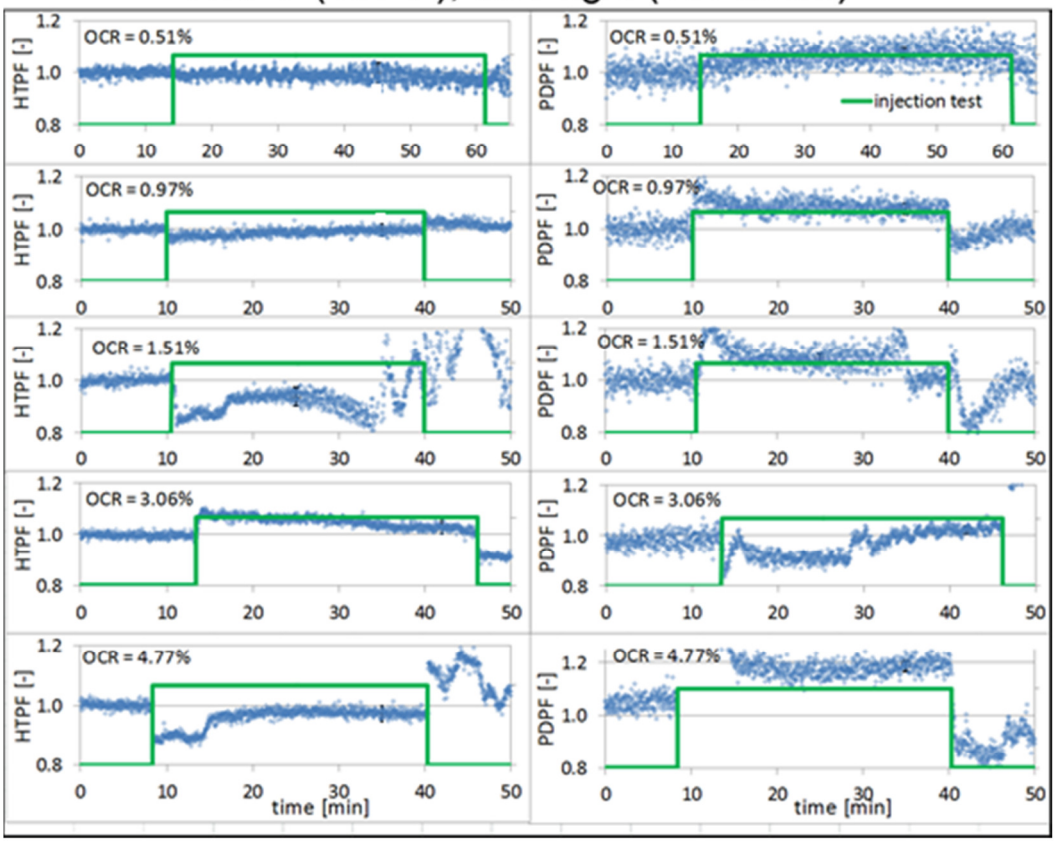

40.6°C (105°F), 0.076 kg/s (600 lbm/h)

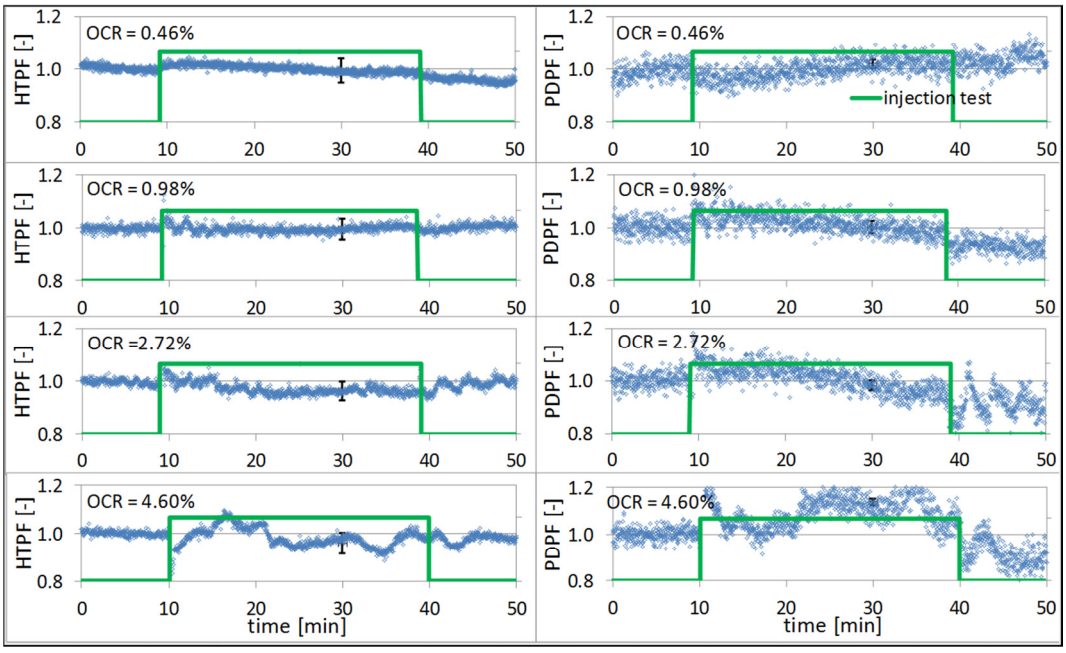

54.4°C (130°F), 0.05 kg/s (400 lbm/h)

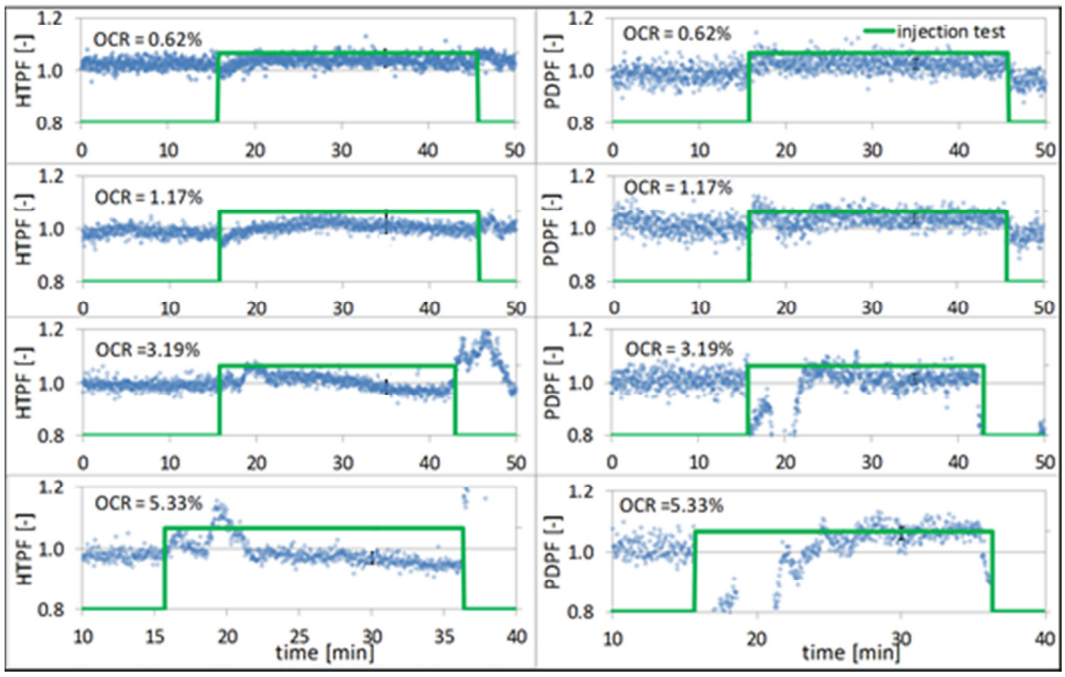

54.4°C (130°F), 0.076 kg/s (600 lbm/h)

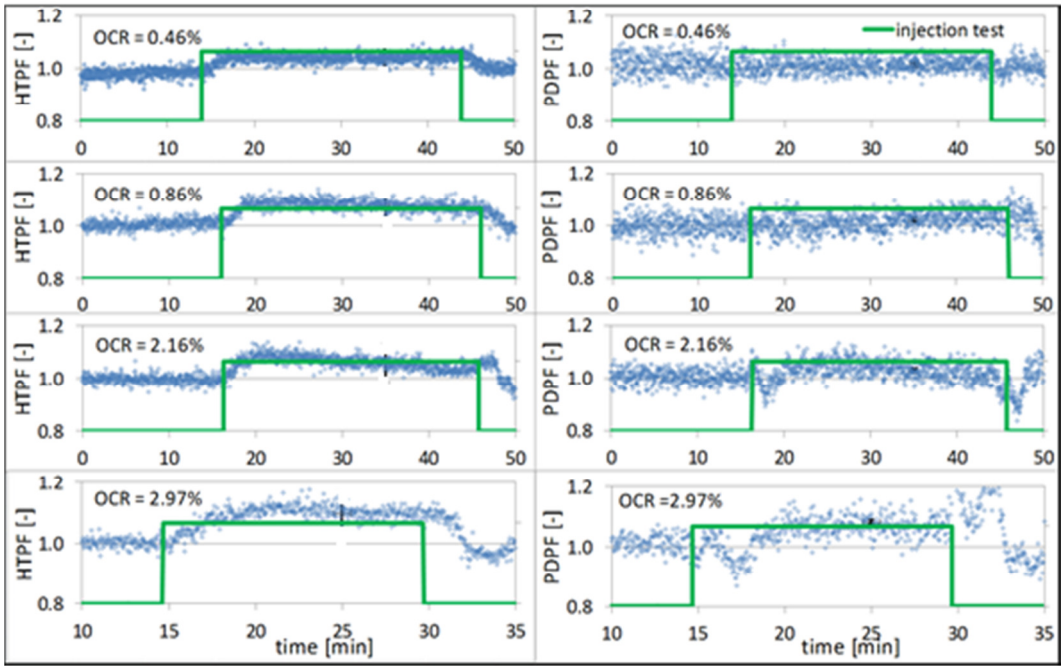

Appendix C: Measured solubility with the sampling cylinder using the gravimetric method.

P	***T***	***S*_sampling cylinder**
[psia]	**[°F]**	**[% w/w]**
262.1	94.1	21.77
273.0	155.0	17.06
274.0	142.0	17.49
274.0	150.0	16.61
276.2	100.8	22.80
277.0	143.0	14.31
277.0	157.0	18.55
278.0	150.0	19.41
278.0	154.0	16.26
281.0	187.0	12.76
289.7	105.4	34.40
290.3	101.8	38.90
296.9	102.2	38.70
313.1	106.2	47.40
315.2	111.0	28.40
320.8	104.2	27.50
354.6	113.3	49.25
359.6	98.6	76.70
360.7	108.9	55.23
361.3	84.3	63.25
363.5	106.2	79.95
364.2	101.7	82.11
495.3	130.0	59.93
495.7	138.4	51.00
496.3	136.2	48.93
496.5	132.5	50.36
496.5	137.8	47.63
496.9	137.2	49.79
497.6	128.2	64.19
498.5	131.6	59.36

Appendix D: VBA codes to calculate the properties of air and volume flow rate at the nozzle bank.

Humidity Ratio of Air

```
Function humidity_ratio(T_db As Double, RH As Double, P As Double)

'inputs: T_db (°F), temperature
'        RH (0 to 1), relative humidity
'        P (in WC gauge), pressure
'output: humidity_ratio (lb_w/lb_da), humidity ratio

Dim C8 As Double, C9 As Double, C10 As Double, C11 As Double, C12 As Double, C13 As Double
Dim T_db_R As Double, p_ws As Double, p_psia As Double, W_s As Double, mu As Double

'Properties of air calculated from
'2001 ASHRAE Fundamentals Handbook, Chapter 6: Psychrometrics'

'water vapor saturated pressure, for temperature range 32 to 392°F (0 to 200°C)'

C8 = -10440.39
C9 = -11.29465
C10 = -0.027022355
C11 = 0.00001289036
C12 = -2.4780681E-09
C13 = 6.5459673

'°F to °R'
T_db_R = T_db + 459.67

p_ws = Exp((C8 / T_db_R) + (C9) + (C10 * T_db_R) + (C11 * T_db_R ^ 2) + (C12 * T_db_R ^ 3) + (C13 *
Application.WorksheetFunction.Ln(T_db_R))) 'p_ws is in psia'

'1 in water = 248.8 N/m2= 0.0361 lb/in2'
p_psia = P * 0.0361 + 14.696

'humidity ratio of saturated moist air, W_s'
W_s = 0.62198 * p_ws / (p_psia - p_ws)

'degree of saturation, mu=W/W_s'
mu = RH / (1 + (1 - RH) * (W_s / 0.62198))

'air humidity ratio, W'
humidity_ratio = mu * W_s

End Function
```

Density of Moist Air - Method 1

```
Function density_air(T_db As Double, RH As Double, P As Double)

'inputs:      Tdb (°F), temperature
'             RH (0 to 1), relative humidity
'             P (in WC gauge), pressure
'output:      density_air (lb_(db+w)/ft^3), density of moist air mixture

Dim p_inHg As Double, W As Double, v As Double, p_psia As Double

W = humidity_ratio(T_db, RH, P)
```

```
'1 in water column = 248.8 N/m2= 0.0361 lb/in2 = 0.0735 in Hg'
p_psia = (P * 0.0361) + 14.696
p_inHg = p_psia * 0.0735 / 0.0361

'specific volume, v'
v = 0.7543 * (T_db + 459.67) * (1 + 1.6078 * W) / p_inHg

'density of moist air mixture, rho_air'
density_air = (1 + W) / v

End Function
```

Density of Moist Air - Method 2

```
Function density_air_with_humidity_ratio(T_db As Double, W As Double, P As Double)

'inputs:      Tdb (°F), temperature
'            W (lb_w/lb_da), humidity ratio
'            P (in WC gauge), pressure
'output:      density_air (lb_(db+w)/ft^3), density of moist air mixture

Dim p_psia As Double, v As Double, p_inHg As Double

'1 in water column = 248.8 N/m2= 0.0361 lb/in2'
p_psia = (P * 0.0361) + 14.696
p_inHg = p_psia * 0.0735 / 0.0361

'specific volume, v'
v = 0.7543 * (T_db + 459.67) * (1 + 1.6078 * W) / p_inHg

'density of moist air mixture, rho_air'
density_air_with_humidity_ratio = (1 + W) / v

End Function
```

Specific Volume of Moist Air

```
Function sp_vol(T_db As Double, W As Double, P As Double)

'inputs:      Tdb (°F), temperature
'            W, humidity ratio
'            P (in WC gauge), pressure
'            del_P(in WC), pressure across the nozzle bank no
'output:      sp_vol (lb/ft^3)^-1, sp.volume of moist air mixture

Dim p_psia As Double, p_inHg As Double

'1 in water column = 248.8 N/m2= 0.0361 lb/in2'
p_psia = (P * 0.0361) + 14.696
p_inHg = p_psia * 0.0735 / 0.0361

'specific volume, v'
sp_vol = 0.7543 * (T_db + 459.67) * (1 + 1.6078 * W) / p_inHg

End Function
```

Specific Enthaly of moist air

```
Function enthalpy_air(T_db As Double, RH As Double, P As Double)

'inputs:      Tdb (°F), temperature
'            RH (0 to 1), relative humidity
'            P (in WC gauge), pressure
'output:      enthalpy (Btu/lb), specific enthaly of moist air
```

```
Dim h_da As Double, h_g As Double, W As Double

W = humidity_ratio(T_db, RH, P)

'specific enthalpy for dry air, h_da'
h_da = 0.24 * T_db

'specific enthalpy for saturated water vapor, h_g'
h_g = W * (1061 + 0.444 * T_db)

'speccific enthalpy of moist air, h [Btu/lbm]'
enthalpy_air = h_da + h_g

End Function
```

***CFM* Calculation**

```
Function CFM_OutdoorNozzleBank(T_db As Double, W As Double, P_inlet As Double, del_P As Double, _
N1 As Double, N2 As Double, N3 As Double, N4 As Double, N5 As Double, N6 As Double, N7 As Double)

'inputs:      Tdb (°F), dry bulb temperature
'            W (lb_w/lb_da), humidity ratio
'            P_inlet (in WC gauge), pressure at the inlet of the nozzle bank
'            del_P(in WC), pressure across the nozzle bank
'            Ni=0 (nozzle Ni is closed), Ni=1(nozzle Ni is open)
'output:      CFM (ft^3/min), volume flow rate of air

Dim rho_air As Double, dia(8) As Double, CA As Double, i As Integer, Re As Double, c As Double
Dim a As Double, alpha As Double, y_ExpFactor As Double, T_db_R As Double

'density of moist air mixture, rho_air'
rho_air = density_air_with_humidity_ratio(T_db, W, P_inlet)

'defining the nozzle diameters'
dia(1) = N1 * 8 / 12
dia(2) = N2 * 7 / 12
dia(3) = N3 * 8 / 12
dia(4) = N4 * 0.5 / 12
dia(5) = N5 * 8 / 12
dia(6) = N6 * 8 / 12
dia(7) = N7 * 8 / 12

'calculation of the CFM of the air is done using the formulas given in ANSI/ ASHRAE 41.2-1987 (RA 92)'
'in the following calculations beta ratio for the nozzle is taken as zero, as beta ratio <<1.
'beta ratio=(nozzle exit diameter)/ (approach duct diameter)'

'initialization'
CA = 0
i = 0

'------------------------------------------------------------------------'
For i = 1 To 7 Step 1
   Re = 1363000 * (dia(i)) * (del_P * rho_air) ^ 0.5
   'note in the equation del_P is in in. WC'
   'for the value of C, curve fit of C=f(Re) is used from the Table 4 of ANSI/ ASHRAE 41.2-1987 (RA 92)'

   'Original Code used by Pratik (bad curve fit):
   'C = (-3.4703E-14 * Re ^ 2) - (0.000000040414 * Re ^ 1) + 0.97725
   '-------------------------------------------------------------------------------------------------
   'Code in the labview (good curve fit)
   'C = (2.20E-31*Re**5)-(6.09E-25*Re**4)+(6.77E-19*Re**3)-(3.90E-13*Re**2)+(1.28E-07*Re)+(9.69E-01)
   '-------------------------------------------------------------------------------------------------
   'Change it to (Pratik got - very good curve fit):
```

```
    If (Re < 76295) Then
        c = -3E-21 * Re ^ 4 + 6E-16 * Re ^ 3 - 0.00000000006 * Re ^ 2 + 0.000002 * Re + 0.9241
    ElseIf (Re >= 76295 And Re < 504164) Then
        c = -2E-27 * Re ^ 4 + 1E-20 * Re ^ 3 - 0.00000000000002 * Re ^ 2 + 0.00000003 * Re + 0.9806
    ElseIf (Re >= 504164) Then
        c = -1E-24 * Re ^ 4 + 2E-18 * Re ^ 3 - 0.0000000000008 * Re ^ 2 + 0.0000002 * Re + 0.9631
    End If
    '   ***************
    '=if(Re<76295,-3E-21* Re ^4+ 6E-16* Re ^3 - 6E-11* Re ^2 + 2E-06* Re  + 0.9241,if(Re>=504164,
    '-1E-24* Re ^4 + 2E-18* Re ^3 - 8E-13* Re ^2 + 2E-07* Re + 0.9631,-2E-27* Re ^4 + 1E-20* Re ^3
    '- 2E-14* Re ^2 + 3E-08* Re  + 0.9806))
    '   ***************

    a = 3.14159265 / 4 * (dia(i) ^ 2)
    CA = CA + (c * a)
Next i
'-------------------------------------------------------------------------'

'°F to °R'
T_db_R = T_db + 459.67
'alpha ratio'
alpha = 1 - (5.187 * del_P / rho_air / 53.35 / T_db_R)

'expansion factor'
y_ExpFactor = 1 - 0.548 * (1 - alpha)

'-----------------------------------------------------------------------------
'volume flow rate [ft^3/min]'
'old equation CFM_OutdoorNozzleBank = 1096 * CA * y_ExpFactor * (del_P / rho_air) ^ 0.5

Dim CF As Double 'CF is correction for CFM
CF = -0.1267 * (1 / rho_air) + 2.9673
CFM_OutdoorNozzleBank = CF * 1096 * CA * y_ExpFactor * (del_P / rho_air) ^ 0.5
'-----------------------------------------------------------------------------

End Function
```

Appendix E: Codes in EES to create the lookup table for R-410A and R-134a.

Code in EES to create the lookup table for R-410A

```
cp_l=Cp(R410A,P=P_sat,x=0)
cp_v=Cp(R410A,P=P_sat,x=1)

h_f=Enthalpy(R410A,P=P_sat,x=0)
h_g=Enthalpy(R410A,P=P_sat,x=1)

rho_f=Density(R410A,P=P_sat,x=0)
rho_g=Density(R410A,P=P_sat,x=1)

s_f=Entropy(R410A,P=P_sat,x=0)
s_g=Entropy(R410A,P=P_sat,x=1)

Phase_f=Phase$(R410A,P=P_sat,x=0)
Phase_g=Phase$(R410A,P=P_sat,x=1)

T_f=Temperature(R410A,P=P_sat,x=0)
T_g=Temperature(R410A,P=P_sat,x=1)

mu_f=Viscosity(R410A,P=P_sat,x=0)
mu_g=Viscosity(R410A,P=P_sat,x=1)
```

$cp_l = Cp('R410A', P = P_{sat}, x = 0)$

$cp_v = Cp('R410A', P = P_{sat}, x = 1)$

$h_f = h('R410A', P = P_{sat}, x = 0)$

$h_g = h('R410A', P = P_{sat}, x = 1)$

$\rho_f = \rho('R410A', P = P_{sat}, x = 0)$

$\rho_g = \rho('R410A', P = P_{sat}, x = 1)$

$s_f = s('R410A', P = P_{sat}, x = 0)$

$s_g = s('R410A', P = P_{sat}, x = 1)$

$Phase_f = Phase\$('R410A', P = P_{sat}, x = 0)$

$Phase_g = Phase\$('R410A', P = P_{sat}, x = 1)$

$T_f = T('R410A', P = P_{sat}, x = 0)$

$T_g = T('R410A', P = P_{sat}, x = 1)$

$\mu_f = Visc('R410A', P = P_{sat}, x = 0)$

$\mu_g = Visc('R410A', P = P_{sat}, x = 1)$

Code in EES to create the lookup table for R-134a

```
cp_l=Cp(R134A,P=P_sat,x=0)
cp_v=Cp(R134A,P=P_sat,x=1)

h_f=Enthalpy(R134A,P=P_sat,x=0)
h_g=Enthalpy(R134A,P=P_sat,x=1)

rho_f=Density(R134A,P=P_sat,x=0)
rho_g=Density(R134A,P=P_sat,x=1)

s_f=Entropy(R134A,P=P_sat,x=0)
s_g=Entropy(R134A,P=P_sat,x=1)

Phase_f=Phase$(R134A,P=P_sat,x=0)
Phase_g=Phase$(R134A,P=P_sat,x=1)

T_f=Temperature(R134A,P=P_sat,x=0)
T_g=Temperature(R134A,P=P_sat,x=1)

mu_f=Viscosity(R134A,P=P_sat,x=0)
mu_g=Viscosity(R134A,P=P_sat,x=1)
```

$cp_l = Cp('R134a', P = P_{sat}, x = 0)$

$cp_v = Cp('R134a', P = P_{sat}, x = 1)$

$h_f = h('R134a', P = P_{sat}, x = 0)$

$h_g = h('R134a', P = P_{sat}, x = 1)$

$\rho_f = \rho('R134a', P = P_{sat}, x = 0)$

$\rho_g = \rho('R134a', P = P_{sat}, x = 1)$

$s_f = s('R134a', P = P_{sat}, x = 0)$

$s_g = s('R134a', P = P_{sat}, x = 1)$

$Phase_f = Phase\$('R134a', P = P_{sat}, x = 0)$

$Phase_g = Phase\$('R134a', P = P_{sat}, x = 1)$

$T_f = T('R134a', P = P_{sat}, x = 0)$

$T_g = T('R134a', P = P_{sat}, x = 1)$

$\mu_f = Visc('R134a', P = P_{sat}, x = 0)$

$\mu_g = Visc('R134a', P = P_{sat}, x = 1)$

Appendix F: Lookup table for R-410A and R-134a.

Lookup Table for R-410A;

P_{sat}	T_f	T_g	h_f	h_g	s_f	s_g	ρ_f	ρ_g	$c_{p,f}$	$c_{p,g}$	μ_f	μ_g
psia	°F	°F	Btu/lbm	Btu/lbm	Btu/lbm-R	Btu/lbm-R	lbm/ft3	lbm/ft3	Btu/lbm-R	Btu/lbm-R	lbm/ft-hr	lbm/ft-h
0.49	-150.6	-150.5	-34.53	100.0	-0.0970	0.3384	94.43	0.0108	0.2903	0.1454	1.3430	0.0163
0.51	-149.8	-149.7	-34.30	100.1	-0.0962	0.3376	94.35	0.0112	0.2906	0.1456	1.3370	0.0163
0.54	-148.7	-148.6	-33.97	100.3	-0.0952	0.3366	94.24	0.0118	0.2912	0.1460	1.3280	0.0164
0.57	-147.6	-147.5	-33.66	100.5	-0.0941	0.3356	94.14	0.0124	0.2917	0.1463	1.3200	0.0165
0.60	-146.5	-146.5	-33.36	100.6	-0.0931	0.3347	94.04	0.0130	0.2922	0.1466	1.3130	0.0166
0.63	-145.6	-145.5	-33.07	100.7	-0.0922	0.3338	93.94	0.0136	0.2927	0.1469	1.3050	0.0166
0.66	-144.6	-144.5	-32.79	100.9	-0.0913	0.3329	93.85	0.0142	0.2931	0.1472	1.2980	0.0167
0.69	-143.7	-143.6	-32.52	101.0	-0.0904	0.3321	93.76	0.0149	0.2935	0.1475	1.2910	0.0168
0.73	-142.5	-142.4	-32.17	101.1	-0.0893	0.3311	93.65	0.0157	0.2941	0.1478	1.2830	0.0168
0.76	-141.7	-141.6	-31.92	101.3	-0.0885	0.3304	93.57	0.0163	0.2944	0.1481	1.2760	0.0169
0.80	-140.6	-140.5	-31.61	101.4	-0.0875	0.3294	93.46	0.0171	0.2949	0.1484	1.2680	0.0170
0.84	-139.5	-139.5	-31.30	101.6	-0.0865	0.3285	93.36	0.0179	0.2954	0.1488	1.2610	0.0170
0.88	-138.6	-138.5	-31.00	101.7	-0.0855	0.3277	93.26	0.0187	0.2959	0.1491	1.2540	0.0171
0.92	-137.6	-137.5	-30.72	101.8	-0.0846	0.3269	93.17	0.0195	0.2963	0.1494	1.2470	0.0172
630.4	150.5	150.7	80.02	117.1	0.1516	0.2124	46.97	15.34	0.7817	0.7473	0.1510	0.0522
637.8	151.5	151.7	80.84	116.8	0.1529	0.2117	46.43	15.76	0.8145	0.7412	0.1480	0.0530
645.3	152.5	152.6	81.70	116.5	0.1543	0.2111	45.86	16.23	0.8558	0.7266	0.1460	0.0540
652.8	153.5	153.6	82.61	116.1	0.1557	0.2104	45.26	16.73	0.9107	0.6991	0.1430	0.0551
660.4	154.5	154.6	83.58	115.8	0.1573	0.2097	44.61	17.30	0.9884	0.6526	0.1410	0.0563
668.1	155.5	155.6	84.65	115.5	0.1590	0.2090	43.90	17.93	1.1040	0.5803	0.1380	0.0577
675.9	156.5	156.6	85.87	115.2	0.1609	0.2084	43.12	18.63	1.2820	0.4798	0.1350	0.0593
683.7	157.5	157.6	87.30	115.0	0.1632	0.2080	42.24	19.39	1.5500	0.3630	0.1320	0.0610
691.6	158.5	158.6	89.06	114.9	0.1659	0.2078	41.23	20.20	1.9330	0.2610	0.1280	0.0630

Lookup Table for R-134a;

P_{sat}	T_f	T_g	h_f	h_g	s_f	s_g	ρ_f	ρ_g	$c_{p,f}$	$c_{p,g}$	μ_f	μ_g
psia	°F	°F	Btu/lbm	Btu/lbm	Btu/lbm-R	Btu/lbm-R	lbm/ft3	lbm/ft3	Btu/lbm-R	Btu/lbm-R	lbm/ft-hr	lbm/ft-h
20.70	-150.6	-150.5	-34.53	100.0	-0.0970	0.3384	94.43	0.0108	0.2903	0.1454	1.3430	0.0163
0.51	-149.8	-149.7	-34.30	100.1	-0.0962	0.3376	94.35	0.0112	0.2906	0.1456	1.3370	0.0163
0.54	-148.7	-148.6	-33.97	100.3	-0.0952	0.3366	94.24	0.0118	0.2912	0.1460	1.3280	0.0164
0.57	-147.6	-147.5	-33.66	100.5	-0.0941	0.3356	94.14	0.0124	0.2917	0.1463	1.3200	0.0165
0.60	-146.5	-146.5	-33.36	100.6	-0.0931	0.3347	94.04	0.0130	0.2922	0.1466	1.3130	0.0166
0.63	-145.6	-145.5	-33.07	100.7	-0.0922	0.3338	93.94	0.0136	0.2927	0.1469	1.3050	0.0166
0.66	-144.6	-144.5	-32.79	100.9	-0.0913	0.3329	93.85	0.0142	0.2931	0.1472	1.2980	0.0167
0.69	-143.7	-143.6	-32.52	101.0	-0.0904	0.3321	93.76	0.0149	0.2935	0.1475	1.2910	0.0168
0.73	-142.5	-142.4	-32.17	101.1	-0.0893	0.3311	93.65	0.0157	0.2941	0.1478	1.2830	0.0168
0.76	-141.7	-141.6	-31.92	101.3	-0.0885	0.3304	93.57	0.0163	0.2944	0.1481	1.2760	0.0169
0.80	-140.6	-140.5	-31.61	101.4	-0.0875	0.3294	93.46	0.0171	0.2949	0.1484	1.2680	0.0170
630.4	150.5	150.7	80.02	117.1	0.1516	0.2124	46.97	15.34	0.7817	0.7473	0.1510	0.0522
637.8	151.5	151.7	80.84	116.8	0.1529	0.2117	46.43	15.76	0.8145	0.7412	0.1480	0.0530
645.3	152.5	152.6	81.70	116.5	0.1543	0.2111	45.86	16.23	0.8558	0.7266	0.1460	0.0540
652.8	153.5	153.6	82.61	116.1	0.1557	0.2104	45.26	16.73	0.9107	0.6991	0.1430	0.0551
660.4	154.5	154.6	83.58	115.8	0.1573	0.2097	44.61	17.30	0.9884	0.6526	0.1410	0.0563
668.1	155.5	155.6	84.65	115.5	0.1590	0.2090	43.90	17.93	1.1040	0.5803	0.1380	0.0577
675.9	156.5	156.6	85.87	115.2	0.1609	0.2084	43.12	18.63	1.2820	0.4798	0.1350	0.0593
683.7	157.5	157.6	87.30	115.0	0.1632	0.2080	42.24	19.39	1.5500	0.3630	0.1320	0.0610
691.6	158.5	158.6	89.06	114.9	0.1659	0.2078	41.23	20.20	1.9330	0.2610	0.1280	0.0630

Appendix G: Codes in VBA to get refrigerant properties from the lookup table.

```
Option Explicit

Function h_gas(P_g As Double)
'input: P_g vapor pressure (psia) - Saturated pressure of the vapor
'output: h_g vapor enthalpy (Btu/lb)
h_gas = -0.000000000000007 * (P_g ^ 6) + 0.00000000002 * (P_g ^ 5) - 0.00000001 * (P_g ^ 4) + _
        0.000007 * (P_g ^ 3) - 0.0017 * (P_g ^ 2) + 0.2317 * (P_g) + 109.25

End Function

'*****************************************************************************************
Function enthalpy_PT_g(P_g As Double, T_g As Double)
'input: P_g vapor pressure (psia) assumed to be saturated pressure of the vapor
'       T_g vapor pressure (psia) - saturated or superheated temperature of the vapor
'output: enthalpy_PT_g vapor enthalpy (Btu/lb)

Dim i As Integer, imax As Integer, p1 As Double, p2 As Double
Dim h1 As Double, h2 As Double, T1 As Double, T2 As Double, cp1 As Double, cp2 As Double
Dim hv As Double, Tv As Double, cpv As Double, ihold As Integer

imax = 312  'imax is the number of rows in the lookup table

For i = 3 To imax Step 1
   p1 = Worksheets("lookup table").Cells(i, 1)
   p2 = Worksheets("lookup table").Cells(i + 1, 1)
   If (p1 < P_g And p2 >= P_g) Then
      h1 = Worksheets("lookup table").Cells(i, 5)
      h2 = Worksheets("lookup table").Cells(i + 1, 5)
      hv = ((P_g - p2) * (h1 - h2) / (p1 - p2)) + h2

      T1 = Worksheets("lookup table").Cells(i, 3)
      T2 = Worksheets("lookup table").Cells(i + 1, 3)
      Tv = ((P_g - p2) * (T1 - T2) / (p1 - p2)) + T2

      cp1 = Worksheets("lookup table").Cells(i, 11)
      cp2 = Worksheets("lookup table").Cells(i + 1, 11)
      cpv = ((P_g - p2) * (cp1 - cp2) / (p1 - p2)) + cp2

      ihold = i
      i = imax
   End If
Next i

If (T_g <= Tv) Then
   enthalpy_PT_g = hv
ElseIf (T_g > Tv) Then
   enthalpy_PT_g = hv + cpv * (T_g - Tv)
End If

End Function

'*****************************************************************************************
Function enthalpy_PT_l(P_f As Double, T_f As Double)
'input: P_f liquid pressure (psia) assumed to be saturated pressure of the liquid
'       T_f liquid pressure (psia) - saturated or subcooled temperature of the liquid
'output: enthalpy_PT_l liquid enthalpy (Btu/lb)

Dim i As Integer, imax As Integer, p1 As Double, p2 As Double
```

```
Dim h1 As Double, h2 As Double, T1 As Double, T2 As Double, cp1 As Double, cp2 As Double
Dim hl As Double, Tl As Double, cpl As Double, ihold As Integer

imax = 312

For i = 3 To imax Step 1
   p1 = Worksheets("lookup table").Cells(i, 1)
   p2 = Worksheets("lookup table").Cells(i + 1, 1)
   If (p1 < P_f And p2 >= P_f) Then
      h1 = Worksheets("lookup table").Cells(i, 4)
      h2 = Worksheets("lookup table").Cells(i + 1, 4)
      hl = ((P_f - p2) * (h1 - h2) / (p1 - p2)) + h2

      T1 = Worksheets("lookup table").Cells(i, 2)
      T2 = Worksheets("lookup table").Cells(i + 1, 2)
      Tl = ((P_f - p2) * (T1 - T2) / (p1 - p2)) + T2

      cp1 = Worksheets("lookup table").Cells(i, 10)
      cp2 = Worksheets("lookup table").Cells(i + 1, 10)
      cpl = ((P_f - p2) * (cp1 - cp2) / (p1 - p2)) + cp2

      ihold = i
      i = imax
   End If
Next i

If (T_f >= Tl) Then
   enthalpy_PT_l = hl
ElseIf (T_f < Tl) Then
   enthalpy_PT_l = hl - cpl * (Tl - T_f)
End If

End Function

'*****************************************************************************************
Function entropy_PT_g(P_g As Double, T_g As Double)
'input: P_g vapor pressure (psia) assumed to be saturated pressure of the liquid
'       T_g vapor pressure (psia) - saturated or superheated temperature of the liquid
'output: entropy_PT_g vapor entropy (Btu/lb-ºR)

Dim i As Integer, imax As Integer, p1 As Double, p2 As Double
Dim s1 As Double, s2 As Double, T1 As Double, T2 As Double, cp1 As Double, cp2 As Double
Dim sv As Double, Tv As Double, cpv As Double

imax = 312

For i = 3 To imax Step 1
   p1 = Worksheets("lookup table").Cells(i, 1)
   p2 = Worksheets("lookup table").Cells(i + 1, 1)
   If (p1 < P_g And p2 >= P_g) Then
      s1 = Worksheets("lookup table").Cells(i, 7)
      s2 = Worksheets("lookup table").Cells(i + 1, 7)
      sv = ((P_g - p2) * (s1 - s2) / (p1 - p2)) + s2

      T1 = Worksheets("lookup table").Cells(i, 3)
      T2 = Worksheets("lookup table").Cells(i + 1, 3)
      Tv = ((P_g - p2) * (T1 - T2) / (p1 - p2)) + T2

      cp1 = Worksheets("lookup table").Cells(i, 11)
      cp2 = Worksheets("lookup table").Cells(i + 1, 11)
      cpv = ((P_g - p2) * (cp1 - cp2) / (p1 - p2)) + cp2
```

```
        i = imax
    End If
Next i

If (T_g <= Tv) Then
    entropy_PT_g = sv
ElseIf (T_g > Tv) Then
    entropy_PT_g = sv + cpv * Application.WorksheetFunction.Ln(T_g / Tv)
End If

End Function

'*************************************************************************************************
Function entropy_PT_l(P_f As Double, T_f As Double)
'input: P_f liquid pressure (psia) assumed to be saturated pressure of the liquid
'       T_f liquid pressure (psia) - saturated or subcooled temperature of the liquid
'output: entropy_PT_l liquid entropy (Btu/lb-°R)

Dim i As Integer, imax As Integer, p1 As Double, p2 As Double
Dim s1 As Double, s2 As Double, T1 As Double, T2 As Double, cp1 As Double, cp2 As Double
Dim sl As Double, Tl As Double, cpl As Double

imax = 312

For i = 3 To imax Step 1
    p1 = Worksheets("lookup table").Cells(i, 1)
    p2 = Worksheets("lookup table").Cells(i + 1, 1)
    If (p1 < P_f And p2 >= P_f) Then
        s1 = Worksheets("lookup table").Cells(i, 6)
        s2 = Worksheets("lookup table").Cells(i + 1, 6)
        sl = ((P_f - p2) * (s1 - s2) / (p1 - p2)) + s2

        T1 = Worksheets("lookup table").Cells(i, 2)
        T2 = Worksheets("lookup table").Cells(i + 1, 2)
        Tl = ((P_f - p2) * (T1 - T2) / (p1 - p2)) + T2

        cp1 = Worksheets("lookup table").Cells(i, 10)
        cp2 = Worksheets("lookup table").Cells(i + 1, 10)
        cpl = ((P_f - p2) * (cp1 - cp2) / (p1 - p2)) + cp2

        i = imax
    End If
Next i

If (T_f >= Tl) Then
    entropy_PT_l = sl
ElseIf (T_f < Tl) Then
    entropy_PT_l = sl - cpl * Application.WorksheetFunction.Ln(Tl / T_f)
End If

End Function

'*************************************************************************************************
Function temperature_PT_g(P_g As Double)
'input: P_g vapor pressure (psia) assumed to be saturated pressure of the vapor
'output: temperature_PT_g vapor temperature (°F)

Dim i As Integer, imax As Integer, p1 As Double, p2 As Double
Dim T1 As Double, T2 As Double
Dim Tv As Double, ihold As Integer

imax = 312
```

```
For i = 3 To imax Step 1
   p1 = Worksheets("lookup table").Cells(i, 1)
   p2 = Worksheets("lookup table").Cells(i + 1, 1)
   If (p1 < P_g And p2 >= P_g) Then

      T1 = Worksheets("lookup table").Cells(i, 3)
      T2 = Worksheets("lookup table").Cells(i + 1, 3)
      Tv = ((P_g - p2) * (T1 - T2) / (p1 - p2)) + T2

      ihold = i
      i = imax
   End If
Next i
temperature_PT_g = Tv

End Function
'*****************************************************************************************
Function temperature_PT_l(P_f As Double)
'input: P_f liquid pressure (psia) assumed to be saturated pressure of the liquid
'output: temperature_PT_l liquid temperature (ºF)

Dim i As Integer, imax As Integer, p1 As Double, p2 As Double
Dim T1 As Double, T2 As Double
Dim Tl As Double

imax = 312

For i = 3 To imax Step 1
   p1 = Worksheets("lookup table").Cells(i, 1)
   p2 = Worksheets("lookup table").Cells(i + 1, 1)
   If (p1 < P_f And p2 >= P_f) Then

      T1 = Worksheets("lookup table").Cells(i, 2)
      T2 = Worksheets("lookup table").Cells(i + 1, 2)
      Tl = ((P_f - p2) * (T1 - T2) / (p1 - p2)) + T2
      i = imax
   End If
Next i
temperature_PT_l = Tl

End Function
```

.

Appendix H: Example to calculate $\boldsymbol{OCR}$, $\boldsymbol{HTPF}$, and $\boldsymbol{PDPF}$ values and their uncertainties.

Example: The oil-refrigerant mixture is injected upstream of the microchannel heat exchanger (at port-A) at a mass flow rate of $\dot{m}_{oil+ref,inj}$ = 27 ± 0.006 lbm/h. The gravimetric method determines the solubility of this injected mixture as S = 47.25 ± 2.18% w/w. The total mass flow rate of the oil-refrigerant mixture at the inlet of the microchannel heat exchanger calculated is $\dot{m}_{ref,test-section}$ = 395.8 ± 0.005 lbm/h. The inlet pressure and superheat temperature observed at the inlet of the microchannel condenser are $P_{mchx,i}$ = 353.04 ± 0.65 and $T_{mchx,i}$ = 111.79 ± 0.36 respectively. The heat transferred by the microchannel condenser to the air during the injection test causes the temperature of the air to rise by $\Delta T_{air@OCR}$= 9.41 ± 0.51°F, the calculated heat transfer is $Q_{air@OCR}$ = 26632.02 ± 1441.37 Btu/h. The oil-refrigerant fluid pressure drop measured by the differential pressure transducer during the injection test is $\Delta P_{@OCR}$ = 2.74 ± 0.03 psi. Using the mapping data the temperature rise, heat transfer, and pressure drop in absence of oil are interpolated at same total flow rate and the inlet pressure as $\Delta T_{air@OCR=0}$ = 9.5 ± 0.51°F, $Q_{air@OCR=0}$ = 27215.63 ± 1441.37, and $\Delta P_{@OCR=0}$ = 2.40 ± 0.03 psi respectively. The aim is to calculate the OCR, $HTPF$, and $PDPF$.

Solution:
$\dot{m}_{oil+ref,inj}$ = 27 ± 0.006 lbm/h
S = 47.25 ± 2.18% w/w
$\dot{m}_{ref,test-section}$ = 395.8 ± 0.005 lbm/h.
$P_{mchx,i}$ = 353.04 ± 0.65
$T_{mchx,i}$ = 111.79 ± 0.36
$\Delta T_{air@OCR}$= 9.41 ± 0.51°F
$Q_{air@OCR}$ = 26632.02 ± 1441.37 Btu/h
$\Delta P_{@OCR}$ = 2.74 ± 0.03 psi
$\Delta T_{air@OCR=0}$ = 9.5 ± 0.51°F
$Q_{air@OCR=0}$ = 27215.63 ± 1441.37
$\Delta P_{@OCR=0}$ = 2.40 ± 0.03
Find OCR, $HTPF$, and $PDPF$.

Using Equation (4.7);

$$\dot{m}_{ref,inj} = {\dot{m}_{oil+ref,inj}}\Big/{\left(1+\frac{100}{S}\right)} = {27}\Big/{\left(1+\frac{100}{47}\right)} = \boldsymbol{\dot{m}_{ref,inj} = 8.63\ \mathbf{lbm/h}}$$

Applying the rule of uncertainty propagation outlined in the book by Taylor (1996)

$$\delta\dot{m}_{ref,inj} = \sqrt{\left[\left({\delta\dot{m}_{oil+ref,inj}}\Big/{\left(1+\frac{100}{S}\right)}\right)^2 + \left({\dot{m}_{oil+ref,inj}\cdot 100}\Big/{(100+S)^2\,\delta S}\right)^2\right]}$$

$$\delta\dot{m}_{ref,inj} = \sqrt{\left[\left(0.006 \Big/ \left(1+\frac{100}{47}\right)\right)^2 + \left(\frac{27\cdot 100}{(100+47)^2} * 2.18\right)^2\right]} = \boldsymbol{\delta\dot{m}_{ref,inj} = \pm 0.27\ \text{lbm/h}}$$

Using Equation (4.8);

$$\dot{m}_{oil,inj} = \dot{m}_{oil+ref,inj} \Big/ \left(1+\frac{s}{100}\right) = 27 \Big/ \left(1+\frac{47}{100}\right) = \boldsymbol{\dot{m}_{oil,inj} = 18.37\ \text{lbm/h}}$$

Applying the rule of uncertainty propagation,

$$\delta\dot{m}_{oil,inj} = \sqrt{\left[\left(\delta\dot{m}_{oil+ref,inj} \Big/ \left(1+\frac{S}{100}\right)\right)^2 + \left(-\dot{m}_{oil+ref,inj}\cdot 100 \Big/ (100+S)^2\,\delta S\right)^2\right]}$$

$$\delta\dot{m}_{oil,inj} = \sqrt{\left[\left(0.006 \Big/ \left(1+\frac{47}{100}\right)\right)^2 + \left(\frac{-27\cdot 100}{(100+47)^2} * 2.18\right)^2\right]} = \boldsymbol{\delta\dot{m}_{oil,inj} = \pm 0.074\ \text{lbm/h}}$$

Using Equation (4.10);

$$\dot{m}_{ref,mchx} = \dot{m}_{ref,test-section} + \dot{m}_{ref,inj} = 395.8 + 8.63 = \boldsymbol{\dot{m}_{ref,mchx} = 404.43\ \text{lbm/h}}$$

Applying the rule of uncertainty propagation,

$$\delta\dot{m}_{ref,mchx} = \sqrt{\left[\left(\delta\dot{m}_{ref,test-section}\right)^2 + \left(\delta\dot{m}_{ref,inj}\right)^2\right]} = \sqrt{[(0.006)^2 + (0.27)^2]}$$

$$\boldsymbol{\delta\dot{m}_{ref,mchx} = \pm 0.27\ \text{lbm/h}}$$

Using Equation (4.11);

$$OCR = \left(\dot{m}_{oil,inj} \Big/ \left(\dot{m}_{oil,inj} + \dot{m}_{ref,mchx}\right)\right) 100$$

$$OCR = \left(18.37 \Big/ (18.37 + 404.43)\right) 100 = \boldsymbol{OCR = 4.34\%}$$

Applying the rule of uncertainty propagation,

$$\delta OCR = \sqrt{\left[\left(\frac{-\dot{m}_{oil,inj} \cdot 100}{\left(\dot{m}_{oil,inj} + \dot{m}_{ref,mchx}\right)^2}\delta\dot{m}_{ref,mchx}\right)^2 + \left(\frac{\dot{m}_{ref,mchx} \cdot 100}{\left(\dot{m}_{oil,inj} + \dot{m}_{ref,mchx}\right)^2}\delta\dot{m}_{oil,inj}\right)^2\right]}$$

$$\delta OCR = \sqrt{\left[\left(\frac{-18.37 * 100}{(18.37 + 404.43)^2} * 0.27\right)^2 + \left(\frac{404.43 * 100}{(18.37 + 404.43)^2} * 0.074\right)^2\right]}$$

$$\delta OCR = \sqrt{\left[\left(\frac{-18.37 * 100}{(18.37 + 404.43)^2} * 0.27\right)^2 + \left(\frac{404.43 * 100}{(18.37 + 404.43)^2} * 0.074\right)^2\right]}$$

$$\boldsymbol{\delta OCR = \pm 0.02\%}$$

Using Equation (4.13);

$$HTPF\_Q_{air} = {Q_{air@OCR}}/{Q_{air@OCR=0}} = {26632.02}/{27215.63} = \boldsymbol{HTPF\_Q_{air} = 0.98}$$

Applying the rule of uncertainty propagation,

$$\delta HTPF\_Q_{air} = \sqrt{\left[\left(\frac{1}{Q_{air@OCR=0}}\delta Q_{air@OCR}\right)^2 + \left(\frac{-Q_{air@OCR}}{{Q_{air@OCR=0}}^2}\delta Q_{air@OCR=0}\right)^2\right]}$$

$$\delta HTPF\_Q_{air} = \sqrt{\left[\left(\frac{1}{27215.63}1441.37\right)^2 + \left(\frac{-26632.02}{27215.63^2}1441.37\right)^2\right]}$$

$$\boldsymbol{\delta HTPF\_Q_{air} = \pm 0.074}$$

Using Equation (4.14);

$$HTPF\_\Delta T_{air} = {\Delta T_{air@OCR}}/{\Delta T_{air@OCR=0}} = {9.41}/{9.5} = \boldsymbol{HTPF\_\Delta T_{air} = 0.99}$$

Applying the rule of uncertainty propagation,

$$\delta HTPF\_\Delta T_{air} = \sqrt{\left[\left(\frac{1}{\Delta T_{air@OCR=0}}\delta\Delta T_{air@OCR}\right)^2 + \left(\frac{-\Delta T_{air@OCR}}{{\Delta T_{air@OCR=0}}^2}\delta\Delta T_{air@OCR=0}\right)^2\right]}$$

$$\delta HTPF\_\Delta T_{air} = \sqrt{\left[\left(\frac{1}{9.5}0.51\right)^2 + \left(\frac{-9.41}{9.5^2}0.51\right)^2\right]} = \boldsymbol{\delta HTPF\_\Delta T_{air} = \pm 0.076}$$

Using Equation (4.15);

$$PDPF = {}^{\Delta P_{@OCR}}\Big/_{\Delta P_{@OCR=0}} = {}^{2.74}\Big/_{2.4} = \boldsymbol{PDPF = 1.14}$$

Applying the rule of uncertainty propagation,

$$\delta PDPF = \sqrt{\left[\left(\frac{1}{\Delta P_{@OCR=0}}\delta\Delta P_{@OCR}\right)^2 + \left(\frac{-\Delta P_{@OCR}}{\Delta P_{@OCR=0}^{\ 2}}\delta\Delta P_{@OCR=0}\right)^2\right]}$$

$$\delta PDPF = \sqrt{\left[\left(\frac{1}{2.4}0.03\right)^2 + \left(\frac{-2.74}{2.4^2}0.03\right)^2\right]} = \boldsymbol{\delta PDPF = \pm 0.019}$$

$$\boldsymbol{OCR = 4.34 \pm 0.02\%}$$

$$\boldsymbol{HTPF\_Q_{air} = 0.98 \pm 0.074}$$

$$\boldsymbol{HTPF\_\Delta T_{air} = 0.99 \pm 0.076}$$

$$\boldsymbol{PDPF = 1.14 \pm 0.019}$$

VITA

Pratik S. Deokar

Candidate for the Degree of

Master of Science

Thesis: DEVELOPMENT OF AN EXPERIMENTAL METHODOLOGY FOR MEASUREMENT OF OIL RETENTION AND ITS EFFECT ON THE MICROCHANNEL HEAT EXCHANGER.

Major Field: Mechanical Engineering

Biographical:

Pratik Deokar is a graduate research assistant at Oklahoma State University. He has 3 years of experimental experience in designing thermal systems, building laboratory test set ups, and lab supervision in universities. While completing his undergraduate and graduate studies, his primary research projects focused on experimentation on enhanced (micro-fin) tubes and microchannel heat exchangers. Through his thesis project work he received good hands-on working experience in the HVAC&R labs. The work has made him expert in performing tests, data analysis/reduction, instrumentation, and troubleshooting. He is proficient in using ASHRAE, AHRI and other standards. He also has coding experience in VBA in Excel and Fortran.

Education:

Completed the requirements for the Master of Science in Mechanical Engineering at Oklahoma State University, Stillwater, Oklahoma in December, 2013.

Completed the requirements for the Bachelor of Engineering (Mechanical) at University of Pune, India in 2010.

Experience:
Worked at HVAC&R labs (Low Temperature Psychrometric Chamber and Air Flow Wind Tunnel Lab) at Oklahoma State University. (Sep 2011- July 2013)
Treasurer of 'ASHRAE Student Branch – Oklahoma State University' (June 2012 – Present)

Professional Memberships:
ASHRAE Student Member
Golden Key International Honour Society